



universität
wien

DIPLOMARBEIT

Titel der Diplomarbeit

Molecular Determinants of the Anti-cancer Activity of Ruthenium
Compound KP1339

angestrebter akademischer Grad

Magistra der Naturwissenschaften (Mag. rer.nat.)

Verfasserin:	Bihter Atil
Matrikel-Nummer:	0409144
Studienrichtung /Studienzweig (lt. Studienblatt):	A441
Betreuerin / Betreuer:	Univ.-Prof. Mag. Dr. Renée Schröder A. o. Univ. Prof. Dr. Walter Berger

Wien, im 22.04.2010

Für meinen lieben, unsterblichen Vater...

Canım, ölümsüz babama...

Ich danke allen, die mir ermöglicht haben, diese Arbeit zu erfassen und fertigzustellen: all den KollegInnen in der Institut für Krebsforschung, all meinen StudiumkollegInnen, und FreundInnen. Mein besonderer Dank geht an A.o. Univ. Prof. Mag. Dr. Renée Schröder, dass sie diese Arbeit betreut hat.

Ich kann A.o. Univ. Prof. Dr. Walter Berger und seiner ganzen Gruppe unendlich danken, für ihre unendliche Unterstützung und Hilfe, für das beste Arbeitsklima, das man sich je vorstellen kann, für die ganze Geduld mit so einem „Zwergl“, „Puppl“, „Kleine“ etc. wie ich... ☺ Für die ganze Hilfe beim Schreiben dieser Arbeit und Einschulung am Anfang meiner Diplomarbeit danke ich besonders Dr. Petra Heffeter, dass sie diese Arbeit wirklich mit mir geschrieben und all diese chaotische Zeit mit mir durchlebt hat. ☺ Daniela Lötsch, Ute Jungwirth, Vera Bachinger, Christine Pirker, Christian Balcarek, Johannes Gojo, Amir Mohamed, Mir Ali Reza Hoda, und Bahil Ghanim... Ihr habt mich alle die ganze Zeit unterstützt, mir mit euren Erfahrungen weitergeholfen und beigestanden.

Ich danke all meine FreundInnen und meine ganze Familie, deren Glauben an mir ich immer gewusst und gefühlt habe, obwohl wir voneinander weit entfernt waren. Besonders einem Menschen, der für mich ihr ganzes Leben geändert und mich zu diesem Abenteuer immer gefördert hat: meiner lieben, einzigartigen Mutter...

DANKE...

TABLE OF CONTENTS

1.	ABSTRACT	9 – 12
2.	INTRODUCTION	
2.1.	What is Cancer?	13 – 20
2.2.	Types of Cancer	21 – 24
2.3.	Hepatocellular Carcinoma	25 – 31
2.4.	Cancer Therapies	32 – 35
2.5.	Ruthenium Drugs	36 – 39
2.6.	Cell Cycle and Cell Cycle Regulation	40 – 44
2.7.	Programmed Cell Death (Apoptosis, Autophagy, and Necrosis)	45 – 49
3.	AIM OF THE STUDY	51
4.	MATERIALS AND METHODS	
4.1.	Cell Culture	53, 54
4.2.	Drugs	53
4.3.	Cell Proliferation and Cell Vitality Assays	
4.3.1.	Cytotoxicity Assay	55, 56
4.3.2.	DNA Synthesis Analysis by ³ H-Thymidine Incorporation Assay	56, 57
4.3.3.	DAPI Staining	58, 59

TABLE OF CONTENTS

4.4.	Flow Cytometry	
4.4.1.	Cell Cycle Analysis by PI Staining	60 – 62
4.4.2.	Mitochondrial Membrane Potential Detections by JC-1 Staining	62, 63
4.5.	Drug Accumulation Assays	
4.5.1.	Total Drug Accumulation	64
4.5.2.	Drug Levels in Cell Fractions	65
4.5.3.	Incorporation of Drugs into DNA	65 , 66
4.6.	Protein Analysis	
4.6.1.	Protein Extraction	67
4.6.2.	Western Blot Analysis	67 – 72
5.	RESULTS	
5.1.	Comparison of KP1019 and KP1339	
5.1.1.	Cell Line-dependent Cytotoxicity of KP1019 and KP1339	73 – 75
5.1.2.	Enhanced Cellular Accumulation of KP1019 As Compared to KP1339	75 – 77
5.1.3.	Different Intracellular Distributions of KP1019 and KP1339	77
5.1.4.	Apoptosis Induction Potential of KP1019 and KP1339	78, 79
5.1.5.	Mitochondrial Membrane Depolarization Induced by KP1019 and KP1339	79, 80
5.1.6.	Apoptosis Detection at Protein Level	81, 82

5.2.	Combination Tests With KP1339 and Other Chemical Compounds	
5.2.1.	Combinations With FeCl ₃ , Gallium nitrate, and Triapine	83 – 86
5.2.2.	Combinations With DNA-Damaging Agents Ara-C, Adriamycin, and Temozolomide	86 – 91
5.2.3.	Combinations With Tubulin-Targeting Agents Taxol and Vinblastine	91 – 93
5.3.	Combination Tests With KP1339 and Tyrosine Kinase Inhibitor Sorafenib	
5.3.1.	Differences in Cytotoxicity of KP1339 Through Sorafenib Co-Treatment	94 – 97
5.3.2.	Enhanced Accumulation of KP1339 in Combination with Sorafenib	98, 99
5.3.3.	Apoptosis-induction by Combination Therapy With KP1339 and Sorafenib	100 – 104
5.3.4.	Effects of KP1339 and Sorafenib Co-treatment on DNA Synthesis	105
5.3.5.	Cell Cycle Alterations Induced by KP1339 and Sorafenib Exposure	106 – 108
5.3.6.	Alterations in p38 MAPK and ERK Pathway Induced by KP1339/Sorafenib Combination	107, 109
6.	DISCUSSION	
6.1.	KP1019 vs. KP1339	111 – 117

TABLE OF CONTENTS

6.2.	Combination Tests With KP1339 and Other Chemical Compounds	118 – 121
6.3.	Combination Tests With KP1339 and Tyrosine Kinase Inhibitor Sorafenib	122 – 128
7.	CONCLUSION	129
8.	ABBREVIATIONS	131 – 134
9.	PUBLICATIONS	135 – 146
10.	REFERENCES	147 – 162
11.	CURRICULUM VITAE	163

1. ABSTRACT

Cancer is one of the major diseases of our century with very high mortality rates. To fight cancer, several strategies such as surgery, radiation therapy, and chemotherapy are used either alone or in combination. Chemotherapy is frequently used for systemic treatment of cancer cells using several chemicals especially at late stages of the disease. Platinum-containing drugs such as cisplatin or oxaliplatin are among the most important chemotherapeutic drugs. However, due to often observed complications, including severe side effects or ineffectiveness through drug resistance, the need for better chemotherapeutics still exists. Due to their promising anti-cancer properties (such as tumor selectivity) ruthenium compounds have attracted much attention. Recently, the ruthenium compound KP1019 (indazolium trans-(tetrachlorobis(1H-indazole)ruthenate(III))) has demonstrated promising anti-cancer activity in a pilot clinical trial. However, due to better pharmacological properties its sodium salt (KP1339) was selected for further clinical development. In this study, both ruthenium complexes were compared in their cytotoxicity, accumulation in the cell, intracellular distribution, and apoptosis induction. Although KP1339 tended to be moderately less cytotoxic than KP1019, almost all analyzes proved that they targets similar components in the cell. Accordingly, both drugs activated apoptosis via caspase activation. Additionally, drug uptake experiments using inductively coupled plasma mass spectrometry (ICP-MS) showed that KP1019 was accumulated in higher levels as compared to KP1339 after 1 hour drug exposure. Interestingly, these compounds differed in their intracellular distribution that KP1019 remained mainly in cytosol while KP1339 was localized in nuclei. This finding related to higher cytotoxic activity of KP1019 suggests that the major targets for these ruthenium drugs are cytosolic rather than nuclear.

As a next step, this study aimed to investigate the impact of KP1339 on the cellular iron homeostasis. To this end KP1339 was combined with several compounds, which are known to interact with the cellular iron regulation such as FeCl₃, gallium nitrate, and triapine. In general, all of these combinations enhanced the anti-tumor potential of KP1339, especially in hepatocellular carcinomas indicating that KP1339 treatment does indeed interact with the cellular iron homeostasis.

Furthermore, KP1339 was combined with the tyrosine kinase inhibitor sorafenib, which led to enhanced cytotoxicity and intracellular accumulation of KP1339. Notably, this was not based on enhanced cell death. In contrast, sorafenib co-treatment reduced the apoptosis level after KP1339 as indicated by a reduced number of apoptotic nuclei and reduced PARP cleavage. However, JC-1 staining revealed that the apoptosis-inducing mitochondrial membrane depolarization was enhanced by combination of KP1339 with sorafenib, indicating that the observed reduction of cell death is not based on reduced apoptosis induction but on hampered apoptosis execution. Finally, the effects of the KP1339/sorafenib combination on cell cycle distribution were analyzed. While KP1339 alone led to G₂/M arrest, addition of sorafenib led to a shift towards G₀/G₁. These data suggest that the synergism between KP1339 and sorafenib is multi-factorial involving transport as well as signal transduction mechanisms. In summary, this study showed that KP1339 is a promising anticancer ruthenium complex targeting specific cancer cell characteristics by a unique mode of action. Moreover, this innovative metal compound demonstrates distinct synergism with novel targeted therapies especially in hepatoma cell lines.

Krebs ist eine der häufigsten Erkrankungen unserer Zeit mit sehr hoher Mortalität. Um gegen Krebs zu kämpfen, wurden viele Strategien entwickelt, welche alleine oder in Kombinationen miteinander verwendet werden. Chemotherapie ist eine oft eingesetzte systemische Behandlung der Patienten mit unterschiedlichen Chemikalien, die besonders im weit fortgeschrittenen Stadium der Krankheit wichtig ist. Zu den am häufigsten verwendeten Chemotherapeutika gehören die Platinverbindungen Cisplatin oder Oxaliplatin. Leider verursachen diese Chemotherapeutika oft schwere Nebenwirkungen und gerade die Uneffektivität durch Resistenzentwicklung stellt ein großes Problem in der Therapie dar. Deswegen besteht immer noch dringender Bedarf an neuen Medikamenten gegen Krebs. Die vielversprechende Eigenschaften (wie Tumor-Selektivität) von Ruthenium-Komplexen haben in den letzten Jahrzehnten Aufmerksamkeit erregt und zu der klinischen Entwicklung solcher Verbindungen geführt. Besonders KP1019 (indazolium trans-(tetrachlorobis(1H-indazole)ruthenate(III))) hat sich in ersten klinischen Studien als sehr vielversprechend herausgestellt. Auf Grund besserer pharmakologischer Eigenschaften, wurde für die weitere klinische Entwicklung das Natriumsalz von KP1019, KP1339 ausgewählt. In der hier präsentierten Arbeit wurden die Zytotoxizität, die zelluläre Aufnahme und Lokalisierung sowie das apoptose-auslösende Potential der beiden Ruthenium-Komplexe miteinander verglichen. Obwohl KP1339 im Vergleich zu KP1019 weniger toxisch war, zeigten all die Analysen, dass beide Substanzen ähnliche Ziele in der Zelle haben. Außerdem wurde es in den Akkumulation-Experimenten mit ICP-MS festgestellt, dass KP1019 besser in die Zelle aufgenommen wird als KP1339. Interessanterweise unterschieden sich die Komplexe stark in ihrer intrazellulären Lokalisation. Während KP1019 größtenteils im Zytosol blieb, reicherte sich KP1339 im Kern an. Diese Ergebnisse lassen vermuten, dass sich die zentralen Angriffspunkte der getesteten Ruthenium-Substanzen im Zytosol befinden. Ein weiterer Schwerpunkt der hier präsentierten Arbeit, lag auf der Untersuchung der Interaktion von KP1339 mit dem intrazellulären Redox und Eisenhaushalt. Hierfür wurde KP1339 mit verschiedenen Verbindungen kombiniert, welche bekannt für ihre Interaktion mit zellulärer

Eisenregulation sind. Im allgemein führte dies immer zu einer verstärkung der KP1339 Wirksamkeit. Diese Erkenntnisse stärken die Hypothese, dass KP1339 mit zellulärer Eisenhomöostase interagieren könnte. Um die Interaktion von KP1339 mit herkömmlicher Chemotherapie zu untersuchen, umfasste der letzte Teil der Studie die Kombination von KP1339 mit klassischen Chemotherapeutika sowie neuen zielgerichteten Medikamenten. Hier zeigte sich, dass KP1339 die Wirkung von Sorafenib synergistisch verstärken kann. Genauere Untersuchungen der zugrundeliegenden Mechanismen ergaben, dass Zugabe von Sorafenib zu erhöhter Aufnahme von KP1339 führte. Bemerkenswerterweise führte die KP1339/Sorafenib-kombination zwar zu erhöhter Apoptose-Induktion, allerdings nicht zu erhöhten Zahlen an sterbenden Krebszellen. Dies legt nahe, dass der Synergismus nicht auf verstärktem Zelltod beruht. Da KP1339 Toxizität zu Zellzyklusarrest in der G₂/M Phase führt, wurde als nächstes der Einfluss von Sorafenib auf diesen Effekt untersucht. Hier zeigte sich, dass die Zugabe von Sorafenib zu einer Verschiebung der Zellzyklusdistribution in die G₀/G₁ Phase führt. Zusammengefasst lassen unsere Daten vermuten, dass der Synergismus zwischen KP1339 und Sorafenib auf einer multi-faktoriellen Interaktion sowohl mit der Substanzaufnahme als auch mit der Signaltransduktion beruht. Zudem zeigt diese Arbeit, dass KP1339 ein vielversprechendes neues Krebsmedikament mit einem gezielt gegen Krebszellen gerichteten Wirkungsmechanismus ist. Außerdem macht die beobachtete synergistische Wirkung von KP1339 mit neuen gezielten Therapien diese neue Rutheniumverbindung gerade für den schwer therapierbaren Leberkrebs besonders wertvoll.

2. INTRODUCTION

2.1. What is cancer?

Cancer is a disease characterized by uncontrolled growth of abnormal cells and their spreading into diverse organs (metastasis). Although diseases of the heart and blood vessels are still the main cause of death in our ageing population, the incidence of cancer is increasing. At least one in three will develop cancer, and one in four men and one in five women will die from it each year [3] (Figure 1).

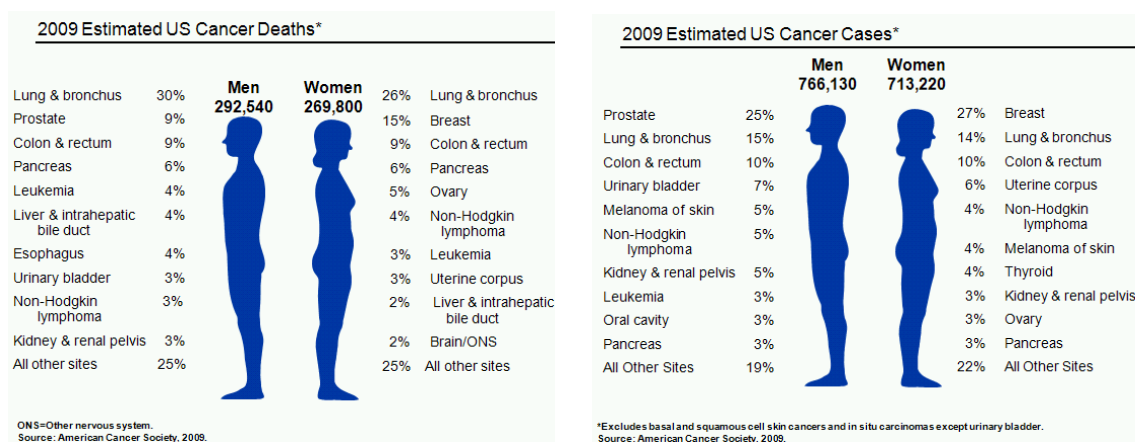


Figure 1: 2009 estimated US cancer deaths and cases (Source: American Cancer Society).

Several discoveries in developmental biology led to increased understanding how tissues in higher organisms are functioning and which molecular mechanisms are involved in this very complex system. The theory on development of cells by Theodor Schwann *et al.* in 1839 was the first to suggest that cells are the basic units of life and arise from pre-existing cells. These theories were crucial for the understanding of tumor development [4].

The process of carcinogenesis is a multi-stage process (Figure 2) [5] requiring a series of changes which allow transformed cell to increase proliferation, avoid cell death and

perform aggressive growth over healthy tissues [6]. It has now become basic knowledge that cancer is caused by stepwise accumulation of changes in the genetic information (the genome) of cells. Such mutations in the genome can occur in oncogenes leading to dominant gain-of-function or in tumor suppressor genes causing recessive loss of function [7]. Current evidence indicates that most cancers arise from one single cell that has undergone malignant transformation driven by such mutations [8].

One current hypothesis suggests that malignant growth is driven by so-called **cancer stem cells**. These cells are able to self-renewal, to proliferate independent from normal growth-regulating mechanisms as well as to invade and destroy healthy tissues [9]. The concept of malignant stem cells is based on the similarity of cancer cells to stem cells.

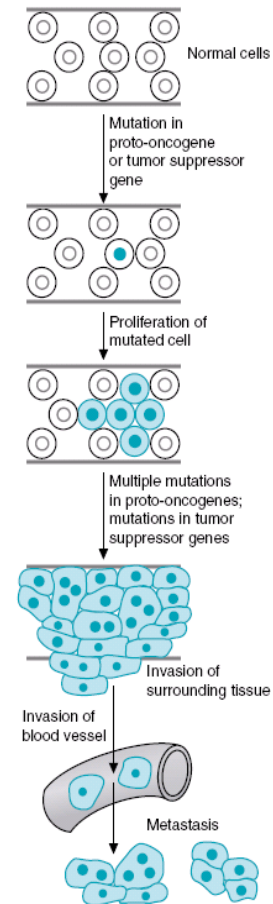
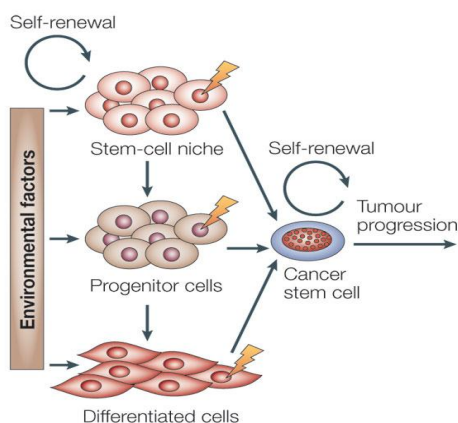


Figure 2: Development of cancer [3].



Copyright © 2005 Nature Publishing Group
Nature Reviews | Cancer

Figure 3: Mutations in stem cells and/or progenitor cells might give rise to cancer stem cells. Environmental factors or mutations can induce changes in the cell program that these abnormal cells proliferate limitless and are able to self-renewal like a stem cell. Thus, these changes can result in uncontrolled growth and disruption of adjacent tissues [8].

Additionally, tumors often originate from malignantly transformed stem cells [10] (Figure 3). This suggests that similar pathways and molecular mechanisms might be responsible for common features of both “normal” and cancer stem cells [11].

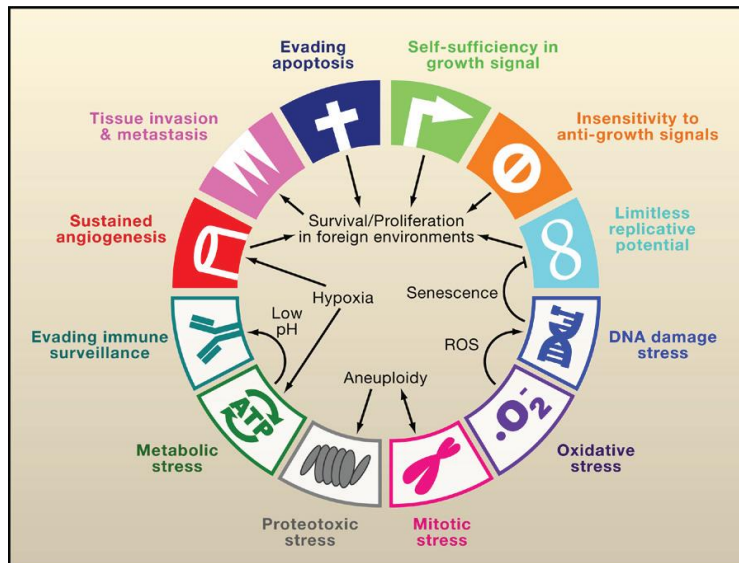


Figure 4: The hallmarks of cancer. In addition to six important alterations in the cell physiology of cancer cells suggested in the review of Weinberg *et al.* [2], another six alterations were proposed by Luo *et al.* [10].

Based on the requirements for tumor development, Weinberg *et al.* suggested in the review “The hallmarks of cancer” that there are six essential alterations in cell physiology causing malignant growth (Figure 4) [7]: self-sufficiency in growth signals, insensitivity to growth-inhibitory (anti-growth) signals, evasion of programmed cell death (apoptosis), limitless replicative potential, sustained angiogenesis and tissue invasion. In 2009, Luo *et al.* have suggested that in addition to these alterations there are also other stress induced mechanisms involved in the tumorigenesis [12]: evading immune surveillance, metabolic stress, proteotoxic stress, mitotic stress, oxidative stress, and DNA damage stress.

2.1.1. SELF-SUFFICIENCY IN GROWTH SIGNALS

Normal cells require mitogenic growth factors for an active proliferation state. In most cases, these signals are transmitted in a paracrin-manner from the microenvironment in order to stimulate cell division. Cancer cells often have the ability to produce growth factors to stimulate themselves in an autocrine loop [7]. For example, it has been shown that the production of platelet-derived growth factor (PDGF) and tumor growth factor α (TGF α) is typical for glioblastomas and sarcomas [13]. Another way to stimulate tumor cell proliferation is the uncontrolled overexpression or activation of cell surface receptors, which transduce stimulatory signals into the cell. This is for example frequently observed in the epidermal growth factor receptor EGFR which is upregulated in stomach, brain, and breast tumors, while the HER2/*neu* receptor is overexpressed in stomach and mammary carcinomas [14-15]. Mutations, gene amplification and overexpression can lead to enhanced activation of these receptors [16].

2.1.2. INSENSITIVITY TO GROWTH-INHIBITORY (ANTI-GROWTH) SIGNALS

Antiproliferative signals are essential for the maintenance of cellular quiescence and tissue homeostasis. Basically, there are two mechanisms [7]: (1) Cells may be forced out of the active proliferative cycle into the G₀ state, or (2) induced to enter into postmitotic states, usually associated with acquisition of specific differentiation-associated characteristics. However, cancer cells must escape from these growth-inhibiting signals to proliferate limitless. Thus, mutations on the components responsible for the regulation of proliferation are frequently observed [7]. One example is retinoblastoma protein (pRb), which controls the expression of several genes essential for progression from G₁ into S cell cycle [17]. Disruption of this pathway causes uncontrolled proliferation and insensitivity to anti-growth factors [18-19].

2.1.3. EVASION OF PROGRAMMED CELL DEATH (APOPTOSIS)

Net growth of cancers is determined not only by higher rates of proliferation but also by the rate of cell death. Programmed cell death, also called apoptosis, is the main mechanism for removal of altered cells and thus a barrier for tumor development [20]. For the survival, tumor cells often acquire resistance to apoptosis. To escape from apoptosis, tumor cells regulate antiapoptotic survival signals or tumor suppressors [7]. Some factors, like *bcl-2* and *c-myc* in follicular lymphoma [21-23], p53 [24], Ras or PTEN [25], have been shown to play major roles in this alteration of tumor cells.

2.1.4. LIMITLESS REPLICATIVE POTENTIAL

For limitless proliferation, tumor cells must also have unlimited replicative potential. This potential can be supported by loss of tumor suppressors like p53 or pRb. Moreover, telomere maintenance at a length above a critical threshold is another key feature required for limitless replicative potential [26-27]. Telomeres are regions of repetitive DNA at the end of chromosomes which protect the ends of chromosomes from deterioration. To inhibit the shortening of telomeres after each replication cycle, telomerases add DNA sequence repeats to the 3' end of DNA strands in the telomere regions. Telomerase is a reverse transcriptase that carries its own RNA molecule which is used as template when it elongates telomeres. The upregulation of telomerase has been shown in most human cancers [28-29], and it is believed that this upregulation of telomerase is required to allow malignant cells to divide after genetic rearrangements enabled by telomere dysfunction [30].

Furthermore, tumors, especially solid tumors, show extreme genomic instability resulting in the accumulation of point mutations, deletions, complex chromosomal rearrangements, and extensive aneuploidy [31]. DNA damages can underlie shortening of telomeres due to replication in the absence of sufficient telomerase activity. This leads to the appearance of double-strand breaks at telomeric ends

initiating breakage-fusion-bridge cycles and results in translocations and gene amplification events [32].

2.1.5. SUSTAINED ANGIOGENESIS

Oxygen and nutrients are crucial for cell function and survival. However, especially rapidly dividing tumor tissues are tend to lack blood supply as compared to normal tissues. Therefore they must have the ability to form new vessels for the maintenance of their aggressive growth. This process is called angiogenesis and allows a better obtainment of nutriment, oxygen and thus energy production. Neoangiogenesis is a prerequisite to metastasize and growth beyond a certain size [7]. One example is the production and secretion of vascular endothelial growth factor (VEGF) (caused e.g. by the activation of *ras* oncogenes) or loss of the VHL tumor suppressor gene [33-34] leading to new blood vessel formation. Notably, two similar processes play a key role which should be distinguished from each other. Vasculogenesis is the blood vessel formation occurring by a *de novo* production of endothelial cells. By contrast, angiogenesis is a physiological process involving the growth of new blood vessels from pre-existing vessels. These two mechanisms used by cancer cells differ in this aspect that angiogenesis denotes the formation of new blood vessels from pre-existing ones, whereas vasculogenesis is the term used for spontaneous blood-vessel formation when there are no pre-existing ones.

2.1.6. TISSUE INVASION

The capability for invasion enables cancer cells to escape the primary tumor mass and to metastasize into distant organs [7]. These distant clones of tumor cells cause about 90% of human cancer deaths [35]. Although the molecular mechanisms of metastasis are not fully understood, the typical alterations leading to enhanced invasion and metastases are loss of E-cadherin expression [36] as well as upregulated production of

extracellular proteases like MMP [37-38]. E-cadherin is a key component in cell-to-environment interactions which is ubiquitously expressed on epithelial cells. E-cadherin bridges can be build between adjacent cells resulting in the transmission of anti-growth and other signals via cytoplasmic contacts with β -catenin to intracellular signaling circuits [36]. The second alteration, upregulation of extracellular proteases, is based on the docking of the active proteases on the cell surface leading to facilitate the invasion into nearby stroma, across basal membranes, blood vessel walls, and through normal epithelial cell layers [7].

2.1.7. STRESS-INDUCED MECHANISMS

In addition to these six alterations of cancer [7], another work by Kroemer and colleagues has suggested that evading immune surveillance is also a key feature to induce tumorigenesis. The metabolic microenvironment of tumor cells may inhibit the function of antitumor immune effectors such as cytotoxic T lymphocytes and natural killer cells. In contrast, attracting inflammatory cells is a double-edged sword and might participate in tumor progression [39]. The microenvironment of tumor tissues is often characterized by enrichment of tumor-associated macrophages (TAMs) which facilitates angiogenesis, migration and induction of immunosuppressive effects [40]. Within TAMs, an essential key factor, hypoxia inducible factor-1 (HIF-1), upregulates glycolysis so that the cells can migrate into tumor beds [41].

Moreover, DNA hyper-replication [42-43] can also increase DSBs and genomic instability [44]. Finally, some mutations of genes involved in either DNA repair programs or the DNA damage response (DDR) pathways can lead to increased DNA damages and genomic instability [45] which cannot be eliminated because of the destruction of the respective genomic control mechanisms. Other mutations in tumors cause rates of chromosome missegregation inducing chromosome instability (CIN) [46]. This phenotype is driven by defects in mitotic proteins [47]. It has been also

shown that mutations of some oncogenes, such as Ras or p53, contribute to the CIN phenotype [48] based on a combination of growth advantage and limited genetic and genomic control.

Aneuploidy and gene copy-number changes imbalance the levels of transcription [49-51] and additionally produce increased amounts of toxic, unfolded protein aggregates [52]. Consequently, tumors exhibit proteotoxic stress evidenced by their frequent constitutive activation of the heat shock response [12] suggesting because of the aneuploidy [53-54].

Due to insufficient blood supply the microenvironment within the tumor is often characterized by low oxygen levels (hypoxia) and enhanced CO₂ levels which lead to an acidic milieu. Thus, in addition of ATP generation through the mitochondrial oxidative phosphorylation, cancer cells frequently produce energy by glycolysis [55]. Due to utilization of this less efficient pathway, tumors are characterized by a high need of glucose and large amounts of the glycolysis endproduct lactic acid [56].

In the microenvironment of tumor tissues, oxidative stress dominates mostly in form of reactive oxygen species (ROS) [57]. Both oncogenic signaling [58] and the downregulation of mitochondrial function [59] in tumors can contribute to ROS generation. ROS also regulate some transcription factors, such as HIF-1, which is a characteristic of hypoxia [60] and promotes the glycolytic switch and neoangiogenesis observed in tumors.

2.2. Types of Cancer

Depending on the stage of disease, tumors can be classified into two broad categories. **Benign tumors** usually resemble their tissue of origin. They grow locally without invasion into adjacent tissues. Generally, they are considered harmless to their hosts based on the possibility for complete surgical removal. However, even benign tumors may cause clinical problems, for example when they release high levels of hormones. In contrast, **malignant tumors** show cellular abnormalities (compare with section 2.1.), invasion into surrounding tissues and potential for metastasis [4]. Malignant tumors have no well-defined fibroblast capsule and grow in a much more disorganized form than benign tumors [6]. Furthermore, malignant tumors can arise from diverse cell types throughout the body (Table 1) [3]. They can be classified in carcinoma (including squamous cell carcinoma and adenocarcinoma), sarcoma, leukemia, lymphoma, and neuroectodermal tumors.

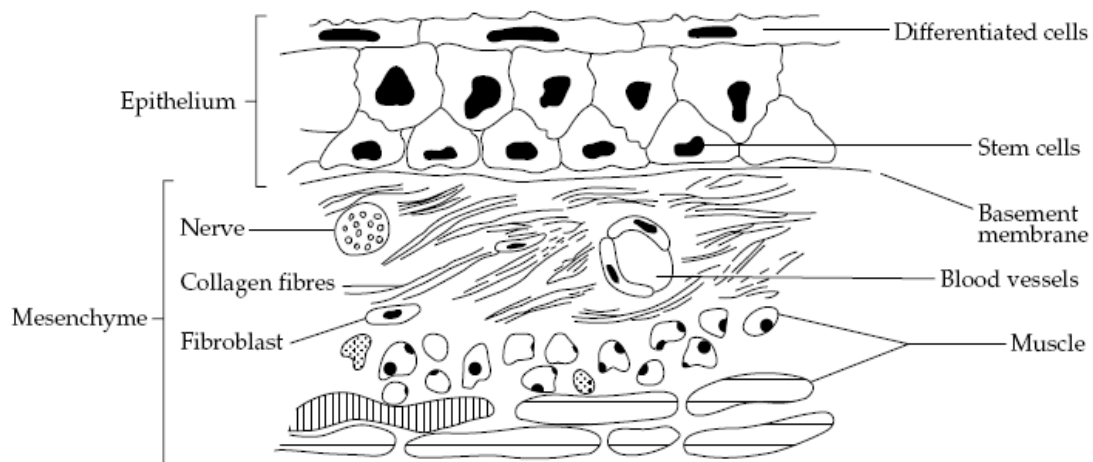


Figure 5: A typical tissue showing epithelial and mesenchymal components [1].

2.2.1. CARCINOMA

The majority of human tumors originates from epithelial tissues and is called **carcinomas** (Figure 5) [3]. This form of malignancies is responsible for more than 80% of the cancer-related deaths in the Western world [4] and comprises two subgroups: squamous cell carcinoma and adenocarcinoma. **Squamous cell carcinomas** arise from epithelial cells which mainly serve to seal cavities or channels that they line and to protect the underlying cell populations [4]. Epithelia occur in all organs which form typical barriers between the host and the external environment, like skin, lips, mouth, esophagus, urinary bladder, prostate, lungs, vagina, and cervix. **Adenocarcinomas** originate from specialized epithelial cells which secrete substances into the ducts or cavities [4].

2.2.2. SARCOMA

Malignant tumors can also occur in non-epithelial tissues throughout the body. For instance, **sarcomas** arise from the various connective tissues which originate from mesenchymal cell types. Some examples for these cells are fibroblasts, adipocytes at adipose tissues, bone marrow-derived osteoblasts, and myocytes in muscles [4].

2.2.3. LEUKEMIA

Another group of cancer is originated from hematopoietic tissues, including cells of the immune system. Malignant growth of any hematopoietic cell type is called **leukemia**. They usually have only a few chromosome rearrangements [61], such as translocations or inversions, and these are used as markers for detecting residual malignant cells after treatment [62]. Leukemia cells need less mutations because of the non-essentiality of invasion and angiogenesis in comparison to solid tumors.

2.2.4. LYPMHOMA

In contrast, **lymphomas** represent tumors of the lymphoid lineages (B and T lymphocytes) that aggregate to form solid tumor masses. Like leukemias, also lymphomas often possess also consistent and, in some cases, highly specific chromosome aberrations [63].

2.2.5. NEUROECTODERMAL TUMORS

Additionally, another major group of nonepithelial tumors are **neuroectodermal tumors**, including gliomas, glioblastomas, neuroblastomas, schwannomas, and medulloblastoma. Neuroectodermal tumors are malignancies originated from various cellular components of the central and nervous systems. These are responsible for about 2.5% of cancer-related deaths [4].

Table 1: Nomenclature of common tumor types [3].

Tissue	Cell type	Benign tumor	Malignant tumor
Epithelium			
Skin	Squamous epithelium	Squamous cell papilloma	Squamous carcinoma
	Melanocytes	Melanocytic naevus	Basal cell carcinoma Malignant melanoma
Upper aero-digestive tract Nose, mouth, pharynx, larynx, and oesophagus	Squamous epithelium	Squamous cell papilloma	Squamous carcinoma
Alimentary tract Stomach, small and large bowel	Columnar epithelium	Adenoma	Adenocarcinoma
Lungs	Respiratory epithelium		Squamous carcinoma Adenocarcinoma Small cell carcinoma Undifferentiated carcinoma
Urinary system Ureters and bladder	Urothelium (transitional epithelium)	Transitional cell papilloma	Transitional cell carcinoma
Solid epithelial organs Liver, pancreas, kidney, prostate, etc.	Specific epithelium	Adenoma	Adenocarcinoma
Gonads			
Ovary	Surface epithelium	Serous cystadenoma Mucinous cystadenoma	Serous cystadenocarcinoma Mucinous cystadenocarcinoma
Ovary	Germ cells	Teratoma	Dysgerminoma Yolk sac tumor Embryonal carcinoma Choriocarcinoma
Testis	Germ cells		Seminoma Teratoma Yolk sac tumor Choriocarcinoma
Mesenchyme			
Fibrous tissue	Fibroblasts	Fibroma	Fibrosarcoma
Fat	Adipocytes	Lipoma	Liposarcoma
Bone	Osteocytes	Osteoma	Osteosarcoma
Cartilage	Chondrocytes	Chondrioma	Chondrosarcoma
Smooth muscle	Smooth muscle cells	Leiomyoma	Leiomyosarcoma
Striated muscle	Striated muscle cells	Rhabdomyoma	Rhabdomyosarcoma
Blood vessels	Endothelial cells	Haemangioma	Angiosarcoma
Peripheral nerve	Schwann cells	Schwannoma Neurofibroma	Malignant peripheral nerve sheath tumor
Haemato-lymphoid			
Haemopoietic system	Red cells, leukocytes, and platelets		Acute myeloid leukemia Chronic myeloid leukemia Myeloproliferative disorders
Immune system	Lymphoid cells		Acute lymphoblastic leukemia Chronic lymphocytic leukemia Non-Hodgkin lymphoma Hodgkin lymphoma Multiple myeloma
Central Nervous System			
Glial cells	Astrocytes and oligodendrocytes		Glioma-Astrocytoma and oligodendroglioma
Meninges	Meningothelial cells	Meningioma	Anaplastic (malignant) meningioma
Embryonal	Neurones		Medulloblastoma and primitive neuroectodermal tumor

2.3. Hepatocellular Carcinoma

Hepatocellular carcinoma (HCC) is a primary malignancy of the liver. It is currently the fifth most common solid tumor worldwide and the fourth leading cause of cancer related-mortality with 610 000 deaths each year (Source: World Health Organization) (Table 2) [64]. HCC represents 83% of all cancer cases (Source: American Cancer Society).

Table 2: The worldwide distribution of HCC and its associated etiologies. HBV... Hepatitis B virus, HCV... Hepatitis C virus [64].

Region	HCC Incidence (occurrences/100 000 population) Males	HCC Incidence (occurrences/100 000 population) Females	No. of HCC Cases	Principal Associations
Asia, Sub-Saharan Africa	30-120	9-30	>500 000 cases per year	HBV, aflatoxin exposure
Japan	10-30	3-9		HCV
Southern Europe, Argentina, Switzerland	5-10	2-5		HCV
Western Europe	<5	<3		HCV
United States	<5	<3	18 000 predicted for 2005	HCV, alcohol

HCC is one of the best studied liver diseases. The high mortality rate of HCC is based on its lack of symptoms in the early stages of the disease and its rapid tumor growth [65]. Although researches have been largely successful in defining the factors of its

pathogenesis [65], the development of more effective therapeutic tools and strategies is urgently needed [66].

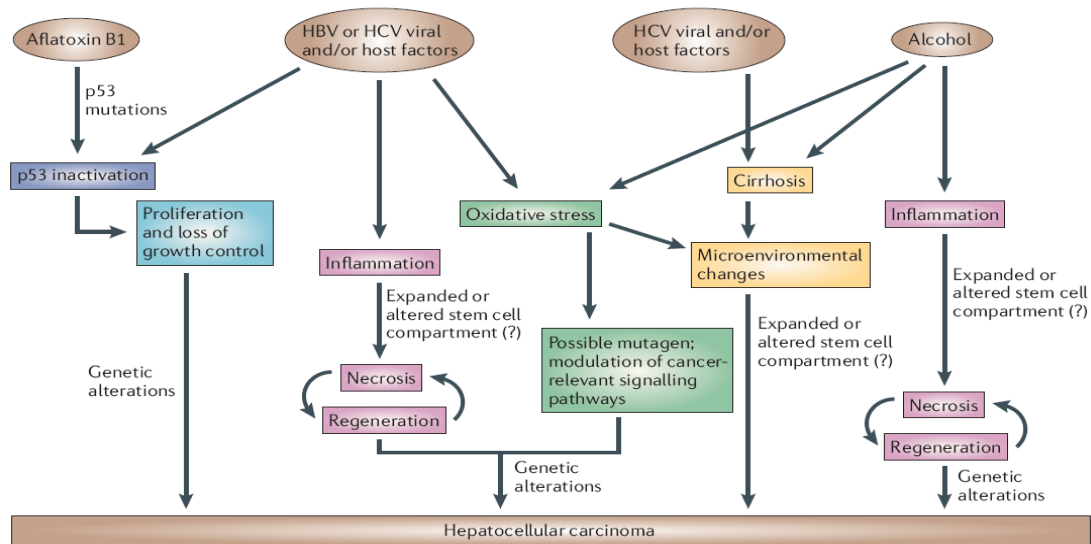


Figure 6: Causes of hepatocellular carcinoma. The main factors in HCC development are aflatoxin B1, which is a fungal toxin, hepatitis B and C viruses, and alcohol [77].

The difficulties to treat HCC are based on several aspects. First, HCC cells are characterized by diverse toxins and thus also high therapeutical resistance because of enhanced cellular drug efflux of several cytotoxic agents. For example, MDR1 (P-gp) and MRP (multidrug resistance protein) proteins of the drug transporter family adenosine triphosphate-binding cassette proteins are upregulated [67-68]. Moreover, it has been hypothesized that certain p53 mutants may contribute to the upregulation of P-gp in cancer cells [69]. Although only approximately half of the clinical specimen studies showed a positive association between p53 mutation and P-gp overexpression [70], numerous other studies suggested that the MDR1 promoter is suppressed by wild-type p53 through a sequence-specific binding [71-74]. Another reason for therapeutical resistance of HCC is the ability of hepatocytes to efficiently metabolize most drugs by non-specific pathways by enzymes in microsomes of the smooth

endoplasmic reticulum. These enzymes convert lipid-soluble compounds into more water-soluble ones thus enabling them to be excreted in the bile or urine [75].

There exists only a limited array of therapeutic options for HCC. At present, surgery or liver transplantation are the best curative methods for HCC at early stage [64]. However, systemic chemotherapy is inefficient in HCC evidenced by low response rates and no demonstrated survival benefits [64].

The orally active multikinase inhibitor **sorafenib** (Nexavar®) allows the targeted therapy of HCC and advanced renal cell carcinoma [76]. It inhibits both cell surface tyrosine kinase receptors, including vascular endothelial growth factor (VEGFR)-1, VEGFR-2, VEGFR-3, platelet-derived growth factor receptor (PDGFR)- β , c-KIT, FMS-like tyrosine kinase (FLT)-3, RET [76] as well as downstream intracellular serine/threonine kinases in the Ras/MAPK cascade, such as Raf-1 (or C-Raf), wild-type B-Raf and mutant B-Raf [77-78].

There are three main mechanisms underlying HCC (Figure 6) [79]: 1) Virus infection (HBV, HCV), 2) alcohol consumption, and 3) aflatoxin-B1-contaminated food.

2.3.1. VIRAL-INDUCED HEPATOCARCINOGENESIS

80% of HCC are caused by viruses [64]. Especially, hepatitis B (HBV) and C virus (HCV) are associated with HCC. HBV annually infects approximately 2 billion individuals worldwide causing 320 000 deaths annually. HBV is a non-cytopathic, partially double-stranded hepatotropic DNA virus classified as a member of the hepadnaviridae family. The HBV-dependent induction of HCC is a multistep heterogeneous process, and several molecular pathways are involved in this process, including p53, nuclear factor- κ B (NF- κ B), mitogen-activated protein kinase (MAPK), c-jun N-terminal kinase (JNK) and PI3 kinase/Akt [80]. This appearance is mostly accompanied by HBV X protein (HBX) which is the most common ORF integrated into the host genome [81]. HBX is an oncogenic protein with no homology to genes in the human genome [82]. The *HBX*

gene is frequently integrated into the genome, and its transcripts are expressed in many cases of HBV-associated HCC [83-84]. Moreover, several studies have shown that HBX transactivates host genes resulting in deregulation of cell-cycle checkpoints [85-86].

In contrast, HCV infection is less aggressive [79], although there are approximately 170 billion infected individuals worldwide. This infection is characterized by inflammatory lesion in the liver, often accompanied by intrahepatic lipid accumulation and progressive fibrosis [80]. In contrast to HBV, HCV is not able to integrate into its host genome [87], and therefore it is suggested that HCV-mediated hepatocarcinogenesis must involve

several indirect mechanisms including the interplay between chronic inflammation, steatosis, fibrosis and oxidative stress, as well as their pathological consequences (Figure 7) [80].

2.3.2. ALCOHOL-INDUCED HEPATOCARCINOGENESIS

It has been shown that chronic alcohol consumption causes the production of proinflammatory cytokines (including $\text{TNF}\alpha$, $\text{IL-1}\beta$, IL6) and initiates increased concentrations of endotoxins with adverse effects on hepatocyte survival [88-89]. Moreover, hepatocytes show increased sensitivity to the cytotoxic effects of tumor necrosis factor α ($\text{TNF}\alpha$) under alcohol consumption [90] and oxidative stress. These factors promote the developments of fibrosis and cirrhosis which are key features of a permissive HCC microenvironment [79]. The key factor $\text{TNF}\alpha$ is a cytokine involved in

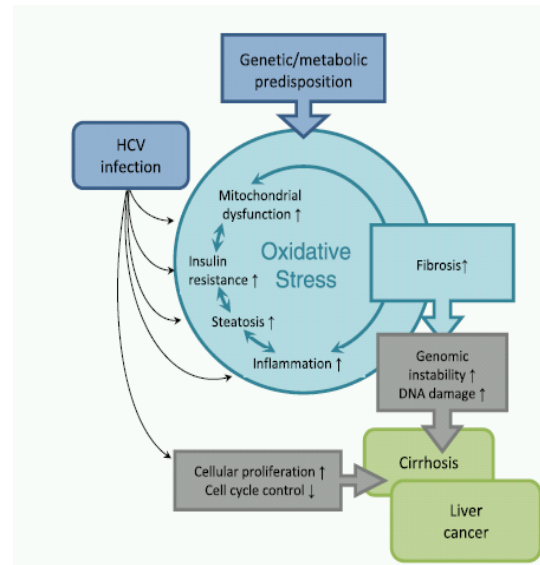


Figure 7: HCV-induced hepatocarcinogenesis [78].

systemic inflammation, has the primary role in the regulation of immune cells and can inhibit tumorigenesis as well as viral replication [91]. It also sets the stage for chronic hepatocyte destruction-regeneration, stellate cell activation, cirrhosis, and ultimately HCC [79].

2.3.3. AFLATOXIN-B1-INDUCED HEPATOCARCINOGENESIS

Aflatoxin B1 (AFB1) (Figure 8) is a fungal toxin naturally produced by many species of *Aspergillus*. AFB1 is metabolized in the liver to an AFB1-8,9-exo-epoxide which forms a promutagenic AFB1-N7-guanine DNA adduct that results in G to T transversion mutations [92]. AFB1-induced HCC is characterized by a specific p53 mutation [93], such as at codon 249 [93], and mutational activation of oncogenes such as *HRAS* [94]. Interestingly, aflatoxin B1 exposure increases the risk of developing HCC by HBV infection by 5-10 fold, although the mechanisms for this synergy are so far unclear [95].

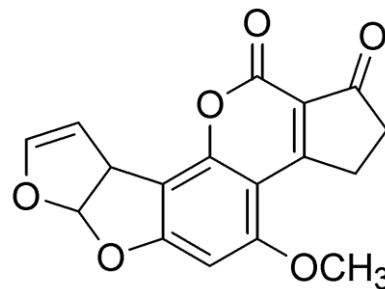


Figure 8: Chemical structure of fungal toxin aflatoxin B1.

In general, the events leading to HCC are accompanied by very typical impact on the genetic alterations of the tumor cells (Table 3) [64]. Some insults can lead to the activation of MAPK pathway or deregulation of some key oncogenes and tumor-suppressor genes, such as *p16 (INK4a)* and E-cadherin. It is widely accepted that the p53 deficiency participates in the development of HCC [79]. Additionally, it was suggested that activation of Wnt signaling plays an early role in hepatocarcinogenesis. **β-catenin** is a downstream component of the Wnt-signaling pathway involved in embryogenesis and cancer. Activated Wnt-signaling induces the stabilization and nuclear translocation of β-catenin leading to transactivation of target genes, including *MYC*, cyclin D1, *COX2*, and matrix metalloproteinase 7 (*MMP7*), which are responsible

for cancer progression [96]. Furthermore, some other oncogenes and signal transductions are also upregulated [97]. For example, the **ErbB** receptors are a family of tyrosine kinase receptors and have been implicated in the development of various cancer types. Several studies have shown that these receptors are overexpressed in HCCs resulting in activation of Akt pathway [90]. Other examples are the overexpression of MET receptor [98] and the specific hypermethylation of *p16(INK4a)* [99], E-cadherin, *COX2* [100], apoptosis-associated speck-like protein (ASC) and deleted in liver cancer 1 (*DLC1*) [97]. Furthermore, HCC can be also induced by genomic instability. These instabilities can be caused by telomere shortening, chromosome segregation defects or mutations in DNA-damage-response pathways [79].

Table 3: Summary of the molecular and genetic mechanisms leading to develop hepatocellular carcinoma [64].

Molecular Event	Comment
Growth factors and receptors:	
EGFR	Overexpression common in chronic hepatitis, fibrosis, cirrhosis, and HCC; known EGFR ligands (EGF, HGF, TGF- β , IGF) mitogenic for hepatocytes and implicated in hepatocarcinogenesis; upregulated HCC cell lines, DN, HCC lesions
ErbB2	Variable (11%-80%) expression in HCC
VEGF	HCC highly vascular tumors; VEGF overexpression in HCC cell lines, DN, tumors; may correlate with tumor invasion and metastases
Intracellular signaling pathways:	MAPK/MEK signaling pathway activated in HCC in vivo model Evidence for role of PKC in HCC is conflicting
Cell cycle control	Cyclin D1 overexpression low to moderate in HCC; cyclin E overexpressed in majority of HCCs and associated with large tumors, poor differentiation, and invasion; may be correlated with p53 mutations Abnormalities in p16/cyclin D1/pRB pathway common in HCC specimens Of the positive cell-cycle regulators, cyclin D1, cyclin A and B1 significantly linked to biologic character of HCC
Oncogenes	No single oncogenes preferentially required for human HCC development; activating mutations seen in <i>ras</i> , <i>Myc</i> , <i>Met</i> , <i>c-fos</i> genes; <i>Ras</i> overexpression in HCC animal model, less so sporadic HCC
Tumor suppressor genes	A variety of p53 aberrations common in HCC (30%-60%); aflatoxin-B-related HCC commonly have consistent codon 249 changes Altered expression of p16, p21, p27 common <i>Rb</i> gene abnormalities seen in 25% HCC
Apoptosis	FAS-Fas-L complex principal component of apoptotic signaling in normal liver; strongly upregulated in chronic hepatitis, cirrhosis; Fas strongly downregulated in HCC
ECM	Genes for ECM and cytoskeleton upregulated early in preneoplastic process; integrins, MMP-14 important

2.4. Cancer Therapies

Several medical therapies are available to treat cancer depending on the type, location and stage of tumor. The most common cancer treatment options are surgery, chemotherapy and radiation therapy, which are used alone or in combination. Additionally, there are also several experimental cancer treatments under development with the aim of specific tumor targeting with less damaging of healthy tissues. The goal of cancer therapy is to reverse the alterations of tumor cells as well as to target them as tumor-specific vulnerabilities, preferably through the combinatorial application of a relatively small number of drugs [12].

Additionally, some carcinomas are hormone-dependent, and based on these characteristics their growth can be prevented through removal or treatment with hormones [101-102]. **Hormone therapy** is frequently used for cancer types derived from hormonally responsive tissues, like breast, prostate, endometrium, and adrenal cortex [6]. Such substances influence the proliferation control of tumor tissues originating from hormone-sensitive tissues [101].

Another treatment option against malignant tumor cells is **radiation therapy**. Ionizing radiation is used in palliative as well as therapeutic settings. Nevertheless, the cellular and molecular changes in cells after radiation are not well understood. It has been shown that DNA is a very sensitive target for radiation, and DNA lesions such as double strand breaks (DSB) can develop chromosomal aberrations blocking cell division [101]. Radiotherapy is frequently combined with surgery, chemotherapy, and hormone therapy.

Furthermore, cancer can be also treated by **immunotherapy**, a method, which aims to stimulate the patient's immune system against tumor cells. For this treatment, therapeutic antibodies, interferons or other cytokines are used, which are normally found in very low concentrations in body [101].

For non-hematological and non-metastatic cancers in early-stage, surgery is often curative. However, late stage disseminated tumors often cannot be cured this way. **Chemotherapy** is a method for systemic treatment of tumor cells using chemicals which mainly target rapidly dividing cells [101]. Consequently, healthy proliferating tissues such as bone marrow and colon are often also affected by these chemicals [6] leading to adverse side effects during therapy. In comparison to chemotherapy, **targeted therapies** are drugs or substances (like imatinib, erlotinib, sunitinib, sorafenib, gefitinib or bortezomib) that block the growth and spread of cancer by interfering with specific molecules involved in tumor growth and progression [60]. However, also in case of these targeted drugs severe side effects are observed due to often unexplored on-target effects against healthy tissues.

Overall, there are diverse types of chemotherapy drugs. Following their mode of action or their chemical structure were classified in alkylating agents, antimetabolites, anti-tumor antibiotics, topoisomerase inhibitors, mitotic inhibitors and corticosteroids.

2.4.1. ALKYLATING AGENTS

The chemotherapeutic alkylating agents exhibit the cytotoxic activity by becoming strong electrophiles through the formation of carbonium ion intermediates or of transition complexes with the target molecules [102]. This involves reactions with guanine in DNA adding methyl or other alkyl groups (C_nH_{2n+1}) at the number 7 nitrogen atom of the imidazole ring. Thus, they inhibit the correct utilization by base pairing and cause disruption of DNA functions, such as inhibition of transcription and translation [103]. This type of anticancer drugs (like cisplatin, BCNU, temozolomid) targets cancer cells based on their higher proliferative rates and deficiency in error-correcting mechanisms. Due to these features, cancer cells are more sensitive to DNA damage in comparison to healthy cells.

There are three mechanisms for alkylating agents (Figure 9) [102]. In the first one, an alkylating agent (such as cobalamin) attaches alkyl groups to DNA bases resulting in DNA fragmentation by repair enzymes in their attempts to replace the alkylated bases. Alkylated bases prevent DNA synthesis and RNA transcription from the affected DNA. In the second mechanism, DNA damages are caused by the formation of cross-bridges. In this process, two bases are linked together by an alkylating agent that has two DNA binding sites, such as BCNU. Bridges can be formed within a single molecule of DNA, or a cross-bridge may connect two different DNA molecules. This cross-linking prevents the separation of DNA strands for synthesis or transcription. The third mechanism is based on the induction of nucleotides leading to mismatches of bases. Following failure of repair mechanisms, such mutations may lead to permanent mutations. An example for such an alkylating agent is MNU.

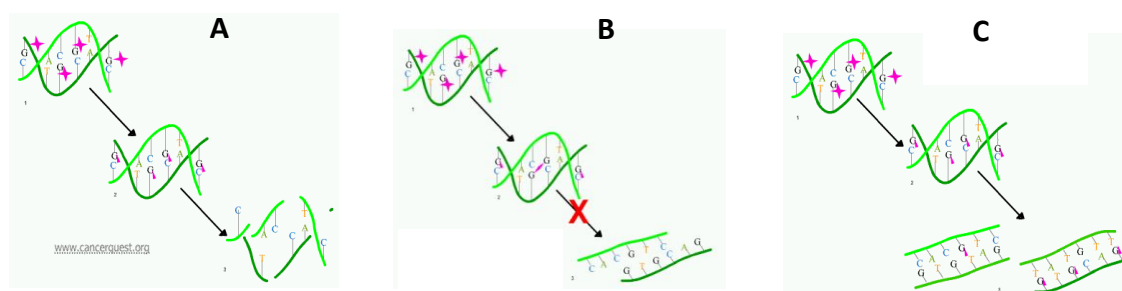


Figure 9: Mechanism of alkylating agents. (A) Fragmentation of DNA, (B) formation of cross-bridges, and (C) mispairing of nucleotides.

2.4.2. ANTIMETABOLITES

These compounds act on tumor cells via interference with DNA and RNA synthesis by substituting for normal nucleic acids leading to stop of cell division and growth of tumors (Source: American Cancer Society). Antimetabolites damage cells during the S phase, and similar to alkylating agents, cancer cells are major targets of these drugs due to their high cell division and proliferation rates [102]. Some examples for antimetabolites are 5FU, gemcitabine and Alimta® (Pemetrexed for injection).

2.4.3. ANTI-TUMOR ANTIBIOTICS AND TOPOISOMERASE INHIBITORS

These agents inhibit cell division by intercalation, DNA strand breaks through a free radical intermediate or by inhibition of the topoisomerase II. Many of the respective compounds are designed to interfere with the topoisomerase enzymes. The key role of topoisomerase enzymes is the control of changes in DNA structure by catalyzing the breaking and rejoining of the phosphodiester backbone of DNA strands during diverse processes including cell cycle. Examples of topoisomerase inhibitors are topotecan, irinotecan and etoposide [101]. *In vitro* studies have shown that such drugs can also induce accumulation of cells in the G₂ phase of the cell cycle displaying chromosomal aberrations, including chromatid breaks, gaps, and fragments, as well as translocations [104]. Most of these substances have been isolated from natural sources and represent antibiotics. Examples for anti-tumor antibiotics are doxorubicin, daunorubicin and actinomycin D.

2.4.4. MITOTIC INHIBITORS

These derivatives from natural substances, such as plant alkaloids, specifically prevent cell division at mitosis. These drugs are cell-cycle-specific agents and work during the M phase [102]. However, they can also damage cells in all cell cycle phases. These agents disrupt microtubule polymerization, which is necessary for division, and lead to cell arrest during metaphase [102]. The inability to segregate chromatids correctly during mitosis consequently leads to cell death. Malignant cells exposed to such drugs undergo changes characteristic for apoptosis [105]. Examples for mitotic inhibitors are taxol, vinblastine and vincristine.

2.5. Ruthenium Drugs

Metallopharmaceuticals are a class of chemotherapeutics, widely used in cancer treatment. Metal compounds came in the focus of interest after discovery of *cis*-diamminedichloroplatinum(II) (cisplatin) by Rosenberg in the 1960s (Figure 10). He discovered that electrolysis of a platinum electrode produces cisplatin which inhibits binary fission in *E.coli* by disrupting of cell division [106-107]. It has been shown that platinum compounds can interact with the plasma membrane [108] and regulatory proteins [109]. However, it is generally accepted that the anticancer activity of platinum complexes arises from their ability to damage DNA by induction of various crosslinking adducts [110]. Moreover, it has been suggested that the effectivity of platinum compounds can underlie the rates of ligand-exchange reactions that are comparable with those of cell-division processes [111]. Antitumor platinum(II) complexes like cisplatin, carboplatin or oxaliplatin, are currently used in the clinic against ovarian and testicular cancer and are highly effective in combination regimens for the treatment of bladder, small cell lung as well as head and neck cancers [112-114]. However, these compounds exhibit several disadvantages. For example, cisplatin displayed limited activity against some of the most common tumors such as colon and breast cancers [115]. Furthermore, it has high systemic toxicity [116], induces a variety of adverse effects [115], and tumor cells frequently develop resistance following the

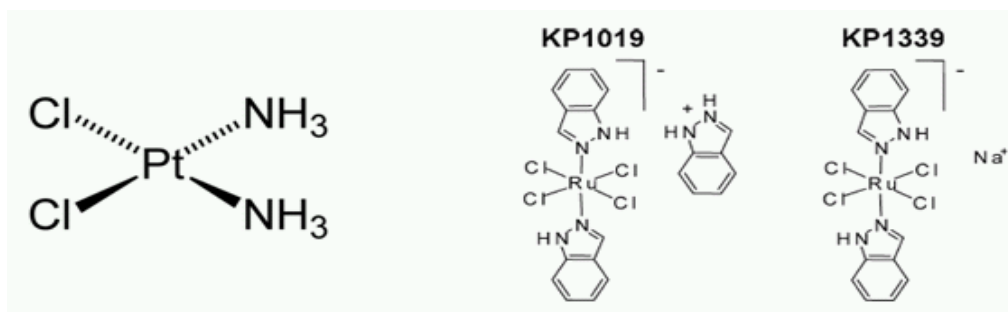


Figure 10: Chemical structures of cisplatin (left), KP1019 (middle), and the analogous salt KP1339 (right).

initial successful treatment [117]. In addition, it has to be administered intravenously due to its limited solubility in water and has severe side effects [113].

Nevertheless, induced by the success of platinum drugs, several novel active antitumor metallodrugs have been synthesized and developed. Ruthenium complexes became interesting candidates for further analysis in middle seventies because of several advantages [118]. For example, ruthenium compounds have shown reduced toxicity and non-cross-resistance in cisplatin-resistant cells [119-120] suggesting that ruthenium compounds have a different mode of action in comparison to platinum complexes [121-122]. Moreover, ruthenium compounds also bind DNA, although much weaker than platinum complexes. Additionally, strong affinity for plasma proteins with a marked preference for surface imidazole groups was discovered [115]. This feature is also expected to be responsible for the tumor selective drug accumulation, which minimizes damages in healthy tissues. Another ability of ruthenium compounds is mimic iron in binding to certain biological molecules like transferrin [123]. Due to this feature of ruthenium compounds, it was hypothesized that they accumulated via transferrin receptor-mediated endocytosis in tumor cells which express a high number of transferrin receptors in order to meet their high iron demand [121, 124]. Moreover, selective toxicity of ruthenium complexes is based on 'activation by reduction' [118]. Tumors utilize more oxygen and other nutrients. Moreover, angiogenesis often fails to keep pace with tumor growth resulting in insufficient blood supply and hypoxia. Thus, hypoxia and higher energy requirements induce lower pH values in tumor tissue [125]. Under these conditions typical for the environment in tumors, Ru(III) is reduced to Ru(II) leading to chemical activation [118].

During last decades, several ruthenium(III) complexes have been developed, and under these complexes some have attracted attention due to their antitumor activities. The first ruthenium drug studied was **ruthenium red**. This drug was found to inhibit *in vivo* tumor growth mainly by impairment of Ca^{++} transport across

mitochondrial and cell membranes [126]. It can also prevent and reduce the anticancer drug cytotoxicity was observed [118]. Another ruthenium-based antitumor drug is imidazolium-*trans*-imidazoledimethyl-sulfoxide-tetrachlororuthenate (**NAMI-A**) representing one of the most studied ruthenium compounds. It was selected because of its very good antimetastatic activity although it had only marginal activity at the primary tumor site [118]. NAMI-A was the first ruthenium drug which has been tested in clinical studies [115].

Among these ruthenium complexes, indazolium *trans*-(tetrachlorobis(1H-indazole)ruthenate(III)) (**KP1019**) and the analog sodium *trans*-(tetrachlorobis(1H-indazole)ruthenate(III)) (**KP1339**) synthesized by Keppler *et al* (Figure 10) belong to the most promising compounds for anticancer treatments [2]. It has been shown that KP1019 and KP1339 are effective tumor-inhibiting drugs in preclinical experiment using autochthonous colorectal carcinomas in rats inducing antineoplastic activity *in vivo* [2, 127], and exhibit moderate cytotoxicity *in vitro* [128]. For example, KP1019 have not shown any symptoms of toxicity as evidenced by 2% body weight gain compared to controls as well as 0% mortality. Generally, the treatment with KP1019 caused not only growth inhibition but also partial remission of established colorectal carcinomas, since the median tumor was decreased by one third in rats [2].

It was suggested that these ruthenium compounds should be taken up into the cells via interaction with transferrin [123, 129-130] and induce apoptotic via the mitochondrial pathway [131-132]. KP1019 has been shown to bind to serum proteins in cell-free experiments, such as albumin [133] as well as apotransferrin [123]. There are two possible mechanisms to explain the apparent tumor selective cytotoxicity of ruthenium compounds such as KP1019: (1) Due to the ability to mimic iron, it can bind to transferrin receptor and might be taken up through endocytosis into the cell in a transferrin-dependent manner. As tumor cells require more iron, KP1019 might accumulate preferentially into the tumor in comparison to healthy cells. (2) KP1019

might serve as prodrug activated by reduction in the environment of tumor tissues leading to the selective cytotoxicity [121, 124].

Moreover, it has been detected that KP1019 induces DNA interstrand and DNA-protein cross-links [119] which are characteristic for many ruthenium and platinum drugs. Interestingly, the binding of KP1019 to serum proteins hampered P-glycoprotein (P-gp)-mediated drug efflux, although cytotoxic effects of KP1019 are not substantially changed by overexpression of drug resistance proteins multidrug resistance-related protein 1, breast cancer resistance protein, and lung resistance protein [134]. P-gp, encoded by the *mdr1* gene, is one of the ABC transporters, which are responsible for the phenomenon of multidrug resistance (MDR). MDR is characterized by a rapidly escalating failure of chemotherapy [135]. This feature makes KP1019 a possible drug for treatment of multidrug-resistant tumor types [134].

KP1019 was tested in a pilot phase I clinical trial. The study was designed as an open-label, dose-escalation trial with an accelerated dose titration in patients with advanced solid tumors without established therapeutic options. Eight patients were selected for the clinical trial and received KP1019 intravenously in doses ranging from 25 to 600 mg twice weekly over three weeks in order to give a dose recommendation for further studies. Disease stabilization has been detected in five of six patients, and two patients dropped out during the study due to adverse events. It has been shown that KP1019 was well tolerated and caused no serious side effects although stabilization of disease [136].

Because of the low water solubility of KP1019 and feasibility problems experienced in clinical trial, KP1339 was selected for further clinical development. KP1339 has a 30-fold more aqueous solubility and has shown similar anticancer activities in the preclinical studies like KP1019.

2.6. Cell Cycle and Cell Cycle Regulation

“Where a cell arises, there must be a previous cell, just as animals can only arise from animals and plants from plants.” After the introduction of cell theory by Theodor Schwann, Matthias Jakob Schleiden and Rudolf Virchow in 1839, this cell doctrine has been widely accepted that cells arise from pre-existing cells, and cell division of these pre-existing cells is the only plausible mechanism to explain this molecular machinery. A cell reproduces by performing an orderly sequence of events in which it duplicates its contents and then divides in two daughter cells [137]. This process is called cell cycle. Although the details of cell cycle vary from organism to organism, certain characteristics are universal and highly conserved throughout evolution.

The eukaryotic cell cycle is traditionally divided into four phases (Figure 11): G_1 , S (synthesis of DNA), G_2 and M (mitosis). G_1 , S, and G_2 together are called interphase. In interphase, cell performs transcription of genes, synthesis of proteins, mass increase and replication of chromosomes. Condensation of replicated chromosomes is the first sign that cell

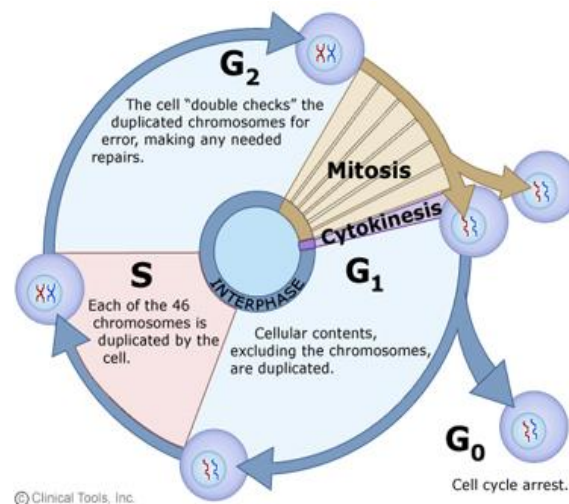


Figure 11: Cell cycle.

is able to enter into the M phase [137]. M phase is also divided in five subphases: prophase, prometaphase, metaphase, anaphase, and telophase. In prophase, chromatin condenses, and chromatids stay connected at the centromere by the cohesion complex. In prometaphase, the nuclear membrane disassembles, and microtubules invade the nuclear space. Furthermore, each chromosome can attach to the spindle microtubule forming two kinetochores at the centromere, one attached at

each chromatid. In metaphase, the metaphase plate is formed by convening the centromeres of chromosomes along this plate. In anaphase, proteins that connect sister chromatids are cleaved allowing them to separate, and the chromosomes move toward the respective centrosomes by shortening of kinetochore microtubules. In telophase, the chromosomes are on the spindle poles, new nuclear membrane is formed, and the division of cytoplasm is initiated [137].

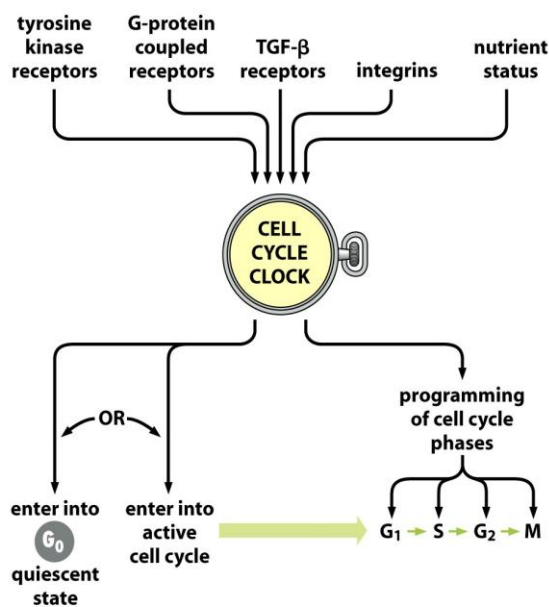


Figure 8-1 The Biology of Cancer (© Garland Science 2007)

Figure 12: The central governor of growth and proliferation: „Cell Cycle Clock“ [2].

A cell that has recently been formed by the processes of cell division (cytogenesis and mitosis) must decide soon thereafter whether it will once again initiate a new round of cell growth and division, or remain into the nongrowing state [4]. The cell cycle clock (Figure 12) apparatus, operating in the cell nucleus, functions as the master controller governing the decision of the cell to proliferate, to enter into reversible quiescence, or to enter into a postmitotic differentiation state [138]. The cell cycle clock is a network of interacting proteins to decide the cell's fate. Therefore, cell cycle machinery needs mitogenic growth factors from the microenvironment and influence this decision strongly [4]. Cell cycle machinery is composed of two major components, cyclin-dependent kinases (CDKs) and cyclins. CDKs phosphorylate target proteins on specific serine or threonine sites underlying regulatory function [138]. Once CDKs are associated with their cyclin partners, cyclin-CDK complexes are able to constitute the engine of the cell cycle clock machinery (Figure 13). Several cyclin-CDK complexes are formed during the cell cycle process. It depends on the levels and availability of cyclins

during various phases of the cell cycle. In contrast, the levels of most CDKs vary only minimally [137]. However, additional levels of control may be superimposed on these complexes [138].

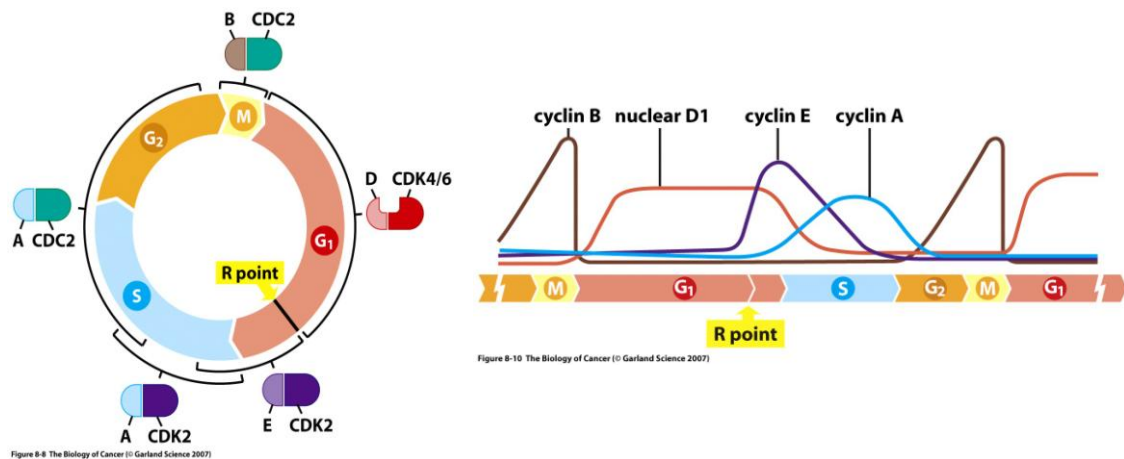


Figure 13: Several cyclin-CDK complexes and their levels during the cell cycle [2].

Arthur Pardee found that cells require growth factor stimulation only during the first two-thirds of their G_1 phase. He has experienced that continuous mitogenic stimulation during this time window allows cells to complete the growth cycle through mitosis in the absence of further exposure to mitogens. This behavior suggests the existence of a decision point at the end of this G_1 which he has called restriction point (R point) [139]. R point decision is the central event in normal cellular proliferation control, and therefore also important for understanding of neoplastic growth deregulation.

In comparison to normal tissues, cancer is a disease of deregulated cell proliferation and survival [140]. These features can be gained by derangement of R point control, mutations by the mechanisms of cell cycle checkpoint, or escape from cell senescence and apoptosis. Cancer cells can induce autocrine production of normally limiting external (paracrine) mitogenic signals [141] due to activation of mitogen receptor tyrosine kinases or G-protein signal transducers such as Ras, or mutations affecting one of the many intermediary signal transducing molecules that convey mitogenic

information to the respective intracellular targets [142]. Cancer cells may also harbor growth-targeting mutations in the late-G₁ cell-cycle checkpoint regulated by phosphorylated retinoblastoma protein (pRB). These alterations include deletion of *RB* gene itself or deregulation of the CDKs that phosphorylate and functionally inactivate pRB [143]. **pRB** serves as the R point switch. In the unphosphorylated or hypophosphorylated state, pRB blocks the R point transition. In phosphorylated state it loses its growth-inhibitory powers and permits cells to enter into late G₁ and furthermore into the remainder of the cell cycle [144]. Another key factor, **Myc**, is a strategic controller of proliferation and is frequently expressed in tumor cells in an uncontrolled manner [145].

Cell-cycle checkpoint refers to mechanisms by which the cell actively halts progression through the cell cycle to ensure that an earlier process, such as DNA replication or mitosis, is complete [146]. Any DNA damages, such as double strand breaks (DSB) caused by free oxygen radicals or ionizing radiation are recognized by several factors or pathways leading to inhibition of cell-cycle progression (Figure 14). Phosphatidylinositol-3-OH kinase (PI3K)-like kinases (PIKKs), ataxia telangiectasia mutated (ATM) and AT- and Rad3-related (ATR) are important components of damage detection [147]. For example, activated ATM phosphorylates p53 leading to stabilisation of p53 [148]. Thus, the binding of p53 to its target sites in the *p21/WAF1* and *GADD45* gene promoter leads to silencing the G₁/s-promoting cyclins and thereby causing G₁ arrest [147].

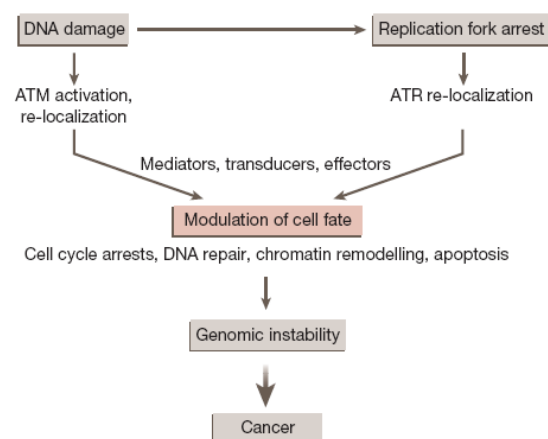


Figure 14: General scheme of responses to DNA damage and replication fork arrest [145].

In S phase, DNA synthesis is also controlled by ATM/ATR signaling machinery [147]. For example, the inhibition of CDK2 activity downstream of this pathway blocks the loading of CDC45 onto chromatin which is required for the recruitment of DNA polymerase α into assembled pre-replication complexes. Thus, the inhibition of CDK2 activity prevents the initiation of new origin firing [149-150]. Furthermore, in G2 checkpoint the critical target is cyclin B/CDK1 kinase whose activation can be inhibited by ATM/ATR, CHK1/CHK2 or p38-kinase. This mediates subcellular sequestration, degradation or inhibition of the CDC25 family of phosphatases responsible for the G₂/M boundary progression [151-154].

Cancer cells can circumvent senescence and apoptosis can be solved by several mutations or deregulations. For example, activation of oncogenes through mutations might play a role, such as *ras* to elicit cell senescence [155-156] and *myc* to escape from apoptosis [157-158]. The senescence response mechanism appears closely tied to the actions of cdk inhibitor, like p16^{INK4A} and p21. Loss of p53 disrupts activation of p21 for inducing senescence and proteins like Bax that are important for triggering apoptosis [138]. Moreover, the inactivation of p19^{ARF} and p53 allows cells to escape from apoptosis due to some possible protection against it [154]. Therefore, p53 plays a key role in tumorigenesis by several mechanisms (Figure 15). Thus, it is termed the “guardian of the genome” in normal cells [159].

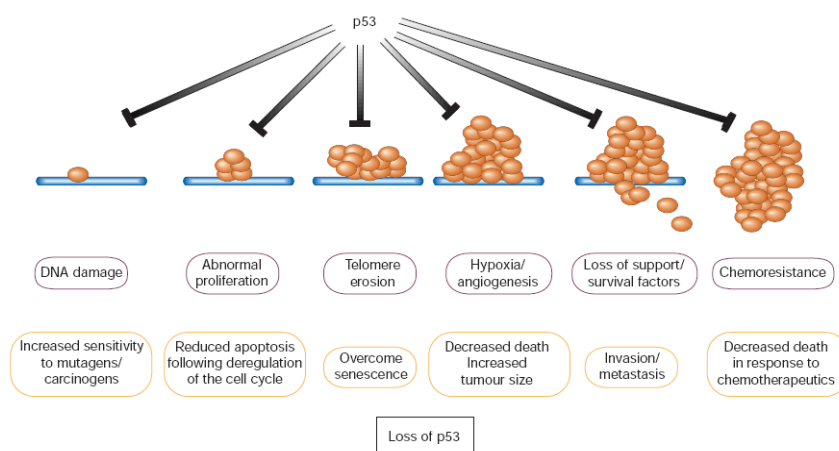


Figure 15: Activities of p53 resulting apoptosis and growth arrest [138].

2.7. Programmed Cell Death (Apoptosis, Autophagy, and Necrosis)

Apoptosis is a physiological cell death program that plays fundamental roles during embryonic development and in the maintenance of tissues by controlling normal cell homeostasis [160-161]. The first observations about this phenomenon was described by Galen, although he did not directly address cell death. He reported the transitional state of the fetal arterial duct allowing the direct circulation of blood from the pulmonary artery to the aorta while bypassing the fetal lung. This disappearance could be explained based on the identification of cells by Schleiden and Schwann in 1839 [162]. First, Vogt has described cell death in 1842 on amphibian metamorphosis, and it was officially recognized in 1871 as both a pathological and physiological process [163]. Furthermore, in 1972, Kerr *et al.* forwarded a theory of cell death defining necrosis and apoptosis. They have defined necrosis as a „violent“ form of cell death initiated by environmental stimuli and resulting in the rapid disruption of cellular homeostasis, and apoptosis as an alternative, programmed form of cell death [20].

In 1990, Clarke has classified programmed cell death (PCD) according to lysosomal involvement [164]. After Clarke's model, apoptosis was called type I PCD which is marked by cell shrinkage, oligonucleosomal DNA fragmentation, chromatin condensation leading to the appearance of apoptotic bodies and involving heterophagocytosis [165]. By contrast, another form of PCD, described as type II PCD or autophagy, is characterized by the formation of autophagic vacuoles, as well as by the dilation of the mitochondria and the endoplasmic reticulum (ER) and the slight enlargement of the Golgi [162]. Furthermore, these double-membraned autophagic vesicles fuse with lysosomes for degradation. However, in necrosis or type III PCD no lysosomes were found. In this form of PCD the intracellular organelles swell, the plasma membrane breaks down, and the cytoplasm is disintegrated.

One of the best characterized PCD mechanism is the mitochondria-mediated apoptosis. Mitochondrion is a membrane-enclosed organelle found in most eukaryotic cells [166]. It is responsible for generation of chemical energy by supplying of adenosine triphosphate (ATP), and involved in a range of other processes, such as signalling, cellular differentiation, cell death, as well as the control of cell cycle and cell growth [167]. Moreover, mitochondria are characterized by an outer and an inner membrane separated by an intermembrane space. The intermembrane space plays key role in releasing of proteins involved in cell death induction. These intermembrane space proteins include caspase-independent death effectors as nucleases and/or proteases, as well as caspase activators [162].

Apoptosis can be induced through two separable pathways leading to caspase activation [168-169] (Figure 16). The extrinsic pathway is initiated by ligands of transmembrane death receptors, such as CD95, TNF and TRAIL receptor, to activate membrane-proximal (activator) caspases (caspase 8 and 10), which in turn cleave and activate effector caspases such as caspase 3 and 7. In contrast, the intrinsic pathway requires disruption of the mitochondrial membrane and the release of mitochondrial proteins including Smac/DIABLO, HtrA2, and cytochrome c [160]. The initiation of apoptosis in this pathway is dependent on the balance between proapoptotic and prosurvival Bcl-2 family proteins [170]. In response to apoptotic stimuli, a subgroup of Bcl-2 family, BH3-only proteins such as Bim, Bid and Bad, are activated. These proteins promote oligomerization of Bax/Bak, permeabilization of the mitochondrial outer membrane and release of factors from IMS. The most important factor releasing from intermembrane space is cytochrome c. Cytochrome c in the cytoplasm forms complexes with apoptosis protease-activating factor 1 (Apaf-1), dATP, and procaspase 9 [171-174]. Apaf-1 recruits the zygomic form of caspase 9 and forms the apoptosome, which leads to dimerization-induced activation of caspase 9. Caspase 9 in turn cleaves other effector caspases [175]. A proteolytic cascade is then initiated

With respect to cytochrome c release, loss of transmembrane potential is a major determinant for induction of cell death. The transmembrane potential is essential for cellular viability. Due to this potential, the ATP production through ATP synthase across the inner membrane is enabled. This process is responsible for the supply of cellular energy. Therefore, the disruption of the transmembrane potential leads to alterations and defects in mitochondrial respiration, energy production, and cell survival [162].

Additionally, the escape of an electron from the mitochondrial electron transport chain can cause the reaction with molecular oxygen leading to production of oxygen radicals. These radicals are normally converted into the hydrogen peroxide or other reactive oxygen species (ROS). High intracellular ROS levels cause significant damages, such as lipid peroxidation or DNA damage [183]. These processes can also introduce damages in the mitochondrial membrane resulting in release of cytochrome c [184]. Cytochrome c plays normally a key role in the generation of ATP via the electron transport chain. Thus, minor alterations or damages in mitochondrial respiration may be amplified rapidly leading to cell death [162].

Interestingly, cancer cells are characterized by increased respiration even under high levels of oxidative stress. This appearance can be caused by the frequently hyperpolarized intermembrane of their mitochondria leading to higher degree of ROS generation and an increased sensitivity to inhibitors of ROS elimination [185]. Furthermore, some tumor cells with postmitochondrial defects are able to survive chemotherapy. Even in the absence of downstream caspase activation, damage to the mitochondrial membrane and release of cytochrome c still disrupts the electron transport chain and enhances ROS production [160]. However, it was shown that mitochondria can restore transmembrane potential and maintain ATP production [186]. This might be explained by two possible mechanisms. It may occur either 1) through relocalization of cytoplasmic cytochrome c back into the mitochondria or 2)

through rapidly recovery of cytochrome c [160]. Interestingly, the capacity of some tumor cells to tolerate mitochondrial dysfunction may be because they frequently express elevated levels of antioxidants [187]. Moreover, tumor cells are often growing in glycolytic conditions and therefore rely less on oxidative phosphorylation than normal cells [188].

3. AIM OF THE STUDY

Metal compounds belong to the most important chemotherapeutics for the treatment of human malignancies at the disseminated stage. Besides platinum-containing drugs, especially ruthenium compounds such as KP1019/KP1339 are very promising candidate in the development of new cancer therapeutics. Recently, KP1019 containing an indazolium counter ion demonstrated exciting anti-cancer activity in a clinical phase I study with low side effects. However, based on the relatively low water solubility large infusion volumes were necessary in this clinical trial. Consequently, the better water soluble sodium salt of trans-[tetrachlorobis(1H-indazole)ruthenate(III)] (KP1339) got in the focus of interest.

The aim of the here presented study was

- 1) To investigate the anti-cancer activity and the mode of action of KP1339 and compare its anti-tumor potential with its precursor drug KP1019. To this end, several analyzes regarding cytotoxicity, drug accumulation, intracellular drug distribution as well as cell death induction were performed.
- 2) To gain more insights into the interaction of KP1339 with the cellular iron homeostasis. Consequently, KP1339 was combined with compounds which are known for their effects on the cellular redox and iron balance.
- 3) To test the efficacy of KP1339 in combination with several clinically used classical chemotherapeutics as well as new tyrosine kinase inhibitors. The most promising combination, namely KP1339 with sorafenib, was then further analyzed for the underlying mechanisms with respect to drug accumulation, cell death induction, and its effects on the cell cycle distribution.

4. MATERIALS AND METHODS

4.1. Cell culture

The cells were maintained in a humidified atmosphere of 5% CO₂ at 37°C using different growth media supplemented with 10% FCS (compare Table 5). The list of used cell lines and their most important genetic alterations are also shown in Table 5.

4.2. Drugs

KP1019, as previously published [189], KP1339, KP46, oxaliplatin, and cisplatin were synthesized at the Institute of Inorganic Chemistry, University of Vienna. All the other drugs and reagents were purchased from Sigma Aldrich (St. Louis, USA) and LC laboratories (Woburn, USA) (Table 4). Final DMSO concentrations were always below 1%.

Table 4: List of used drugs and reagents. IIC... Institute of Inorganic Chemistry, University of Vienna.

Drugs / Reagents	Specification	Solvent	Source
KP1019	Ruthenium drug	DMSO	IIC
KP1339	Ruthenium drug	DMSO	IIC
FeCl₃	-	H ₂ O	Sigma Aldrich
Gallium nitrate	-	H ₂ O	Sigma Aldrich
Adriamycin	DNA intercalating agent, Topo II inhibitor	0.9 % NaCl	Sigma Aldrich
Ara-C	Anti-metabolite	Serum-free medium	Sigma Aldrich
Temozolomid	Alkylating agent	Serum-free medium	Asca
Triapine	Ribonucleotide-reductase inhibitor	DMSO	IIC
Taxol	Microtubuli stabilisation	DMSO	Sigma Aldrich
Vinblastine	Tubulin binding, inhibition of microtubules	0.9% NaCl	Sigma Aldrich
Sorafenib	Tyrosine kinase inhibitor	DMSO	LC Laboratories

Table 5: List of used cell lines and their growth medium. SCC... Squamous cervix carcinoma, HCC... Hepatocellular carcinoma, NSLC... Non-small lung carcinoma, ICR... Institute of Cancer Research, Vienna. HBV... Hepatitis B virus

Cell line	Tissue	Growth medium	Specification	Source
Hep3B	HCC	RPMI 1640	HBV, p53-, cox-2+, EGFR++, ERB2-, Erb3-, ERB4-, all ras wt	ATCC
HepG2	HCC	MEME + 0.2% Na-pyruvate + 1% non essential amino acids (NEAA)	p53+, P-gp+, triglyceride lipase active, 3-hydroxy-3-methylglutaryl CoA reductase active, N-ras mut (Codon-61), c-myc+, K/H-ras wt, cox-2+, EGFR-, ERB2+, ERB3++, ERB4-, Aurora A/B+, increased Aurora B activity	ATCC
HCC1.1	HCC	RPMI 1640	Fibrosis, EGFR+, ERB2-, ERB3-, ERB4-, all ras wt	ICR
HCC1.2	HCC	RPMI 1640	Fibrosis, EGFR+, ERB2++, ERB3++, ERB4-, all ras wt	ICR
KB-3-1 (HeLa)	Cervix carcinoma	RPMI 1640	p53 and Rb downregulated by HPV18	W. Shen, BETHESDA, USA
VL-8	SCC	RPMI 1640	Ras wt	ICR
A549	NSLC, Adenocarcinoma	RPMI 1640	p53 wt, Ras mutated (hom)	ATCC
Calu-6	NSLC, Adenocarcinoma	MEME + 0.2% Na-pyruvate + 1% non essential amino acids (NEAA)	Ras (mut +/-), p53 (mut -/-), EGFR wt	ATCC
VM-1	Melanome	RPMI 1640	lymphnode metastasis, b-Raf mut (het?), N-ras wt	ICR
VM-48	Melanome	RPMI 1640	Brain metastasis, b-Raf mut (hom), N-ras wt	ICR
B1	HCC	RPMI 1640		
HCC2	HCC	RPMI 1640	Cirrhosis, EGFR-, ERB2-, ERB3++, ERB4+, all ras wt	ICR
HCC3	HCC	RPMI 1640	Cirrhosis, EGFR+, ERB2-, ERB3+, ERB4-, all ras wt	ICR
A427	NSLC, Adenocarcinoma	MEME + 0.2% Na-pyruvate + 1% non essential amino acids (NEAA)	Ras (mut +/-), p53 wt, EGFR wt	ATCC
SW480	Colorectal carcinoma	MEME	p53mut, Pgp+, myc+, mycb+, k-ras mut, h-ras mut, Fos+, SIS+, Src-, N-ras (nd), EGFR+, Her2 -	ATCC
HCT116	Colorectal carcinoma	McCoy	p53+, MMR-, k-Ras mut (codon13), EGFR+, Her2-	B. Vogelstein, John Hopkins University, Baltimore
VM-21	Melanome	RPMI 1640	b-Raf mut (hom), N-ras wt	

4.3. Cell Proliferation and Cell Vitality Assays

4.3.1. CYTOTOXICITY ASSAYS

Background:

The MTT assay is a standard colorimetric assay for measuring the activity of enzymes that reduce 3-(4,5-Dimethylthiazol-2-yl)-2,5-diphenyltetrazolium bromide (MTT) to formazan giving a purple color. In cell vitality assays, MTT is reduced by mitochondrial reductase causing the typical colorimetric reaction (Figure 17). This colorimetric reaction can be measured at a wavelength (450 and 620 nm) by a spectrophotometer, and the cytotoxic effects of drugs on the cell number can be examined due to the ratio of viable and dead cells. MTT assays are widely used to determine the cytotoxic activity of drugs and drug combinations.

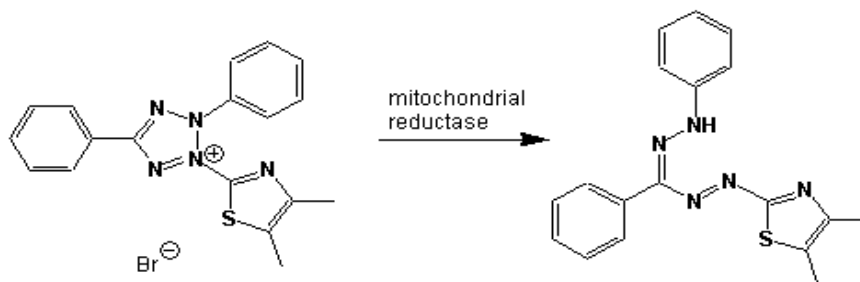


Figure 17: The reduction of 3-(4,5-Dimethylthiazol-2-yl)-2,5-diphenyltetrazolium bromide (MTT) by mitochondrial reductase to formazan.

In combination tests, the complementary cytotoxicity of both drugs was determined. Modes of interactions between drugs were classified as synergism, additivism or antagonism [190-191]. Drug **synergism** occurs when drugs can interact in ways that enhance or magnify one or more effects, or side effects, of those drugs. **Additivism** is another variant of interpretation of drug treatment calculated the sample sum of drug cytotoxicities. In comparison to these, **antagonism** defines the reduction of overall drug effectivity, if they are used in combination with each other.

Preparation:

Cells were plated ($2-3 \times 10^3$ cells in 100 μ l growth medium per well) in 96-well plates and allowed to recover for 24 hours. Drugs were added in other 100 μ l growth medium, and cells were exposed for other 72 hours. After drug exposure, the proportion of viable cells was determined by MTT assay following the manufacturer's procedure (EZ4U, Biomedica, Vienna, Austria). After incubation for 2-5 hours (depending on the metabolic capacity of the cells in the control wells) plates were gently shaken before extinction measurement at 450 nm. 620 nm was used as reference wavelength. Cytotoxicity was expressed as IC_{50} values calculated by software GraphPad Prism 5.0 from dose-response curves (drug concentrations inducing a 50% reduction of cell survival in comparison with the control cultured in parallel without drugs).

4.3.2. DNA SYNTHESIS ANALYSIS BY 3H -THYMIDINE INCORPORATION ASSAY**Background:**

Thymidine (Figure 18) is a pyrimidine deoxynucleoside which pairs with deoxyadenosine in double stranded DNA. In its composition, deoxythymidine is a nucleoside composed of deoxyribose joined to the pyrimidine base thymine. Tritiated thymidine (3H -Thymidine) is commonly used in cell proliferation assays. During S phase, thymidine is incorporated into the DNA of dividing cells, and after cell lysis the level of incorporation and accordingly radioactivity can be measured using scintillator solution via a liquid scintillation counter. This analysis is based on the measurement of fluorescence level of a transparent crystal (usually phosphor or organic liquid) which fluoresces when struck by ionizing radiation. In

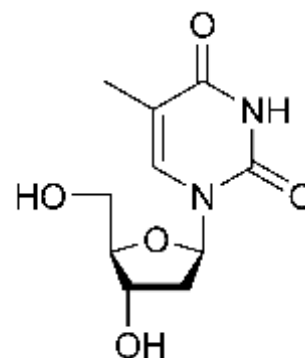


Figure 18: Chemical structure of thymidine, also called deoxythymidine.

contrast to MTT assay, which determines cell viability, the level of ^3H -thymidine incorporation is proportional to the DNA-synthesis rate.

Preparation:

Cells were plated (5×10^4 cells in 100 μl growth medium per well) in 96-well plates. After recovery for 24 hours, drugs were added. To determine the effects of our test drugs on DNA-synthesis rate, test solutions were replaced with 100 μl of a 2 nM ^3H -thymidine solution (GE Healthcare). Cells were incubated for 1 hour at 37°C. Then, cells were washed three times with 100 μl PBS. After washing, the cells were lysed in 100 μl lysis buffer for ^3H -thymidine incorporation. Subsequently, cell lysates were transferred into scintillator tubes. The 96-wells were washed again with 100 μl PBS, and this PBS was also transferred to the cell lysates. After adding of 2 ml scintillator solution into each tube, the samples were mixed by turning up side down. The radioactivity was measured with liquid scintillation analyser Tri-Carb 1900TR (Packard). Radioactivity was expressed as IC_{50} values calculated by software GraphPad Prism 5.0 from dose-response curves (drug concentrations inducing a 50% reduction of cellular thymidine incorporation in comparison with the control cultured in parallel without drugs).

Receipts:

10x PBS:

95 g 0.53 M $\text{Na}_2\text{HPO}_4 \times 2 \text{H}_2\text{O}$
32 g 0.23 M $\text{NaH}_2\text{PO}_4 \times \text{H}_2\text{O}$
44 g 0.75 M NaCl
 Σ 1 l ddH₂O

Lysis buffer for ^3H -thymidine incorporation:

10 mM Tris-HCl, pH= 7.8
1% SDS
 Σ 1 l ddH₂O

4.3.3. DAPI STAINING

Background:

4',6-diamidino-2-phenylindole (DAPI) (Figure 19) is a fluorescent nuclear stain that intercalates strongly to DNA. It associates with the minor groove of double strand DNA, preferentially binding to AT clusters. DAPI can pass through an intact cell membrane, and viable as well as fixed cells can be analyzed using fluorescence microscopy. When bound to double-stranded DNA the absorption maximum of DAPI is at 358 nm and its emission maximum at 461 nm. DAPI binds also to RNA, but the resulting fluorescence is not as strong as when DAPI is bound to DNA. Using DAPI DNA can be stained, and informations on nuclear morphology, apoptosis and necrosis induction as well as cell division can be gained.

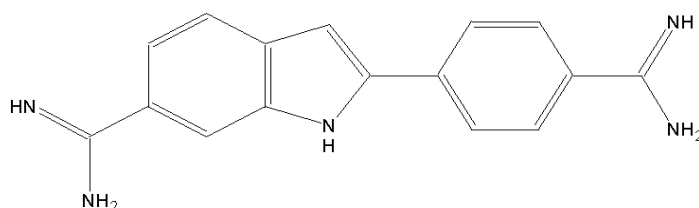


Figure 19: Chemical structure of 4',6-diamidino-2-phenylindole (DAPI).

Preparation:

Cells were plated in 6-well plates (2×10^5 cells in 2ml growth medium per well) and allowed to recover for 24 hours. After recovery the cells were treated with test drugs. After drug exposure, cells were collected by trypsinisation, washed once with PBS, and centrifuged (5 minutes, 1100 rpm). The pellet was resuspended in 300 μ l PBS. For each sample two slides were prepared, and cytopspins were performed. The slides were mounted with the paper pad and the cuvette in the metal holder and placed in the cytocentrifuge. 50-75 μ l of each sample were aliquoted into the appropriate wells of the cytopspin. The cells were cytopspined, fixed using a 1:1 methanol-aceton solution for

10 minutes and stained with DAPI containing antifade solution (Vector Laboratories, Inc., Burlingame, CA). Nuclear morphology was examined using a Leica DMRXA fluorescence microscope (Leica Microscopy and System, Wetzlar, Germany) equipped with appropriate epifluorescence filters and a COHU charge-coupled device camera.

4.4. Flow Cytometry

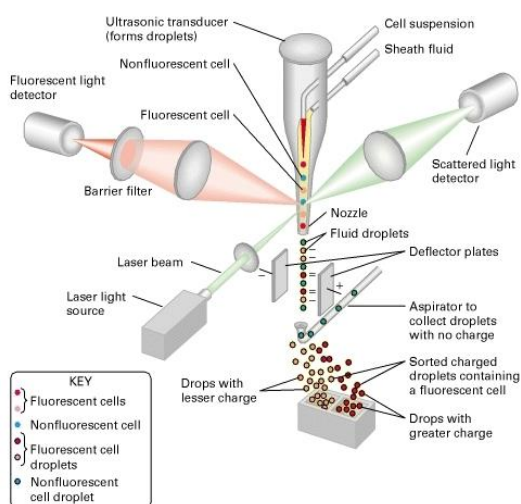


Figure 20: A functional diagram of flow cytometry.

Flow cytometry is a technique for counting and examining microscopic particles, such as cells and chromosomes, by suspending them in a stream of fluid and passing them by an electronic detection apparatus (Figure 20). Samples can be stained with a fluorescent antibody or dye. Using this method, analysis about cell cycle, mitochondrial membrane potential or proteins on cell surface or can be performed.

4.4.1. CELL CYCLE ANALYSIS BY PI STAINING

Background:

Propidium iodide (PI) is an intercalating agent and is able to fluoresce after excitation with 488 nm (Figure 21). PI binds with little or no sequence preference to DNA at a stoichiometry of one dye per 4-5 base pairs. PI is frequently used for the analysis of cell cycle distribution via flow cytometry (Figure 22).

During cell cycle, normal diploid cells run through four stages: G_0/G_1 , S, G_2 and M phase. G_0 is the post-mitotic phase, and nonproliferative cells enter this quiescent state. G_1 is the first phase within interphase providing basis for cell duplication with high biosynthetic activities but the amount of DNA is still $2n$. DNA replication starts at the beginning of S phase, and at the end of

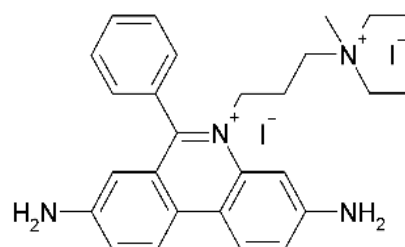


Figure 21: Chemical structure of intercalating agent propidium iodide (PI).

this phase the DNA amount has changed from $2n$ to $4n$. Significant protein synthesis and production of microtubules required for mitosis occurs in G_2 phase. In G_2 , the cell ensures if DNA replication is complete and without any errors before entering M phase. Following to G_2 the cells enter M phase involving cell division.

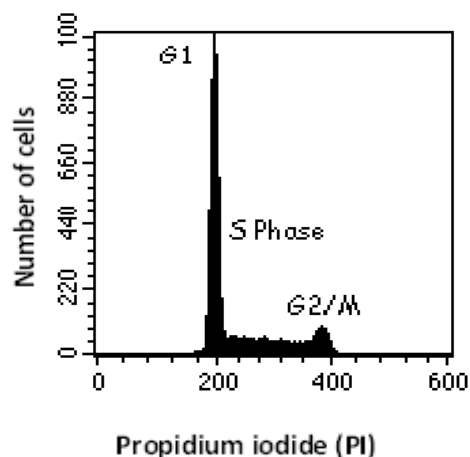


Figure 22: DNA histogram using PI staining.

The levels of PI-fluorescence directly correlate with the DNA content which changes during phases of cell cycle. As shown in Figure 21, cells in G_0/G_1 phase show a distinct $2n$ peak. The height of peaks is dependent on the number of cells. In comparison to this, no peak can be detected by cells in S phase where DNA replication starts, and therefore the level of fluorescence increases. However, in G_2/M phase cells are $4n$ causing the highest fluorescence level because of the large amount of DNA.

Preparation:

Cells were seeded (5×10^5 cells in 2 ml growth medium per well) in 6-well plates and treated with drug after 24 hours recovery. Then, cells were collected by trypsinisation and washed once with FACS-PBS. The all pellets were resuspended in 100 μ l 0.9% NaCl and dropped slowly into 70% ice-cold ethanol. Due to the treatment with NaCl and ethanol, cell membranes become permeabilized, and PI can diffuse into the cell intercalating into DNA. After at least 1 hour incubation at -20°C , cells were centrifuged again (1 minute, 8000 rpm) and resuspended in 1 ml FACS-PBS. 0.79 Kunitz units/ml RNase A were added, and samples were incubated at 37°C for 30 minutes. Cells were filtrated into FACS tubes, stained with 1 mg/ml of PI for another 30 minutes at 4°C , and fluorescence was measured by flow cytometry (FACS Calibur – Becton Dickinson, Palo Alto, CA) using Cell Quest Pro software.

Receipts:**FACS-PBS:**11.5 g Na₂PO₄ x 2 H₂O2 g KH₂PO₄

2 g KCl

80 g NaCl

Σ 1 l ddH₂O**4.4.2. MITOCHONDRIAL MEMBRANE POTENTIAL DETECTIONS BY JC-1 STAINING****Background:**

JC-1 (5,5',6,6'-tetrachloro-1,1',3,3'-tetraethyl-benzimidazolocarbo-cyanine iodide) is a dual-emission potential-sensitive probe that can be used to measure mitochondrial membrane potential. At low membrane potential e.g. in cytoplasm, JC-1 (Figure 23) is a green-

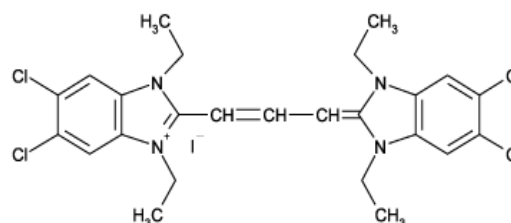


Figure 23: Chemical structure of JC-1 (5,5',6,6'-tetrachloro-1,1',3,3'-tetraethyl-benzimidazolocarbo-cyanine iodide).

fluorescent monomer. At higher mitochondrial potentials, typical in healthy mitochondria, JC-1 forms red-fluorescent “J-aggregates”. If the mitochondrial membrane depolarization occurs, mitochondria are unable to build polymers leading to loss of red-fluorescent. Underlying these features, fluorescent signals can be measured using FACS. The ratio of red to green fluorescence of JC-1 is dependent only on membrane potential, and not influenced by mitochondrial size, shape, or density.

Preparation:

Cells were seeded (1x10⁶ cells in 5 ml growth medium per T25 cm² culture flask) and treated with the test compounds after 24 hours recovery. Following drug exposure, cells were collected by trypsinisation and washed once with ice-cold FACS-PBS. The cells were resuspended in 1 ml JC-1 solution (10 µg/ml in DMSO) and incubated for 10

minutes at 37°C. After incubation, cells were centrifuged (5 minutes, 1200 rpm). The pellet was washed again with FACS-PBS, and resuspended in 1 ml FACS-PBS, and cells were filtrated into FACS tubes. The samples were analyzed by flow cytometry using Calibur (Becton Dickinson, Palo Alto, CA).

4.5. Drug Accumulation Assays

INDUCTIVELY-COUPLED PLASMA-MASS SPECTROSCOPY (ICP-MS)

Inductively-coupled plasma-mass spectrometry (ICP-MS) is a type of mass spectrometry designed for the determination of a range of metal and several non-metals. This analysis method is based on the ionization of the metals in the sample in argon plasma at ~10000 Kelvin followed by a mass spectrometer for their separation and detection. The ions are separated based on their mass-to charge ratio, and the detector receives an ion signal proportional to the concentration of this ion. This very sensitive method allows the exact quantification of metal contents in liquid and solid samples.

4.5.1. TOTAL DRUG ACCUMULATION

Preparation:

Cells were plated ($1-2 \times 10^5$ cells in 2 ml growth medium per well) in 6-well plates and were exposed after 24 hours recovery with the test drug. After 1 hour drug exposure, cells were washed with ice-cold PBS and lysed by 400 μ l tetramethylammonium hydroxide (TMAH). After adding 1.6 ml 0.6 N HNO₃, the lysates were filled up with ddH₂O to 25 ml. To determine the unspecific binding of ruthenium to cell culture flask plastic, a blank well containing only growth medium and drug was also prepared. The ruthenium concentrations were determined by inductively-coupled plasma mass spectrometry (ICP-MS) using an Elan 6100 (Perkin-Elmer/Sciex Corporation) at the Institute for Geology, University of Vienna.

4.5.2. DRUG LEVELS IN CELL FRACTIONS

Preparation:

Cells were seeded (1×10^6 in 5 ml growth medium per T25 cm² culture flask or 1×10^7 in 20 ml growth medium per T150cm² culture flask) and allowed to recover for 24 hours. Drugs were added, and after drug exposure 1 ml from cell culture medium was stored at -80°C for determination of drug concentration in medium. Cells were collected by trypsinisation and washed twice with ice-cold PBS. Cells were counted microscopically and lysed in lysis buffer for cell fractionation. Total cell lysis was checked immediately microscopically by trypan blue staining. Cell lysates were centrifuged (5 minutes, 14000 rpm, 4°C). Supernatants (cytosolic fractions) were aliquoted in 500 µl eppendorf tubes, and pellets (nucleic fractions) as well as supernatants (containing protein lysates) were stored at -80°C. The samples were analyzed by size exclusion chromatography combined with ICP-MS (SEC-ICP-MS) using ELAN DRC-II (PE SCIEX, Ontario, Canada) at the Institute of Analytical Chemistry; BOKU, Vienna. Moreover, protein concentrations of cytosolic fractions were determined using by Micro BCA™ Protein Assay Reagent Kit (Pierce Biotechnology, Rockford, USA).

Receipts:

Lysis buffer for cell fractionation:

500 µl lysis buffer

0.5% Triton X-100

10 µl/ml phenylmethanesulphonylfluoride (PMSF) –serine protease inhibitor, Roche-

25 µl/ml Complete (protease inhibitor cocktail tablets, Roche)

4.5.3. INCORPORATION OF DRUGS INTO DNA

Preparation:

Cells were seeded (1×10^6 cells in 5 ml growth medium per T25 cm² culture flask) and allowed to recover overnight. Then, drugs were added, and after drug exposure cells

were collected by trypsinisation. Following washing with PBS, cells were lysed in 400 μ l DNA lysis buffer and incubated for 15 minutes at -20°C . 1.58 Kunitz units/ml RNase A were added. After 1 hour at 37°C , 15 mg/ml Proteinase K were added and incubated for 24 hours at 37°C . 400 μ l phenol/chloroform/isoamylalcohol solution (25:24:1) were added, the solution was centrifuged (5 minutes, 12000 rpm). The supernatant was transferred in an eppendorf tube and washed twice with 400 μ l chloroform/isoamylalcohol (24:1). The supernatant was transferred again into a new eppendorf tube. Then, 40 μ l Na-acetat were added and followed by 1 ml 100% ethanol. The solution was mixed and allowed to precipitate for 20 minutes on ice. Cells were centrifuged (15 minutes, 15000 rpm), and the supernatant was removed. The pellet was resuspended in 100 μ l ddH₂O, DNA concentrations were measured using NanoDrop Spectrophotometer ND-1000 (PepLab Biotechnology GmbH, Germany). After adding 1.6 ml 0.6 N HNO₃, the DNA samples were filled up with ddH₂O to 25 ml. The ruthenium concentrations were determined by ICP-MS using an Elan 6100 (Perkin-Elmer/Sciex Corporation) at the Institute for Geology, University of Vienna.

Receipts:

DNA lysis buffer:

1 ml 0.5 M EDTA
2.5 ml 1 M Tris-HCl, pH= 8
5 ml 5% Sarcosin
 Σ 50 ml ddH₂O

4.6. Protein analysis

4.6.1. PROTEIN EXTRACTION

Preparation:

Cells were plated ($3\text{-}5 \times 10^5$ cells in 2 ml growth medium per well) in 6-well plates and allowed to recover for 24 hours. After drug exposure, cells were collected by scratching. After washing with PBS, cells were lysed in lysis buffer for total protein extraction and were incubated for 10 minutes on ice. Subsequently, the lysates were treated with ultrasound for 3 minutes and centrifuged for another 15 minutes (14000 rpm, 4°C). Supernatants (protein lysates) were collected, and the protein concentrations were determined by using Micro BCA™ Protein Assay Reagent Kit (Pierce Biotechnology, Rockford, USA).

Receipts:

Lysis buffer for total protein extraction:

500 µl lysis buffer

5 µl phenylmethanesulphonylfluoride (PMSF) –serine protease inhibitor, Roche-

12.5 µl Complete (protease inhibitor cocktail tablets, Roche)

25 µl PhosSTOP (phosphatase inhibitor cocktail tablets, Roche)

4.6.2. WESTERN BLOT ANALYSIS

Background:

Western Blot is an analytical technique developed to detect specific proteins in a given sample using electric current to protein-separation. For this method, the proteins are denatured in SDS-containing lysis buffer for protein extraction. SDS is an anionic detergent that binds most proteins and unfolds them. SDS masks also the native charge of the proteins, so that all proteins have the same charge to mass ratio and the same shape. So, it is gained that the samples are separated only due their molecular

weight. Additionally, samples are often treated to 95°C in mercaptoethanol-containing loading buffer. Protein denaturation means that the secondary and tertiary structures are destroyed leaving only peptide bonds between the amino acids are intact. The sample proteins are then separated by gel electrophoresis due to protein size and electrophoretic mobilities. In our study, SDS-PAGE protein electrophoresis, a system consisting two different polyacrylamide gels, a collecting and a separating gel, have been used. In the collecting gel, the denatured proteins become sandwiched into very thin, sharp bands before entering the separating gel, the samples are fractionated by size. The two gels differ mainly in their amount of acrylamide which leads to different size of pores in the gel. The separating gel has a higher percentage of polyacrylamide compared to collecting gel allowing a better separation of proteins. Additionally, these two gels have different pH values. In course of electrophoresis, the chloride and glycinate ions from the electrode buffer migrate through the collecting gel. Because of the pH value of this gel (pH= 6.8), glycine molecules are zwitterionic and their mobility is very low. In comparison to that, chloride ions have a much higher mobility and migrate in front. Thus, the mobility of proteins is between these two ions, and the proteins are stacked into thin distinct layers in order of their electrophoretic mobility. Due to the higher pH value in the separating gel, glycine ions become negatively charged increasing their mobility. The ion front moves ahead of the proteins which are now separated by size.

Sufficiently separated proteins have to be transferred to a solid membrane to be detectable by antibodies. For our analyzes, the proteins were transferred to a PVDF membrane. The procedure of electroblotting uses electric current to pull negatively charged proteins out of the gel on the PVDF membrane. The protein binding occurs via hydrophobic interactions, as well as interactions between the membrane and protein.

After blotting, the membrane with bounded proteins is washed with TBST (tris-buffered saline with Tween). Using TBST, unbound components can be washed away

without suppressing antigen-antibody binding interactions, thereby reducing nonspecific background and increasing the specific signal. To prevent unspecific bindings and interactions of antibodies with PVDF membrane, the membrane must be blocked. Commonly bovine serum albumin (BSA) and non-fat dry milk solution with TBST are used for this purpose. The proteins in this solution attach everywhere on the membrane where no target proteins from the gel have been bound avoiding unspecific binding of antibodies to the membrane.

After washing and blocking, a dilute solution of primary antibody directed against a specific protein is incubated with the membrane overnight at 4°C (Table 6). In order to detect primary antibody bound to the target protein, secondary antibody, which is directed against the species-specific region of the first antibody, is used. Commonly, this secondary antibody is linked to horseradish peroxidase, a reporter enzyme, which cleaves an added substrate resulting in a luminescent signal. For the detection, a sensitive photographic film is placed against the membrane, and the luminescence blackens the film at the specific protein bands (Figure 24).

Preparation:

Denatured protein samples (25 µg, 3 minutes at 95°C) were resolved by SDS-PAGE (sodium dodecyl sulphate polyacrylamide gel electrophoresis) using 10% separating gel and 4.5% collecting gel. Electrophoresis was conducted with 90 V till protein bands reached the end of the gel chamber. After the separation of proteins due their molecular weight using electrophoresis, proteins were transferred onto a polyvinylidene difluoride (PVDF) membrane (activated in methanol) using Trans-Blot SD (Bio-Rad) with 0.08 mA for 45 minutes. In semi-dry blotting, the gel and membrane are sandwiched between to stacks of filter paper. These filters are soaked with a cathode and an anode buffer acting as ions-reservoirs. After blotting, the membranes were blocked with milk solution (0.5% BSA + 1% milk powder) for at least 1 hour, washed with TBST and incubated with primary antibody (1:1000 dilution in 3% BSA) at

4°C overnight. After incubation, the membranes were washed again three times with TBST for 10 minutes and incubated with HRP-coupled secondary antibody (anti-mouse or anti-rabbit, 1:10000 dilution in 1% BSA) for at least 1 hour. The membranes were washed against three times with TBST each for 10 minutes. Following to washing, the proteins were detected using Santa Cruz Biotechnology Detection Kit.

Table 6: List of the antibodies used for the detection of several protein expression

Antibodies	Species	Concentration	Source
Caspase 3	Rabbit	1:1000	Apoptosis Sampler Kit – Cell Signaling
Caspase 7	Rabbit	1:1000	Apoptosis Sampler Kit – Cell Signaling
Caspase 8	Rabbit	1:1000	Apoptosis Sampler Kit – Cell Signaling
Caspase 9	Rabbit	1:1000	Apoptosis Sampler Kit – Cell Signaling
CDC2 = CDK1	Rabbit	1:1000	Santa Cruz Biotechnology
CDK2	Rabbit	1:1000	Santa Cruz Biotechnology
Cleaved Caspase 7	Rabbit	1:1000	Apoptosis Sampler Kit – Cell Signaling
Cleaved PARP	Rabbit	1:1000	Apoptosis Sampler Kit – Cell Signaling
ERK 1/2	Rabbit	1:1000	p44/42 MAP Kinase Antibody – Cell Signaling
IRE1 α	Rabbit	1:1000	ER Stress Antibody Sampler Kit – Cell Signaling
p38	Rabbit	1:1000	Santa Cruz Biotechnology
PARP	Rabbit	1:1000	Apoptosis Sampler Kit – Cell Signaling
pERK	Rabbit	1:1000	Phospho-p44/42 MAP Kinase (Thr202/Tyr204) Antibody – Cell Signaling
pp38	Rabbit	1:1000	Phospho-MAPK Family Antibody Sampler Kit – Cell Signaling
β -actin	Mouse	1:5000	Santa Cruz Biotechnology

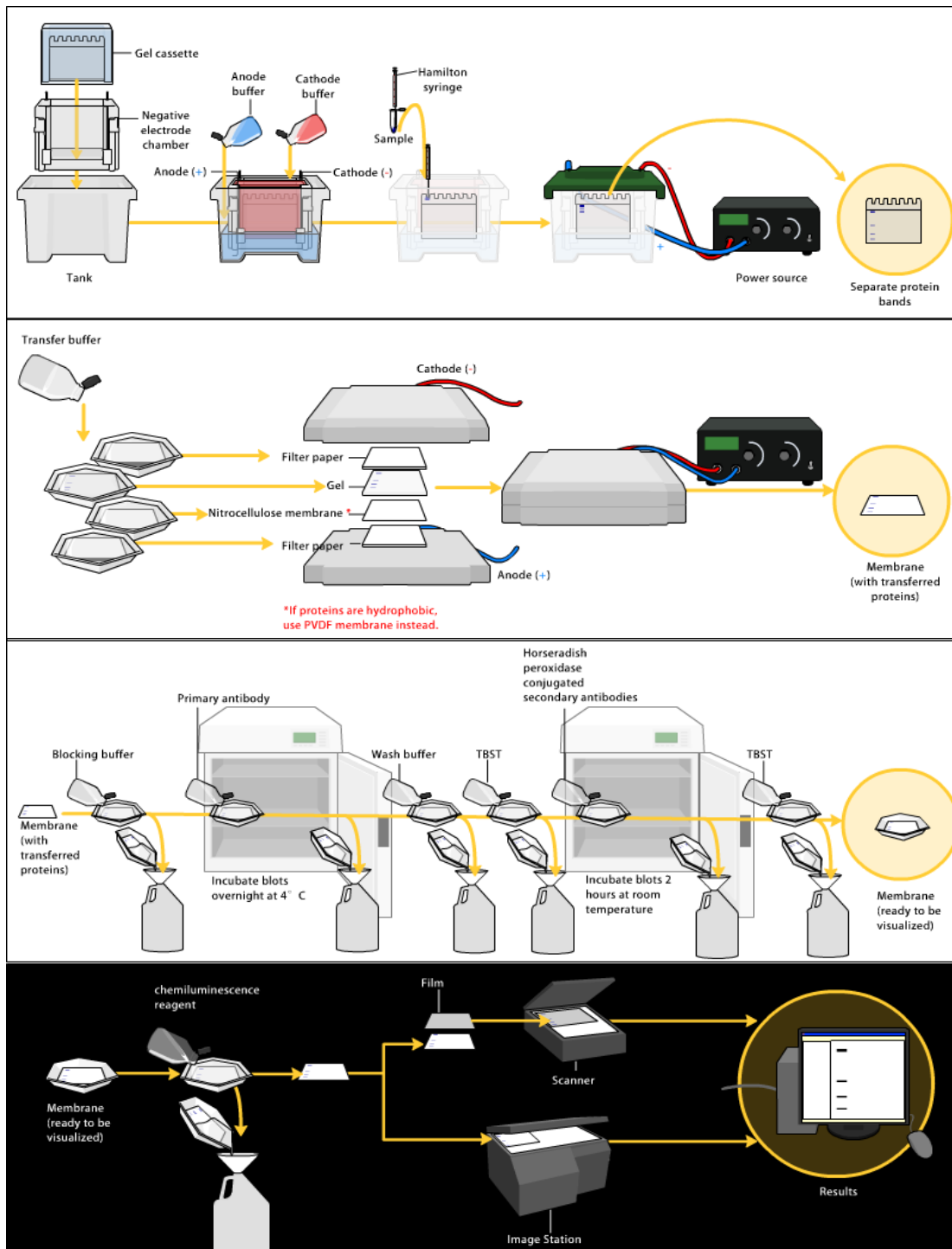


Figure 24: The main steps of Western blotting: Gel electrophoresis, blotting and detection of proteins using specific antibodies.

Receipts:**Tris-HCl 1.5 M, pH= 8.8:**

18.2 g Tris
Σ 100 ml ddH₂O, pH= 8.8

Lysis buffer:

50 mM Tris-HCl, pH= 7.6
300 mM NaCl
0.5% Triton X-100
Σ 500 ml ddH₂O

10x TBS:

120 g Tris
90 g NaCl
Σ 1 l ddH₂O, pH= 7.6

10x Laemmli-Electrophoresis buffer:

30 g Tris
144 g Glycine
10 g SDS
Σ 1 l ddH₂O

Bjerrumbuffer with Methanol:

5.82 g Tris
2.93 g Glycine
200 ml Methanol
Σ 1 l ddH₂O

SDS-PAGE – 10% Separating gel:

3.65 ml ddH₂O
1.875 ml Acrylamid
1.875 ml 1.5 M Tris-HCl, pH= 8.8
75 µl 20% SDS
5 µl 10% APS
5 µl TEMED

Tris-HCl 0.5 M, pH= 6.8

3 g Tris
Σ 50 ml ddH₂O, pH= 6.8

4x Sample loading buffer:

4 ml 10% Glycine
2 ml 2-Mercaptoethanol
0.92 g SDS
2.5 ml 1 M Tris-HCl (pH= 6.8)
Σ 10 ml ddH₂O

1x TBST:

100 ml 10xTBS
900 ml ddH₂O
1 ml Tween 20 (Bio-Rad)

Bjerrumbuffer with SDS:

5.82 g Tris
2.93 g Glycine
0.375 g SDS
Σ 1 l ddH₂O

SDS-PAGE – 4.5% Collecting gel:

1.56 ml ddH₂O
0.281 ml Acrylamid
0.625 ml 0.5 M Tris-HCl, pH= 6.8
25 µl 20% SDS
12.5 µl 10% APS
2.5 µl TEMED

5. RESULTS

5.1. Comparison of KP1019 and KP1339

5.1.1. Cell line-dependent cytotoxicity of KP1019 and KP1339

Cytotoxicity assays were performed using several cell lines after 72 hours drug exposure (Figure 25). Hepatoma cell lines tested with KP1019 and KP1339 included Hep3B, HepG2, HCC1.1 and HCC1.2 cells. Although levels of cytotoxicity differed from cell line to cell line, KP1019 showed generally higher cytotoxic activity than KP1339 in hepatoma cell lines. The same effect was demonstrated in cervix carcinoma cell line KB-3-1. However, in colorectal carcinoma cell line HCT116 KP1339 seemed to be more cytotoxic in comparison to KP1019. IC_{50} values of all tested cell lines were calculated by software GraphPad Prism 5.0 and shown in Table 7.

Table 7: The half maximal inhibitory concentration (IC_{50}) values of Hep3B, HepG2, HCC1.1, HCC1.2, KB-3-1, HCT116 cell lines with KP1019 or KP1339.

Cell lines	IC_{50} values with KP1019	IC_{50} values with KP1339
Hep3B	79.906 μ M	199.918 μ M
HepG2	42.128 μ M	161.544 μ M
HCC1.1	72.656 μ M	126.984 μ M
HCC1.2	83.026 μ M	123.764 μ M
KB-3-1	114.364 μ M	176.013 μ M
HCT116	44.265 μ M	35.253 μ M

In Hep3B hepatoma cells, differences in cytotoxicity between KP1019 and KP1339 became detectable at concentrations higher than 50 μ M. At concentrations higher than 150 μ M KP1019 led to 100% cell death. In contrast, treatment with 200 μ M

KP1339 induced viable cell number reduction to 15%. Nevertheless, the curve progressions of Hep3B cells exposed to KP1019 and KP1339 were parallel at concentrations higher than 50 μM .

The second hepatoma cell line HCC1.1 demonstrated similar sensitivity to the tested ruthenium drugs. Again up to 50 μM , both drugs did not differ in levels of cytotoxicity with enhanced activity of KP1019 at higher concentrations. Interestingly, KP1339 did not display dose-dependent cytotoxicity at the two highest concentrations (150 and 200 μM), but rather stabilization in cell number.

Also the hepatoma cell line HCC1.2 was responsive to KP1019 and KP1339. Both drugs at the concentrations lower than 75 μM showed similar levels of cytotoxicity. The cytotoxicity curve of KP1019 demonstrated an almost linear progression, and concentrations higher than 150 μM led to 100% cell death. Comparable to Hep3B and HCC1.1 cell lines, 100% cytotoxicity induced by KP1339 could not be reached.

The fourth hepatoma cell line, HepG2, responded differently to the investigated ruthenium drugs. KP1339 stimulated HepG2 cell proliferation up to a concentration of 100 μM . In comparison to Hep3B cells, almost 100% cell death could be achieved at the concentration of 200 μM KP1339. The highest cytotoxicity of KP1339 was observed at the highest concentration used (200 μM). In contrast, KP1019 caused no stimulated proliferation and was much more toxic in comparison to the previous experiment with Hep3B cells. Additionally, HepG2 cells were highly sensitive against KP1019. Concentrations higher than 100 μM induced 100% cell death.

The anticancer activity of KP1019 and KP1339 were also tested in KB-3-1 cells, a cervix carcinoma cell line. At concentrations lower than 100 μM , KB-3-1 cells reacted almost similar to KP1019 and KP1339. At higher doses the differences between these two curve progressions became significant. KP1019 showed an almost linear curve progression in a dose-dependent manner. Although KP1339 did not induce 100% cell

death, at the highest concentration (200 μM) of KP1019 all cells underwent cell death.

In HCT116, a colorectal carcinoma cell line, KP1339 showed highest cytotoxicity of all tested cell lines with $\text{IC}_{50} < 50 \mu\text{M}$ for both compounds (compare Table 7). KP1019 and KP1339 showed similar activity at almost all concentrations leading to total cell death at concentrations of 150 μM and 200 μM .

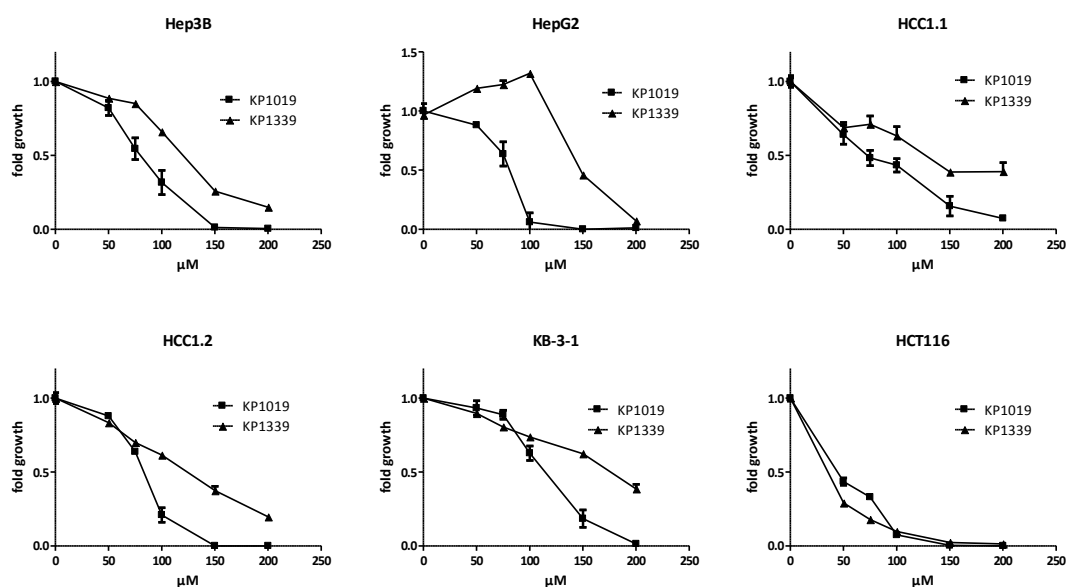


Figure 25: Activity of KP1019 and KP1339 against Hep3B, HepG2, HCC1.1, HCC1.2, KB-3-1 and HCT116 cells. The values given are means and standard deviations of six independent experiments.

5.1.2. Enhanced cellular accumulation of KP1019 as compared to KP1339

Cytotoxicity analyzes showed that in most cell lines KP1019 was more active in comparison to KP1339. This might be explained by alterations on the uptake levels of these drugs. To test this hypothesis, total intracellular ruthenium levels were determined using ICP-MS after 1 hour drug exposure. ruthenium levels were set in relation to the cell number of each sample, and expressed in ng per 10^5 cells (Figure 26). These analyzes were performed with Hep3B, KB-3-1, HCC1.1, HCC1.2 and HCT116 cells. As shown in Table 8 and Figure 26, the highest uptake levels of KP1019 and

KP1339 were found in HCC1.1 and Hep3B cells.

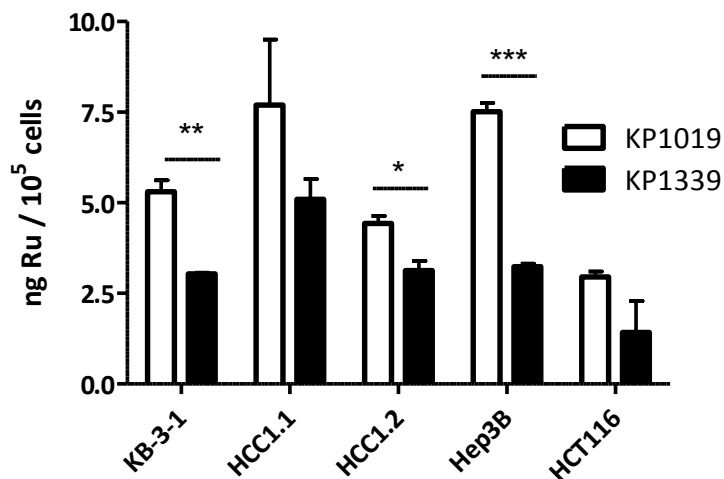


Figure 26: Ru uptake levels in KB-3-1, Hep3B, HCC1.1, HCC1.2 and HCT116 cell lines after 1 hour KP1019 and KP1339 exposure. Ru values were calculated relating to the cell number of each sample by using GraphPad Prism 5.0

Table 8: Absolute values and their standard derivations of each cell line.

Cell lines	KP1019		KP1339	
	Mean	SD	Mean	SD
KB-3-1	5.3	0.556777	3.033334	0.057735
HCC1.1	7.7	2.545584	5.1	0.964365
HCC1.2	4.433333	0.351189	3.133333	0.461880
Hep3B	7.508928	0.428160	3.239361	0.143549
HCT116	2.952	0.269	1.425	1.5

Notably, HCT116 cells displayed the lowest drug accumulation levels of all cell lines tested, arguing against the hypothesis that drug accumulation levels are the only factor responsible for drug efficacy.

Especially in Hep3B and HCT116 cells, the uptake level of KP1019 was up to 2-fold higher than KP1339 accumulation. A similar difference in uptake levels between two ruthenium drugs was also found in KB-3-1 cells (~1.75-fold). Nevertheless, although uptake of KP1019 occurred more efficient in all cell lines analyzed, no significant

correlation between total cellular uptake and cytotoxicity was found in case of both drugs indicating that more drug accumulation is not decisive for the exerted levels of cytotoxicity.

5.1.3. Different intracellular distributions of KP1019 and KP1339

Furthermore, the localisation of KP1019 and KP1339 in the cell might influence the mechanisms underlying their efficacy or mode of action (Figure 27). As the intracellular fate of the tested ruthenium drugs is still widely unknown, the intracellular distribution between cytosol and nucleus was examined. KP1019 and KP1339 were significantly and completely accumulated in the tumor cells within the first hour of drug incubation. Longer drug exposures did not cause enhanced uptake levels leading to suggest that within 1 hour the accumulation of both drugs had reached a stage. Moreover, ruthenium amount in cytosol and in nuclei increased in a concentration-dependent manner. Generally, KP1019 remained predominantly in cytosol, while KP1339 was enriched in nuclei. At all concentrations and time points, about 75% of KP1019 were detected in the cytosolic fraction. In contrast, 90% of KP1339 accumulated in the nucleus.

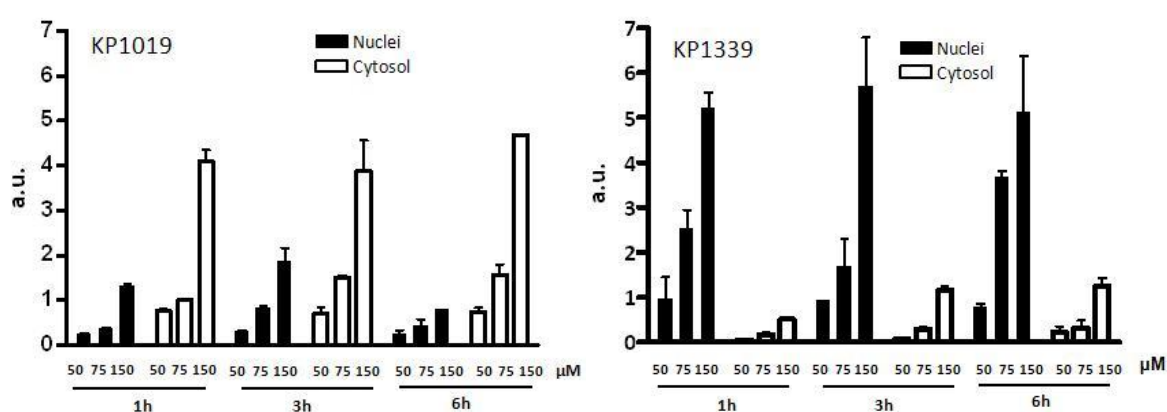


Figure 27: Ru levels in cytosol and nuclei fractions after 1, 3 and 6 hours drug exposure in KB-3-1 cells. The values were calculated relative to the cell number of each sample and normalised using GraphPad Prism 5.0.

5.1.4. Apoptosis induction potential of KP1019 and KP1339

As a next step, it was examined whether the differences in activity between KP1019 and KP1339 were accompanied by alterations in apoptosis induction. The potential of KP1019 and KP1339 to induce apoptosis can be examined using DAPI staining and fluorescence microscopy. KB-3-1 cells were analysed and compared based on their morphological appearances. As expected, after 24 hours drug exposure higher amounts of apoptotic/necrotic cells were detected, and the number of normal cells decreased in a concentration-dependent manner (Figure 28). In general, KB-3-1 cells treated with both drugs exhibited typical signs of apoptosis including chromatin condensation and fragmentation of nuclei into apoptotic bodies (Figure 29). In case of KP1019, pronounced apoptosis induction was observed after treatment with 150 μM (38.9%) and 200 μM (77.1%), while KP1339 only led to 11.5% and 12.9% apoptotic cells at 150 μM and 200 μM , respectively. Treatment with 400 μM KP1339 strongly increased the proportion of apoptotic cells to 93.7%.

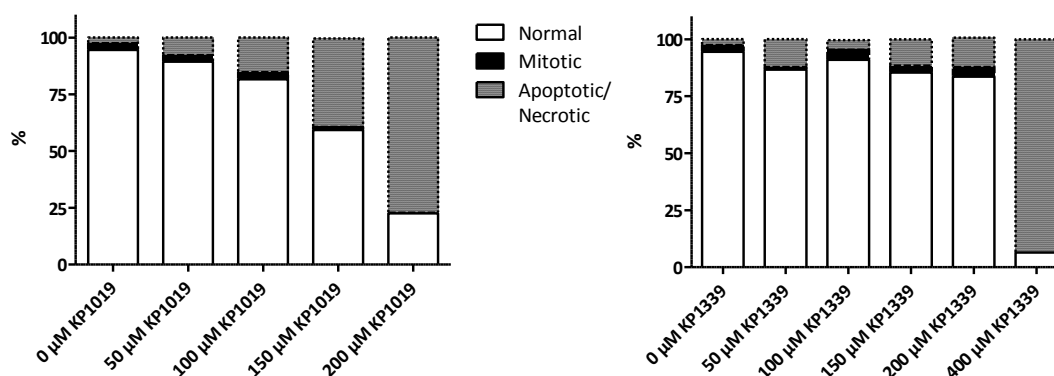


Figure 28: Comparison of the apoptosis-inducing potential of KP1019 with KP1339 in KB-3-1 cells. After 24 hours drug exposure, morphological features of about 200 nuclei of at least two slides for each concentration were analyzed. Percentages of normal, mitotic and apoptotic/necrotic nuclei are shown.

In accordance to MTT assay data, KP1339 caused a 2-fold weaker apoptotic response. The level of mitotic cells also showed a decrease of 3.3%, and there were no mitotic cells found at the highest concentrations (200 μ M KP1019 and 400 μ M KP1339) displaying apoptotic morphology in more than 80% of the treated cell.

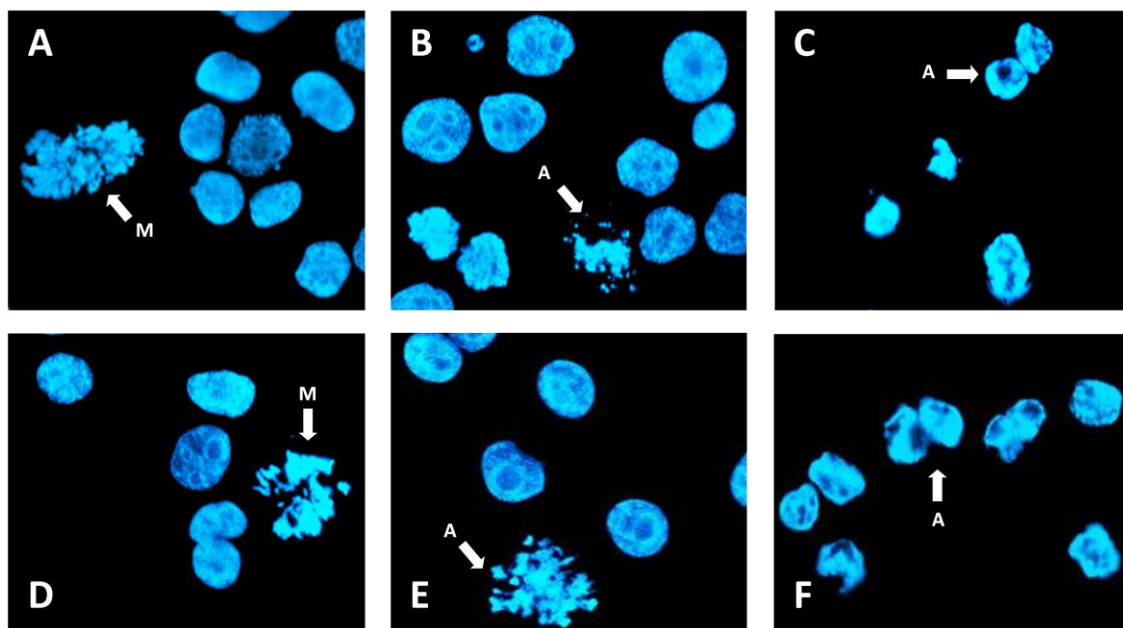


Figure 29: DAPI staining. KB-3-1 cells were treated with (B) 100 μ M KP1019, (C) 200 μ M KP1019, (D) 100 μ M KP1339, (E) 200 μ M KP1339 or (F) 400 μ M KP1339 for 24 hours. A sample of untreated KB-3-1 cells (A) was also stained to compare the morphological changes in treated cells. After cytopsin and fixation with 1:1 aceton/methanol, 300-500 nuclei of at least two slides for each concentration were counted and analyzed. A... apoptotic bodies, M... mitosis.

5.1.5. Mitochondrial membrane depolarization induced by KP1019 and KP1339

To identify the molecular mechanisms underlying the observed apoptosis induction, KB-3-1 cells were treated with increasing concentrations of KP1019 and KP1339 for 24 hours, and the samples were stained using JC-1. JC-1 staining allows determination the mitochondrial regulation of apoptosis. 24 hours treatment with KP1019 and KP1339 induced depolarisation of mitochondrial membrane in a concentration-dependent manner. A detectable increase (from 4.57% to 8.33%) of cells with depolarized mitochondria was observed already using 100 μ M KP1019. Exposure to 200 μ M

KP1019 resulted in profound mitochondrial depolarization in 78.72% of cells. Interestingly, when the cells were treated in a 2-fold higher concentration of KP1339 as the one used for KP1019, the percentages of apoptotic cells were very similar (Figure 30). Treatment with 200 μM KP1339 resulted in 7.03% cells with depolarized mitochondria and 400 μM KP1339 in 65.67%. This supports the hypothesis that ruthenium drugs act in the cell via similar pathways although with less activity in case of KP1339.

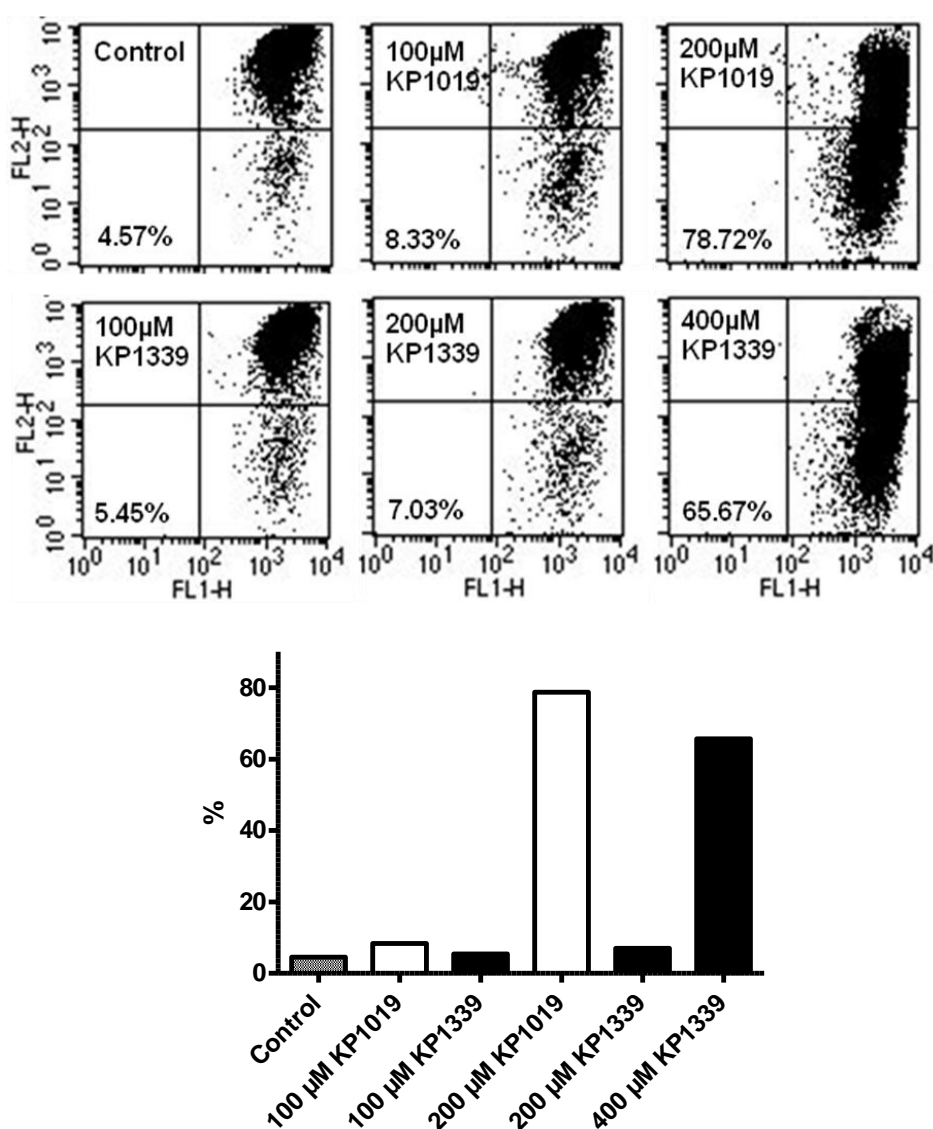


Figure 30: JC-1 staining histograms of KB-3-1 cells after 24 hours drug exposure in several concentrations. The highest concentrations of KP1019 and KP1339 induced more than 65% mitochondrial apoptosis.

5.1.6. Apoptosis detection by KP1019 and KP1339 at protein level

For Western blot analysis, proteins were isolated after 24 hours drug exposure, separated by SDS-PAGE, blotted to PVDF membrane, and detected with several antibodies for typical apoptosis-related in Hep3B, HepG2 and KB-3-1 cells (Figure 31). In case of Hep3B and HepG2, cells were treated with 75 and 150 μM KP1019 or KP1339. Caspase-mediated cleavage of PARP was observed in Hep3B exposed with 150 μM drug, especially with KP1019. 75 μM KP1019 and KP1339 did not induced any cleavage of PARP in comparison to untreated Hep3B cells. Moreover, no changes in

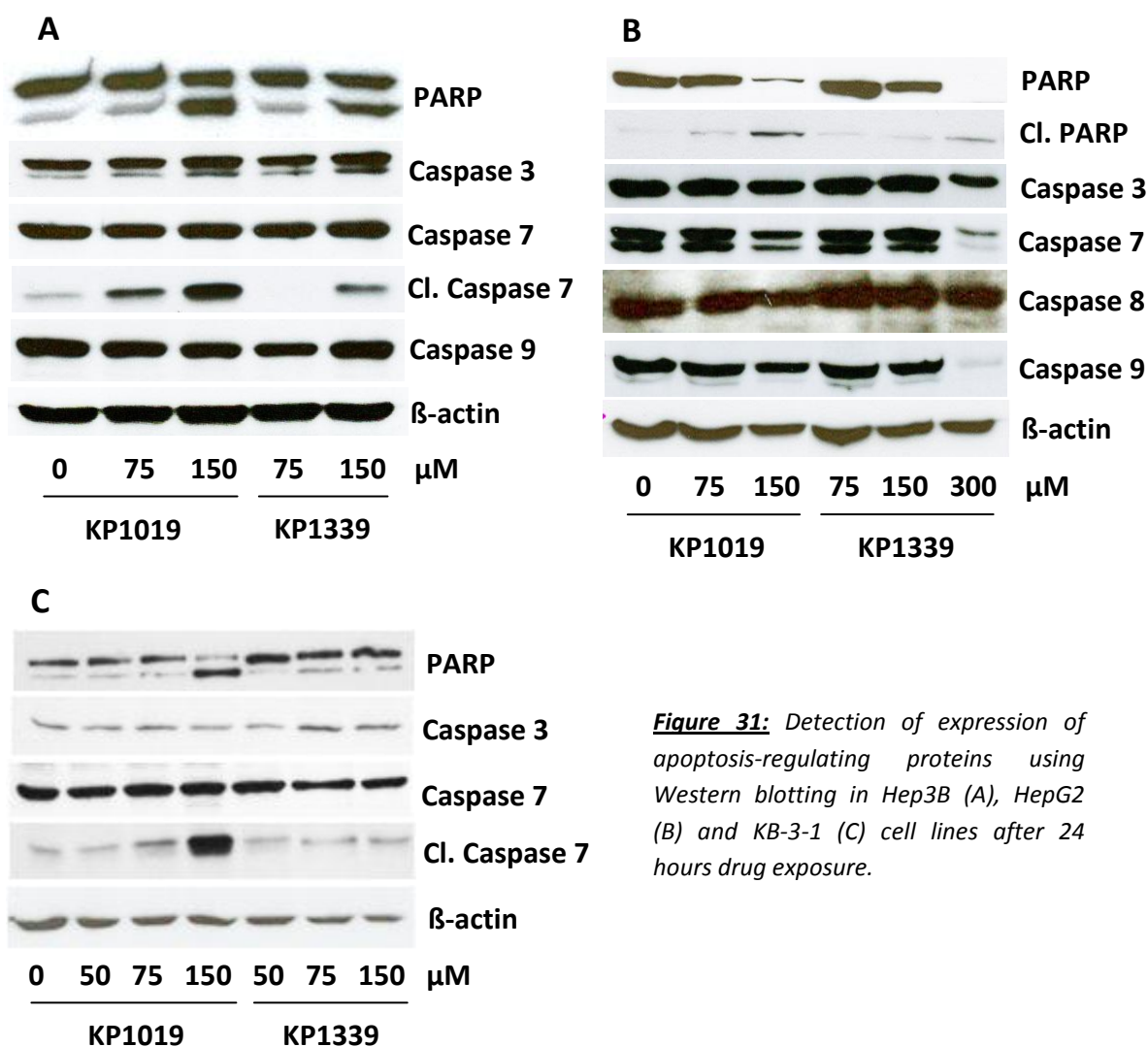


Figure 31: Detection of expression of apoptosis-regulating proteins using Western blotting in Hep3B (A), HepG2 (B) and KB-3-1 (C) cell lines after 24 hours drug exposure.

signal intensity of caspase 3, 7 and 9 were demonstrated after drug exposure. Interestingly, caspase 7 was mainly cleaved by 150 μ M KP1019, while KP1339 showed lower efficiency to cleave this protein.

A different efficiency of PARP cleavage was obtained in HepG2 cells. Comparable to Hep3B cells, the cleavage was induced with increasing concentrations of drugs. The strongest PARP cleavage was detected in HepG2 cells exposed to 150 μ M KP1019. Similar to Hep3B cells, caspase 3 and caspase 8 were not activated compared to caspase 7 and caspase 9, which were downregulated in a drug-dependent manner.

KB-3-1 cells were also investigated for alterations of apoptosis-related proteins. In comparison to other cell lines, 150 μ M KP1019 induced a very strong cleavage of PARP, while 75 μ M and 150 μ M KP1339 were not so active for PARP cleavage. Similar to Hep3B cells, uncleaved caspase 3 and caspase 7 levels remained unchanged, although upregulation of caspase 7 cleavage in cells exposed with 150 μ M KP1019 was observed (Figure 31).

5.2. Combination tests with KP1339 and other chemical compounds

5.2.1. Combinations with FeCl₃, Gallium nitrate, and triapine

FeCl₃ and Gallium nitrate compounds were examined for their activity in cell lines Hep3B, HepG2, HCC1.1, HCC1.2, and KB-3-1. Furthermore, they were also combined with KP1339 to detect the alterations in cytotoxicity.

Based on the theory that both KP1019 and KP1339 are taken up via interaction with transferrin, cells were pre-incubated with FeCl₃ for 6 hours. Without removing FeCl₃, cells were exposed with KP1339 for another 72 hours (Figure 32, Table 9). In case of Hep3B, FeCl₃ led to higher sensitivity against KP1339 in a dose-dependent manner, especially at concentrations higher than 50 μM, although 10 μM and 30 μM FeCl₃ did not differ in the induction of sensitivity. This enhancement of KP1339 activity was also observed in HepG2 and HCC1.1 cells at the concentrations higher than 100 μM KP1339, but in lower levels. Interestingly, only in HCC1.2 hepatoma cell line FeCl₃ induced resistance to KP1339 in a drug-dependent manner. In contrast, increase of intracellular iron levels did not sensitize KB-3-1 cells to KP1339.

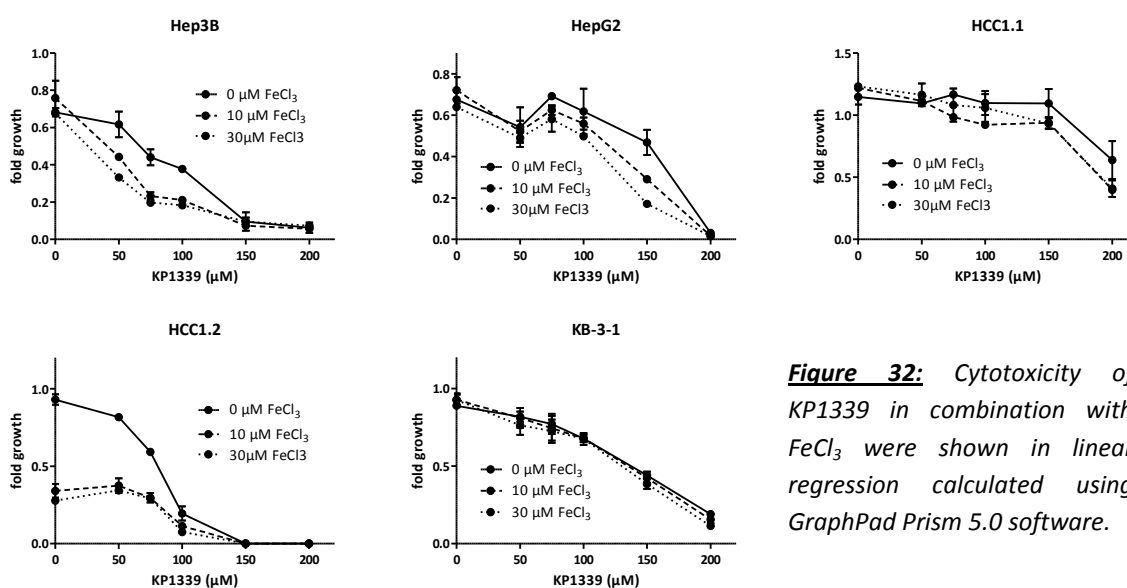


Figure 32: Cytotoxicity of KP1339 in combination with FeCl₃ were shown in linear regression calculated using GraphPad Prism 5.0 software.

Table 9: The half maximal inhibitory concentration (IC_{50}) values for Hep3B, HepG2, HCC1.1, HCC1.2, and KB-3-1 of KP1339, $FeCl_3$ or co-treatment of both drugs.

Cell lines	IC_{50} values with $FeCl_3$	IC_{50} values with KP1339	IC_{50} values in combination with 10 μM $FeCl_3$ and KP1339
Hep3B	> 30 μM	106.517 μM	57.464 μM
HepG2	> 30 μM	164.834 μM	
HCC1.1	> 30 μM	> 200 μM	180.477 μM
HCC1.2	7.791 μM	123.805 μM	190.779 μM
KB-3-1	> 30 μM	148.958 μM	142.031 μM

To gain more insights into the interaction of KP1339 with iron homeostasis combination experiments with Gallium nitrate were performed. Simple gallium salts share some characteristics with Fe^{3+} and have been shown to accumulate in tumor cells via the transferrin receptor. This leads to deficiencies in iron uptake. Consequently, resistance to Gallium nitrate was based on transferrin receptor overexpression [192]. In both Hep3B and KB-3-1 cells, Gallium nitrate induced sensitivity against KP1339 (Figure 33, Table 10). Generally, Hep3B cells were very

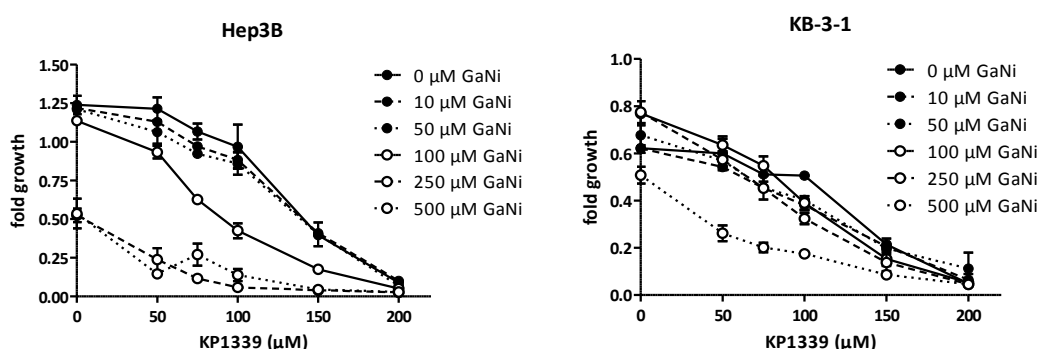


Figure 33: Cytotoxicity assays in Hep3B and KB-3-1 cells after co-treatment of Gallium nitrate and KP1339 for 72 hours. The values were calculated using GraphPad Prism 5.0 software and shown in linear regression.

sensitive against Gallium nitrate mono-therapy at a concentration of 250 μM and 500 μM . In combination, even lowest concentrations of KP1339 displayed strong cytotoxic activities. KP1339 higher than 150 μM in combination with 10 μM , 50 μM , and 100 μM Gallium nitrate led to stabilized cell number of Hep3B cells, while 10 μM and 50 μM Gallium nitrate with KP1339 higher than 100 μM Gallium nitrate caused almost total cell death. Moreover, KB-3-1 cells showed also synergistic activity in combination therapy. The highest sensitivity was found with 500 μM Gallium nitrate, especially in combination with 50 μM , 75 μM and 100 μM KP1339. Additionally, KB-3-1 cells were less sensitive against Gallium nitrate in comparison to Hep3B cells.

Table 10: The half maximal inhibitory concentration (IC_{50}) values for Hep3B, and, KB-3-1 cells of KP1339, Gallium nitrate and combination therapy.

Cell lines	IC_{50} values with Gallium nitrate	IC_{50} values with KP1339	IC_{50} values in combination with 250 μM Gallium nitrate and KP1339
Hep3B	240.66 μM	152.03 μM	42.2 μM
KB-3-1	> 500 μM	135.434 μM	87.694 μM

The next tested agent was Triapine. Triapine is an experimental drug in phase II clinical trial. It exerts its anti-neoplastic activity by inhibition of the enzyme ribonucleotide reductase and generation of ROS after formation of an intracellular iron complex [193]. Ribonucleotide reductase inhibition by triapine results in depletion of cellular dNTP pools leading to DNA synthesis arrest and apoptosis induction. The combination of triapine with KP1339 was tested in two cell lines, Hep3B and KB-3-1 (Figure 34, Table 11). In both cell lines investigated, triapine mono-treatment did not induce strong cytotoxic activity. Combination with KP1339 in Hep3B cells had strong synergistic activity with CI values ranging from 0.2 up to 0.7. Notably, the increase of triapine concentrations was directly associated with a decrease of the respective CI

values. In case of KB-3-1 cells, no synergistic activity between KP1339 and triapine was

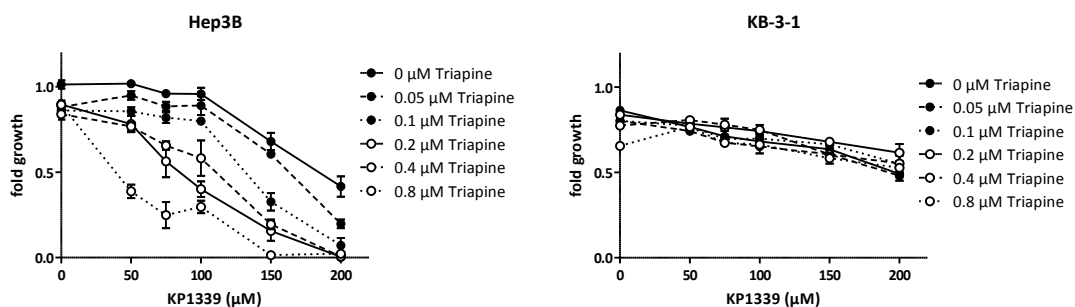


Figure 34: Triapine was tested in combination with KP1339, and the cytotoxic activity was detected after 72 hours drug exposure in Hep3B and KB-3-1 cells.

observed indicating that synergism with triapine is cell type-dependent.

Table 11: The half maximal inhibitory concentration (IC_{50}) values of Hep3B, and KB-3-1 cells with triapine, KP1339 or co-treatment of both drugs.

Cell lines	IC_{50} values with triapine	IC_{50} values with KP1339	IC_{50} values in combination with 0.4 μ M triapine and KP1339
Hep3B	> 0.8 μ M	185.315 μ M	120.912 μ M
KB-3-1	> 0.8 μ M	> 200 μ M	> 200 μ M

5.2.2. Combinations with DNA damaging agents Ara-C, adriamycin, and temozolomide

Ara-C is an anti-cancer chemotherapy drug, which is classified as an anti-metabolite. Incorporation of this modified nucleic acid during DNA synthesis leads to cell cycle arrest in S-phase and DNA damage. Ara-C is used to treat different forms of leukemia. After 72 hours simultaneous treatment of KP1339 with Ara-C, cytotoxicity was evaluated using MTT assay (Figure 35A, Table 12). In this setting Ara-C treatment

alone displayed potent cytostatic activity against both Hep3B and KB-3-1 cells. KB-3-1 cells were found to more sensitive to Ara-C with an IC_{50} value of 6 μM . In contrast, treatment with up to 100 μM Ara-C was not sufficient to reach IC_{50} levels in Hep3B cells. Co-incubation revealed that Ara-C acted in most combinations interacted with KP1339 in an additive to synergistic manner (CI values between 0.4 and 1.2). However, in selected cases, especially at higher concentrations of Ara-C in KB-3-1 cells, antagonism was observed. Moreover, sequential drug treatment settings such as adding KP1339 after 6 hours pre-treatment with Ara-C (data not shown) or Ara-C after 3 hours pre-treatment with KP1339 (Figure 35B, Table 12) did not enhance the activity of this drug combination.

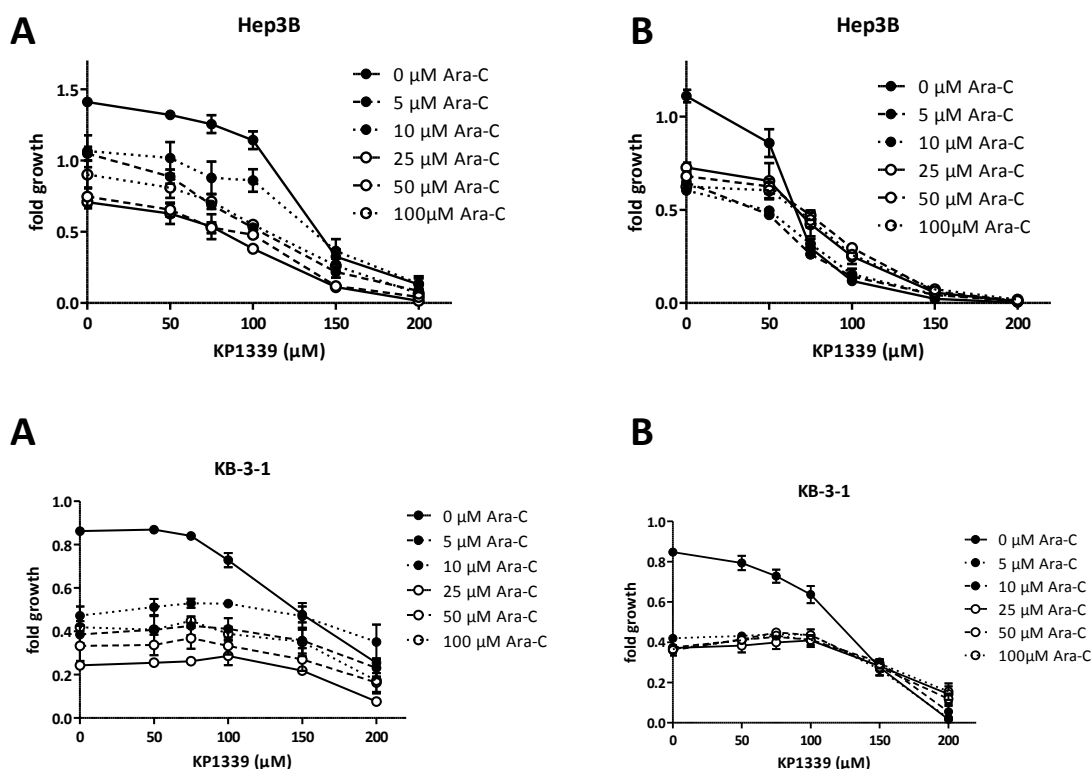


Figure 35: Cytotoxic activities were determined in Hep3B and KB-3-1 cells (A) after simultaneously treatment of Ara-C and KP1339, and (B) Ara-C exposure following to pre-treatment of KP1339 for 3 hours.

Table 12: The half maximal inhibitory concentration (IC_{50}) values for Hep3B and KB-3-1 cells of Ara-C, KP1339 or co-treatment of both drugs after pre-treatment (B) or contemporaneously treatment (A).

Cell lines	IC_{50} values with Ara-C	IC_{50} values with KP1339	IC_{50} values in combination with 50 μ M Ara-C and KP1339
Hep3B (A)	> 100 μ M	121.885 μ M	110.115 μ M
Hep3B (B)	> 100 μ M	63.454 μ M	93.721 μ M
KB-3-1(A)	5.98 μ M	160.366 μ M	198.918 μ M
KB-3-1 (B)	6.107 μ M	129.42 μ M	180.573 μ M

As a next step, the combination of KP1339 with adriamycin was tested for efficacy against several cancer cell models. Adriamycin (also called doxorubicin) is a DNA damaging drug, which leads to DNA lesions by topoisomerase II inhibition and ROS generation. This antibiotic drug of the anthracycline family is frequently used for the treatment of bladder, breast as well as head and neck cancers. Figure 36 shows the impact of simultaneous application of adriamycin with KP1339 on KB-3-1, Hep3B, VL-8 and A549 cells. In general, co-treatment with adriamycin did enhance KP1339 anti-cancer activity in an additive manner (CI values between 0.8 and 1.5). However, at some concentration combinations tested also antagonistic effects were detected. Especially in the rather adriamycin-resistant A549 cell model (IC_{50} of 145 μ M in comparison with e.g. the IC_{50} of 42.5 μ M in KB-3-1 cells) CI values up to 3.9 were observed (Table 13). Consequently, it was evaluated whether sequential application was able to enhance the efficacy of combination of KP1339 with adriamycin. To this end, Hep3B and KB-3-1 cells were either pre-treated with KP1339 for 3 hours or with adriamycin for 6 hours before adding adriamycin or KP1339, respectively. In both settings, no antagonistic effects were observed, but KP1339 and adriamycin were found to act additively (all CI values between 0.9 and 1.2).

Table 13: The half maximal inhibitory concentration (IC_{50}) values of Hep3B, KB-3-1, VL8 and A549 cells with adriamycin, KP1339 or co-treatment of both drugs after pre-treatment (B) or contemporaneously treatment (A).

Cell lines	IC_{50} values with adriamycin	IC_{50} values with KP1339	IC_{50} values in combination with 100 μ M adriamycin and KP1339
Hep3B (A)	> 250 μ M	147.684 μ M	128.146 μ M
Hep3B (B)	> 250 μ M	97.821 μ M	104.672 μ M
KB-3-1 (A)	42.305 μ M	186.593 μ M	> 200 μ M
KB-3-1 (B)	65.043 μ M	144.053 μ M	182.463 μ M
VL-8	8.577 μ M	103.208 μ M	163.755 μ M
A549	144.65 μ M	175.861 μ M	197.739 μ M

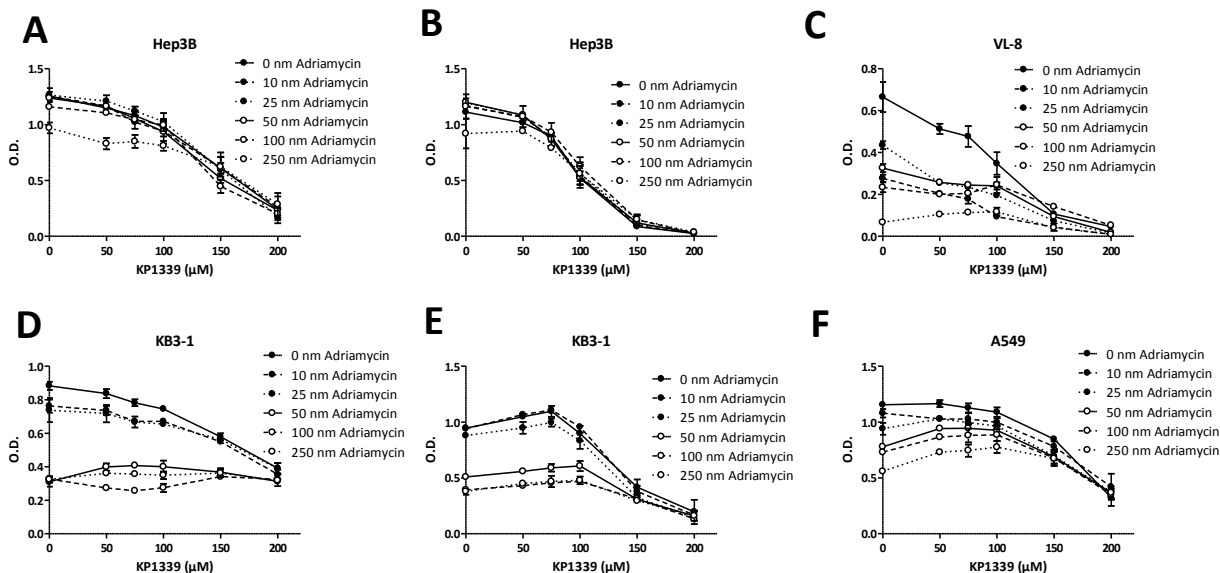


Figure 36: The cytotoxicity of adriamycin and KP1339 in combination was detected against Hep3B, KB-3-1, VL-8 and A549 cells. Drugs were either added simultaneously to the cells, such as in (A), (C), (D), and (F), or cells were exposed with adriamycin following to pre-incubation with KP1339 shown in (B) and (E).

Temozolomide is an alkylating agent which is clinically used for the treatment of glioblastoma (Grade IV astrocytoma) and melanoma. Alkylating agents exert their anticancer activity due to DNA methylation and/or cross linking. The resulting DNA lesions lead to cell cycle growth arrest and apoptotic cell death. The combination of temozolomide with KP1339 was tested additionally to Hep3B and KB-3-1 cells also in the melanoma cell lines VM-1, VM-21, and VM-48 (Figure 37). Temozolomide mono-treatment induced significant cytotoxicity in all cell lines (compare IC₅₀ values in Table 13) with the exception of VM-1 cells, which had an IC₅₀ of higher than 2 mM. Figure 38 shows that co-treatment of the two test drugs had in general additive effects in all temozolomide-responsive cell lines (CI values of 0.8 to 1.2). Notably, in KB-3-1 and VM-21 cells combination of KP1339 with 2 mM temozolomide resulted frequently in synergistic activity with CI values between 0.33 and 0.82. In contrast, mainly antagonistic activity was observed in the temozolomide-resistant VM-1 cell line (CI values up to 6.2).

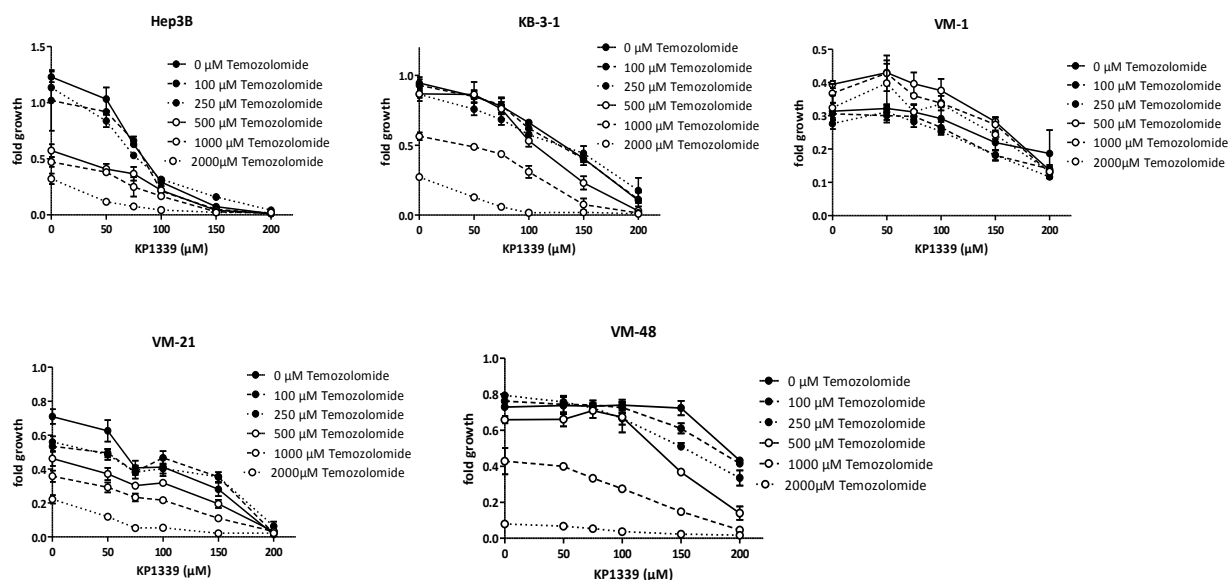


Figure 37: Cytotoxicity of temozolomide and KP1339 in Hep3B, KB-3-1, VM-1, VM-21 and VM-48 cells were identified using MTT assay. The values after calculation in GraphPad Prism 5.0 were shown in linear regression.

Table 13: The half maximal inhibitory concentration (IC_{50}) values of Hep3B, KB-3-1, VM1, VM21 and VM48 cells with Temozolomid, KP1339 or co-treatment of both drugs.

Cell lines	IC_{50} values with temozolomid	IC_{50} values with KP1339	IC_{50} values in combination with 1 mM temozolomid and KP1339
Hep3B	712.223 μ M	76.111 μ M	85.971 μ M
KB-3-1	1311.137 μ M	136.753 μ M	105.857 μ M
VM-1	> 2000 μ M	> 200 μ M	180.991 μ M
VM-21	1024.139 μ M	121.429 μ M	117.5 μ M
VM-48	1183.381 μ M	> 200 μ M	123.822 μ M

5.2.3. Combinations with tubulin-targeting agents taxol and vinblastine

Taxol and vinblastine are characterized by their interaction with the cellular cytoskeleton, which subsequently leads to impaired mitosis and cell death. Taxol binds specifically to the β -tubulin subunit, which inhibits the disassembly of microtubules and interferes with the normal breakdown of microtubules during cell division. In contrast, vinblastine inhibits the assembly of microtubules. Taxol is clinically used in the treatment of lung, ovarian as well as head and neck cancer. Consequently, the combination with KP1339 was tested in VL-8 lung cancer cells (Figure 38, Table 14). Taxol mono-treatment was very cytotoxic with an IC_{50} values of 11.9 nM. With regard to the combination effects of our test drugs, the simultaneous application of taxol with KP1339 had mainly antagonistic activity in VL-8 cells (CI values up to 240), especially at low KP1339 concentrations (50 μ M). To test whether sequential application is able to reduce this antagonism, other application schemas were tested. In these experiments, pre-incubation with KP1339 for 3 hours (Figure 38 B) or taxol for 6 hours (Figure 38 C) caused mostly antagonistic activity with CI values higher than 1.5, and only in some concentrations such as co-treatment with 50 μ M KP1339 after 6 hours pre-incubation with taxol.

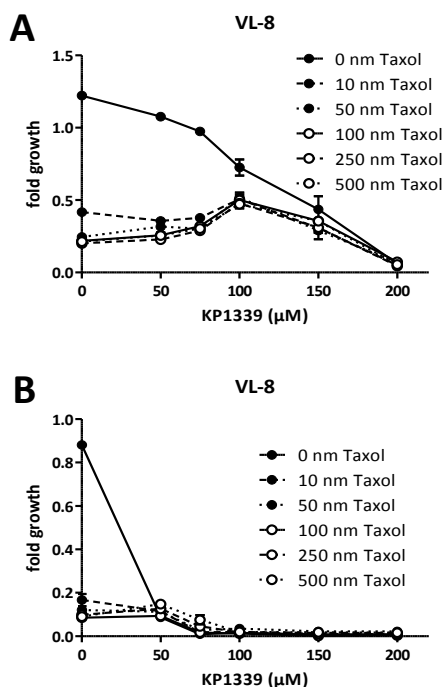


Figure 38: Cytotoxic activity of taxol and KP1339 were determined using MTT assays in VL-8 cells. In (A), the cells were treated for 72 hours. In contrast, in (B) they were pre-incubated with KP1339 for 3 hours, and in (C) with taxol for 6 hours.

Table 14: The half maximal inhibitory concentration (IC_{50}) values of VL-8, KB-3-1, and A549 cells with taxol, KP1339 or co-treatment of both drugs with simultaneously treatment (A), pre-incubation for 3 hours with KP1339 (B), and for 6 hours with taxol (C).

Cell lines	IC_{50} values with taxol	IC_{50} values with KP1339	IC_{50} values in combination with 10 nM taxol and KP1339
VL-8 (A)	11.858 nM	119.775 μ M	166.697 μ M
VL-8 (B)	9.847 nM	27.748 μ M	58.14 μ M
VL-8 (C)	9.798 nM	30.633 μ M	61.865 μ M
KB-3-1 (A)	8.332 nM	> 200 μ M	> 200 μ M
A549 (B)	11.892 μ M	67.794 μ M	110.647 μ M
A549 (C)	11.684 μ M	55.631 μ M	89.721 μ M

Vinblastine is frequently used in treatment of Hodgkin's lymphoma, non-small cell lung cancer, breast, head, neck as well as testicular cancer. Thus, for the experiments

with vinblastine KB-3-1 and VL-8 cells were used (Figure 39, Table 15). Vinblastine alone had strong cytotoxic effects against KB-3-1 cells with an IC_{50} of 3.1 nM, while VL-8 cells turned out to be vinblastine-resistant with an IC_{50} of higher than 10 nM. The combination of vinblastine with KP1339 had at most concentrations tested additive effects (CI values from 0.8 to 1.5). Notably in the VL-8 cell model, addition of KP1339 was found to synergistically enhance the activity of 10 nM vinblastine leading to CI values between 0.4 – 0.7. This suggests that KP1339 might be able to synthesize resistant tumor cells to vinblastine treatment.

Table 15: The half maximal inhibitory concentration (IC_{50}) values of A549, KB-3-1 and VL8 cells with vinblastine. KP1339 or co-treatment with both drugs.

Cell lines	IC_{50} values with vinblastine	IC_{50} values with KP1339	IC_{50} values in combination with 5 nM vinblastine and KP1339
KB-3-1	3.143 nM	183.85 μ M	> 200 μ M
VL-8	> 200 μ M	133.147 μ M	124.169 μ M

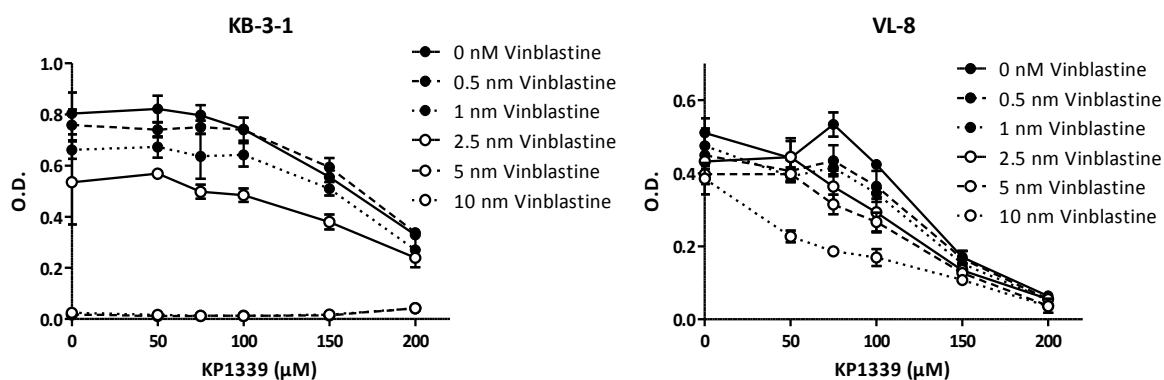


Figure 39: The activity of vinblastine and KP1339 was determined in KB-3-1 and VL-8. The cells were exposed to drugs for 72 hours. The linear regression of the cytotoxicity values was calculated in GraphPad Prism 5.0 software.

5.3. Combination tests with KP1339 and tyrosine kinase inhibitor sorafenib

Sorafenib is an oral, dual inhibitor of Raf and vascular endothelial growth factor receptor (VEGFR). The molecule has demonstrated preclinical antineoplastic activity against a wide spectrum of human cancers [78]. Moreover, it has exhibited *in vitro* inhibitory effects against Raf-1, B-Raf, VEGFR-2, platelet-derived growth factor receptor (PDGFR), and VEGFR-3. It is approved for the treatment of advanced renal cell carcinoma and hepatocellular carcinoma [194].

5.3.1. Differences in cytotoxicity of KP1339 by sorafenib co-treatment

The tyrosine kinase inhibitor sorafenib was tested in addition to several hepatoma cell lines (Hep3B, HepG2, HCC1.1, HCC1.2, HCC2 and B1) also in the lung carcinoma cell lines VL-8, Calu-6 and several melanoma cell lines (Table 16). Most cell lines were rather sensitive to sorafenib mono-treatment with IC_{50} values of $\sim 3 \mu\text{M}$. Most resistant to sorafenib were HCC1.1 and VL-8 cells (IC_{50} higher than $10 \mu\text{M}$), while B1 and Calu-6 were the most sensitive ones with IC_{50} values of $0.5 \mu\text{M}$ and $0.3 \mu\text{M}$, respectively. Notably, all melanoma cell lines tested showed only little sensitivity against sorafenib.

With regard to the drug combination, sorafenib co-treatment with KP1339 showed additive to synergistic activity in all cell lines investigated (Figure 40). Especially, combination of KP1339 with $10 \mu\text{M}$ sorafenib was always highly synergistic with CI values between 0.1 and 0.5. In general, at lower KP1339 concentrations ($50 - 100 \mu\text{M}$) mainly additive effects were observed (CI values of 0.9-1.5). Furthermore, higher KP1339 doses ($100 - 200 \mu\text{M}$) increased the anticancer activity of sorafenib synergistically. Especially in HepG2 and VM-1 cells this led to a drastic reduction in CI values (CI values from 1.8 to 0.1 in HepG2 cells and from 1.3 to 0.4 in VM-1 cells).

Notably, synergistic activity of KP1339 with sorafenib was found in sorafenib-resistant (HCC1.1. and VL-8) as well as sorafenib-responsive cell lines (e.g. Hep3B, HepG2, HCC2, HCC1.2). Only, in the very sorafenib-sensitive hepatoma model B1, KP1339 with sorafenib solely additive effects were observed. This indicates that KP1339 co-treatment in general enhances the activity of sorafenib and is able to overcome sorafenib resistance.

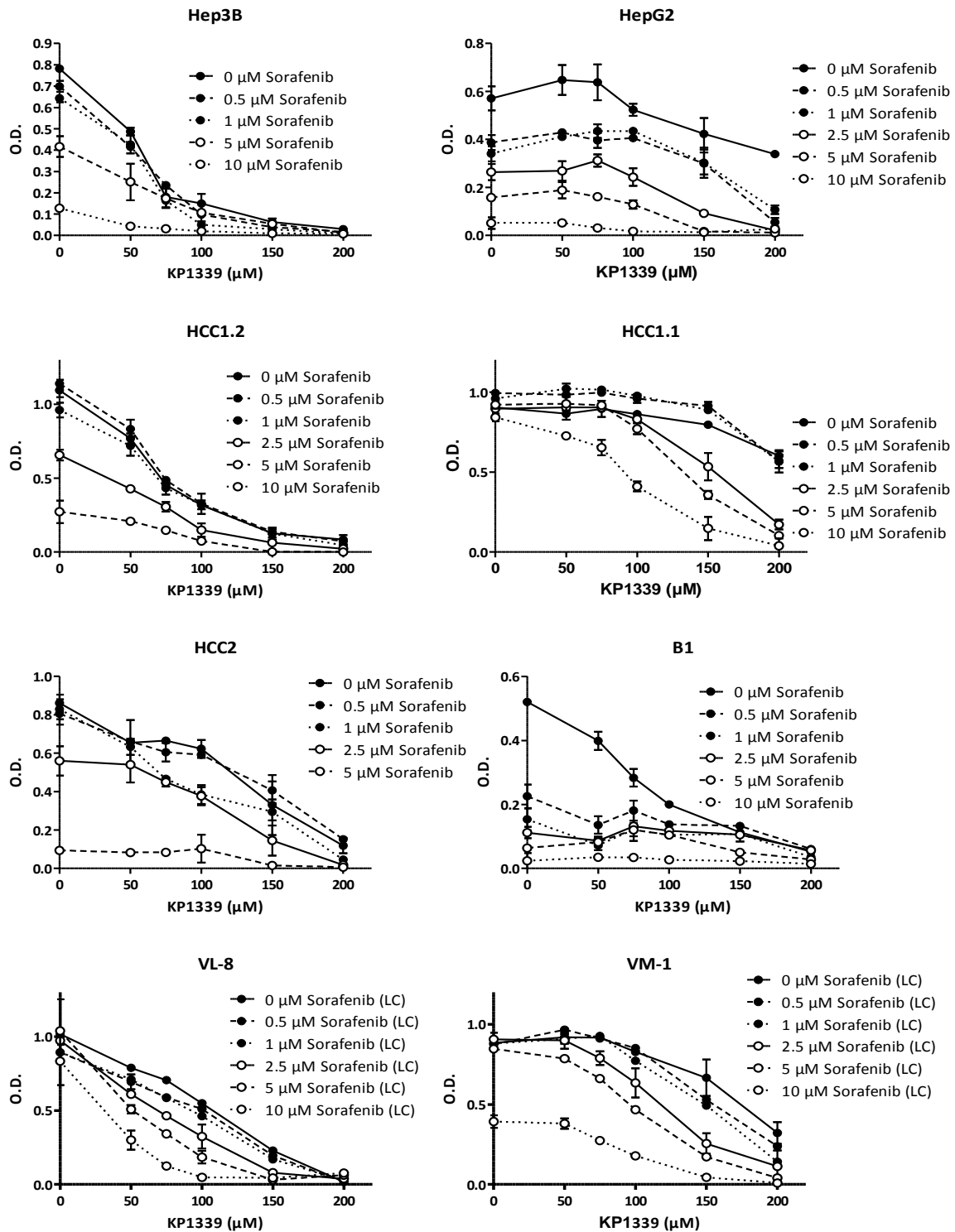


Figure 40: The indicated liver (Hep3B, HepG2, HCC1.1, HCC1.2, HCC2, and B1), lung cancer (VL-8) as well as melanoma cell lines (VM-1) were tested in combinations with sorafenib and KP1339. Cells were exposed for 72 hours, and their cytotoxicity was analysed by MTT assays.

Table 16: *IC₅₀ values were determined from the cytotoxicity tests of different carcinoma cell lines.*

Cell lines	IC ₅₀ values for sorafenib	IC ₅₀ values for KP1339	IC ₅₀ values in combination with 5 μM sorafenib and KP1339
Hep3B	5.443 μM	78.801 μM	63.815 μM
HepG2	2.79 μM	-	128.422 μM
HCC1.1	-	-	137.494 μM
HCC1.2	3.211 μM	67.582 μM	120.486 μM
B1	0.534 μM	103.046 μM	191.492 μM
HCC2	3.194 μM	132.796 μM	131.939 μM
HCC3	4.55 μM	29.898 μM	102.531 μM
KB-3-1	-	-	-
KBC-1	-	169.753 μM	155.619 μM
VL-8	-	106.139 μM	38.585 μM
A427	0.836 μM	186.845 μM	169.653 μM
A549	8.769 μM	-	-
AHWG	-	101.691 μM	90.361 μM
Calu-6	0.308 μM	135.284 μM	-
VM-1	9.341 μM	177.178 μM	108.031 μM
VM-21	6.073 μM	116.989 μM	116.849 μM
VM-48	9.475 μM	136.71 μM	128.126 μM
GLC4	5.19 μM	127.157 μM	126.532 μM
GLC4-ADR	4.075 μM	90.837 μM	118.312 μM
HCT116	3.791 μM	42.438 μM	29.566 μM
HCT116 p21 KO	4.155 μM	29.501 μM	26.065 μM

5.3.2. Enhanced accumulation of KP1339 in combination with sorafenib

As the cytotoxicity assays revealed that co-treatment with sorafenib enhanced the efficacy of KP1339 in most of the investigated cell lines, we aimed to identify the underlying mechanisms responsible for the observed synergism. Sorafenib has been recently reported to inhibit multiple ATP-binding cassette (ABC) transporters, which are responsible for multidrug resistance due to enhanced drug efflux [195] for several drugs (e.g. doxorubicin [196], etoposide [197], topotecan [198], imatinib [199], gefitinib [200]). Thus, one possible explanation for the enhanced activity of the KP1339/sorafenib combination might be that sorafenib influences KP1339 efflux or uptake.

Therefore, ruthenium levels after simultaneous treatment of KP1339 with sorafenib were determined by ICP-MS (Figure 41). Comparable to the results shown in Section 3.3.1., significant KP1339 accumulation in a range of 5-10 ng/ 10^5 cells was detected in cells after treatment with 75 μ M KP1339. Moreover, treatment with 150 μ M KP1339 led to further increase of the intracellular ruthenium levels in most cell lines (Hep3B, HCC1.2, VL-8, A549, and SPC111). With regards to the drug combination, sorafenib co-treatment dose-dependently enhanced KP1339 uptake in most cell lines (Hep3B, HepG2, HCC1.1, HCC1.2, VL-8, SPC111). Especially, Hep3B, HepG2, and VL-8 cells turned out to be very responsive to the modulator effects of sorafenib with an increase of intracellular ruthenium of \sim 10-fold. Remarkably, in the ABC-transporter-overexpressing and highly drug-resistant A549 cell model, sorafenib co-treatment had no significant effect on intracellular KP1339 accumulation. This suggests that although sorafenib leads to enhanced KP1339 levels, these effects seem to be not based on inhibition of ABC transporter function. This is in accordance with experiments using KB-3-1 and KBC-1 cell line which differs from KB-3-1 cell line in its ABCB1-overexpression [201]. However, in case of the P-gp overexpressing KBC-1 cells no

synergistic activity of sorafenib in combination with KP1339 could be detected (data not shown).

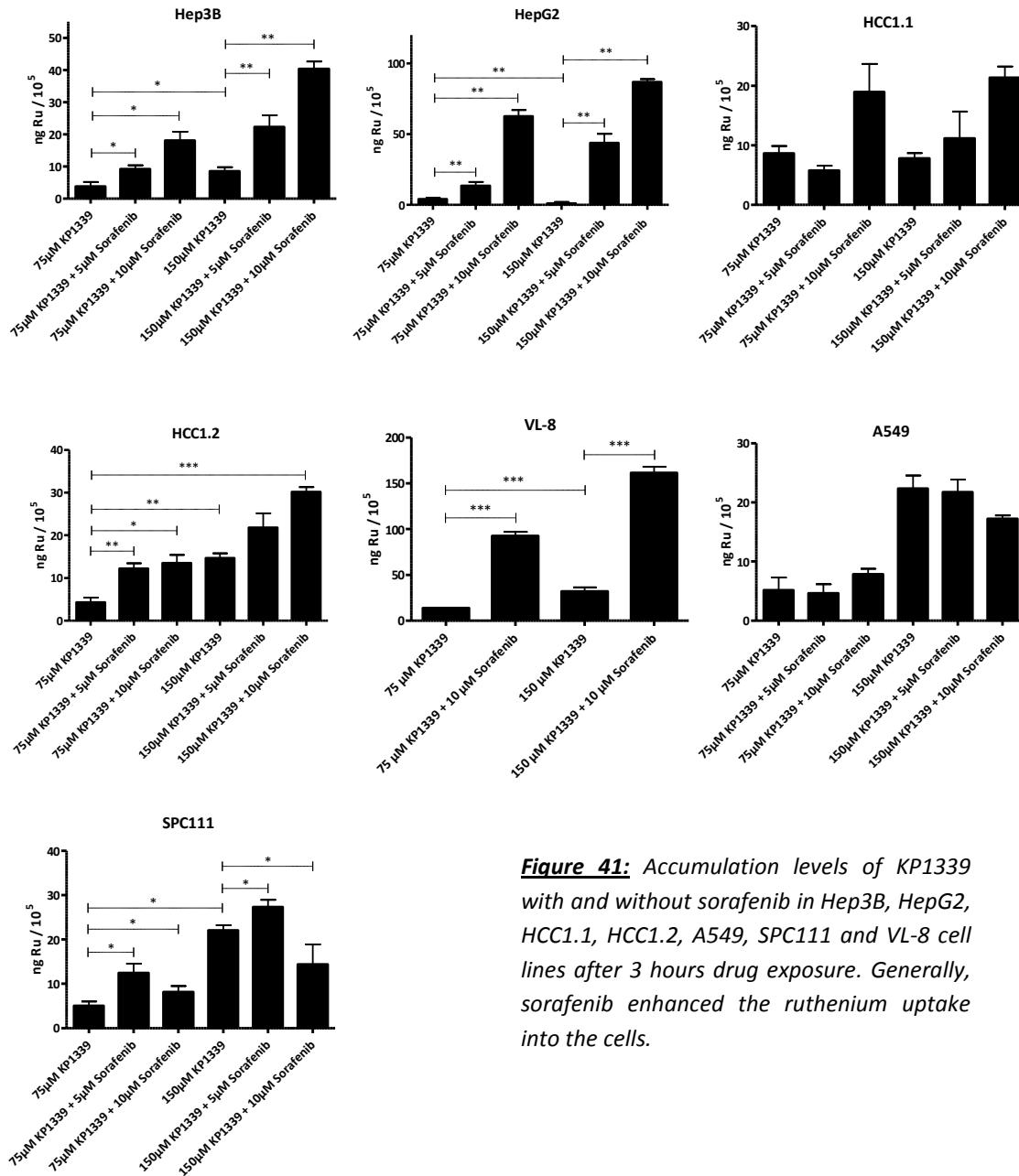


Figure 41: Accumulation levels of KP1339 with and without sorafenib in Hep3B, HepG2, HCC1.1, HCC1.2, A549, SPC111 and VL-8 cell lines after 3 hours drug exposure. Generally, sorafenib enhanced the ruthenium uptake into the cells.

5.3.3 Apoptosis-induction by combination therapy with KP1339 and sorafenib

Cytotoxicity and uptake experiments indicated that sorafenib enhanced activity and accumulation of KP1339 in almost all cell lines investigated. To gain more insights into the mode of action underlying this drug combination, levels of apoptosis induction after drug treatment were determined. To this end, typical signs of apoptosis were examined in drug-treated cells after 24 hours exposure using DAPI staining (Figure 42 and 43), and the number of normal, mitotic, and apoptotic cells were counted.

Comparable to the results obtained in KB-3-1 cells (compare Figure 28 and 29), KP1339 mono-treatment dose-dependently increased the level of apoptotic cells also in Hep3B cells. This resulted in an increase in apoptotic cells from 4.5% in the control to 10 % and 47.7% after treatment with 75 μ M and 150 μ M, respectively (Figure 42). This was accompanied by a significant decrease in the number of mitotic cells from 1.8% to 0.6% and 1.3%, respectively. Also treatment with sorafenib alone (5 and 10

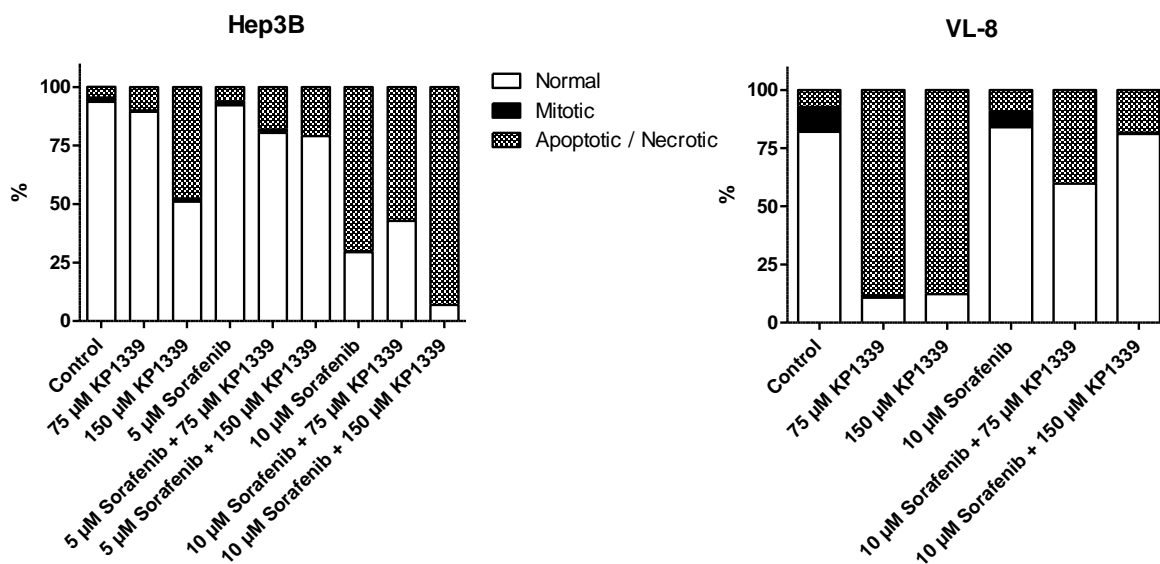


Figure 42: Detection of morphological changes of nuclei after single and combined drug treatment with sorafenib and KP1339. DAPI staining of Hep3B and VL-8 cells was analyzed after 24 hours incubation with the indicated drug concentrations. Percentages of normal, mitotic and apoptotic/necrotic cells are shown.

μM) led to an increase in the number of apoptotic cells to 6.1% and 18.2%, respectively. After exposure to 10 μM sorafenib, a reduction in mitotic cells to 0.4% was observed.

Combination of KP1339 with sorafenib did not enhance the levels of apoptotic cells and was at several concentrations even less effective in apoptosis induction than the single compounds. For example, while 150 μM KP1339 led to 47.7% apoptotic cells, addition of 5 μM sorafenib caused only 20% cell death. Also combination of 75 μM KP1339 with 10 μM sorafenib induced about 20% less cell death than 10 μM sorafenib alone. In contrast, sorafenib co-treatment significantly enhanced the anti-mitotic effects of KP1339 leading to complete loss of mitotic cells after combination of 75 μM KP1339 with 10 μM sorafenib or 150 μM KP1339 with 5 and 10 μM sorafenib.

The combination therapy was also tested for its apoptosis-inducing potential in lung cancer cell line VL-8 (Figure 42). In comparison to Hep3B cells, KP1339 treatment resulted in higher apoptotic levels. Thus, after treatment with 75 μM and 150 μM KP1339 the percentages of normal cells decreased from 82% up to 11% and the amount of apoptotic/necrotic cells increased from 7.3% up to 88%. Again, KP1339 induced very strong anti-mitotic activity reducing the number of mitotic cells from 10.72% to 1% and 0% after treatment with 75 μM and 150 μM, respectively. Mono-treatment of 10 μM sorafenib induced only minor changes in percentages of normal (from 82% to 83.9%), mitotic (from 10.7% to 7%) or apoptotic/necrotic cells (from 7.3% to 9%). Comparably to the results obtained in Hep3B cells, combination of KP1339 with sorafenib was again strongly antagonistic in its apoptosis-inducing potential. Addition of 10 μM sorafenib reduced the number of dead cells from 88% to 40% and 18%, respectively. With regard to the mitotic fraction, the combination of KP1339 with sorafenib again caused total disappearance of mitotic cells (from 10.72% to 0%). This suggests that the synergism of KP1339 with sorafenib is not based on enhanced apoptosis induction but a stronger cytostatic activity.

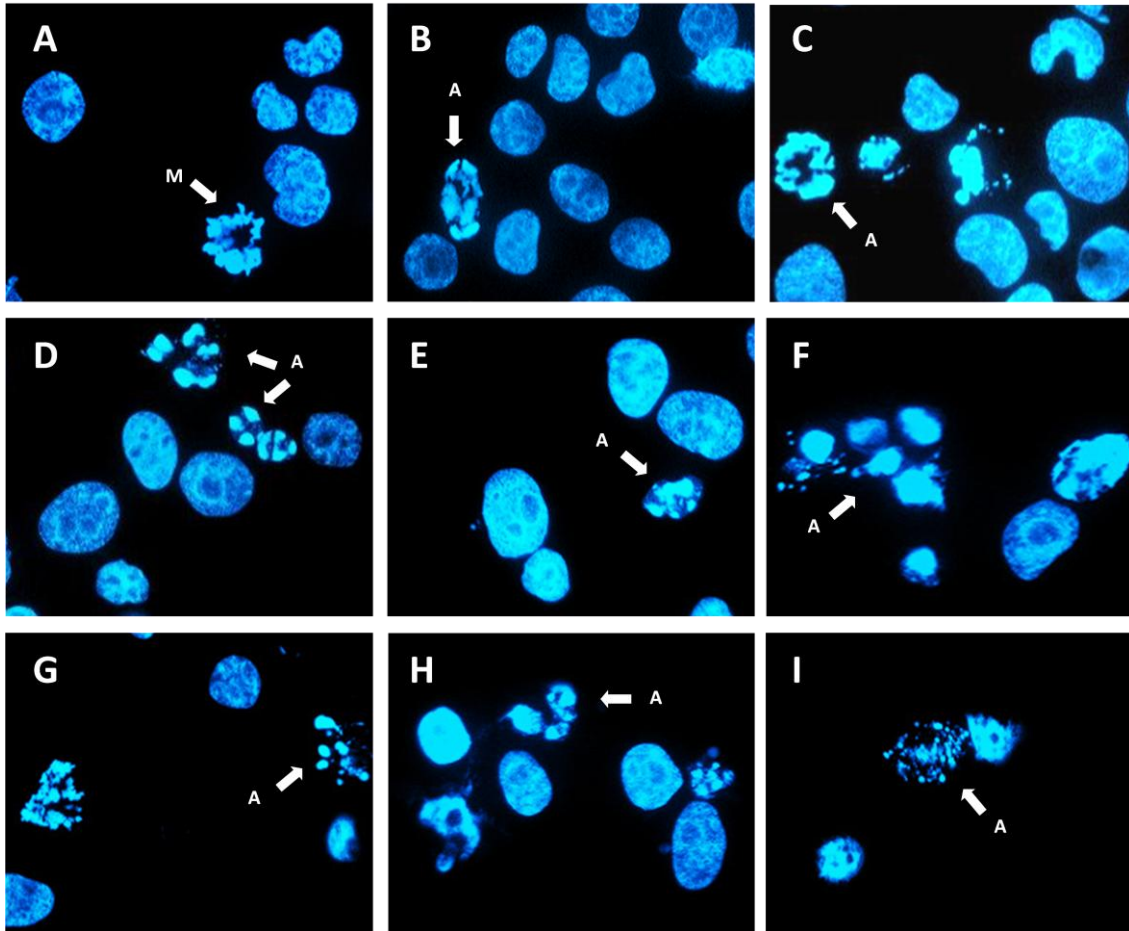


Figure 43: DAPI staining of Hep3B nuclei. The analyses were performed using fluorescence microscopy to visualize the morphological changes after drug exposure for 24 hours. (A) untreated cells, (B) 75 μ M KP1339, (C) 150 μ M KP1339, (D) 5 μ M sorafenib, (E) 5 μ M sorafenib and 75 μ M KP1339, (F) 5 μ M sorafenib and 150 μ M KP1339, (G) 10 μ M sorafenib, (H) 10 μ M sorafenib and 75 μ M KP1339, (I) 10 μ M sorafenib and 150 μ M KP1339. M... mitosis, A... apoptotic bodies.

The reduced apoptosis-inducing potential of the KP1339/sorafenib combination was further analyzed by Western blotting using apoptotic PARP cleavage as a marker. As shown in Figure 44, PARP cleavage in Hep3B cells was induced in a dose-dependent manner after KP1339 mono-treatment. 150 μ M KP1339 led to ~50% cleavage of PARP protein. In accordance to the results obtained by DAPI staining, the levels of apoptotic PARP cleavage were strongly diminished by sorafenib co-treatment.

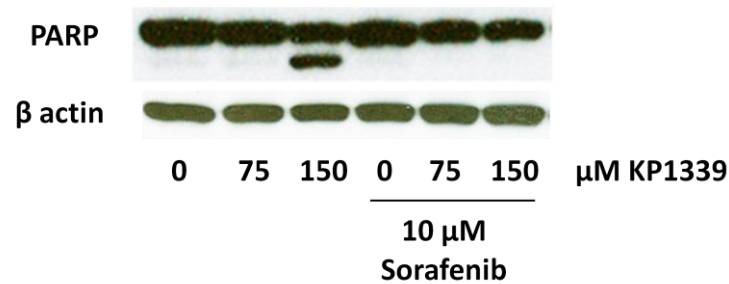


Figure 44: Detection of PARP cleavage in Hep3B cells after 24 hours drug exposure.

Apoptosis is executed either intrinsically via mitochondria or extrinsically by activation of death receptors. One major characteristic of the intrinsic pathway is the disruption of the mitochondrial membrane potential, which leads to release of cytochrome c into the cytosol which then activates the caspase cascade. As shown in section 4.1., KP1339 is able to induce apoptosis via mitochondrial membrane depolarisation and activation of caspase 7. To test whether the combination of Sorafenib with KP1339 has an impact on the KP1339-induced mitochondrial membrane depolarisation, the mitochondrial integrity of Hep3B cells after drug treatment was determined via JC-1 staining (Figure 45). The influence on the mitochondrial membrane potential was detected after 3 and 24 hours drug exposure. Comparable to the results obtained in section 3.1., KP1339 slightly increased the level of depolarised of mitochondria after 3 hours as well as 24 hours treatment. Also exposure with 5 μM sorafenib for 3 hours and 10 μM sorafenib for 24 hours led to increased mitochondrial disruption (from 4% to 8.3% and 6.3%, respectively). With regard to the drug combination, after 3 hours sorafenib cotreatment in general doubled the effects of KP1339 on mitochondria. After 24 hours, the levels of depolarized mitochondria further increased to 15% and 18%, respectively. These data indicate that the reduction in the apoptotic cell number observed in DAPI staining and PARP cleavage is not due to reduced apoptosis induction by the KP1339/ sorafenib combination but due to reduced apoptosis execution.

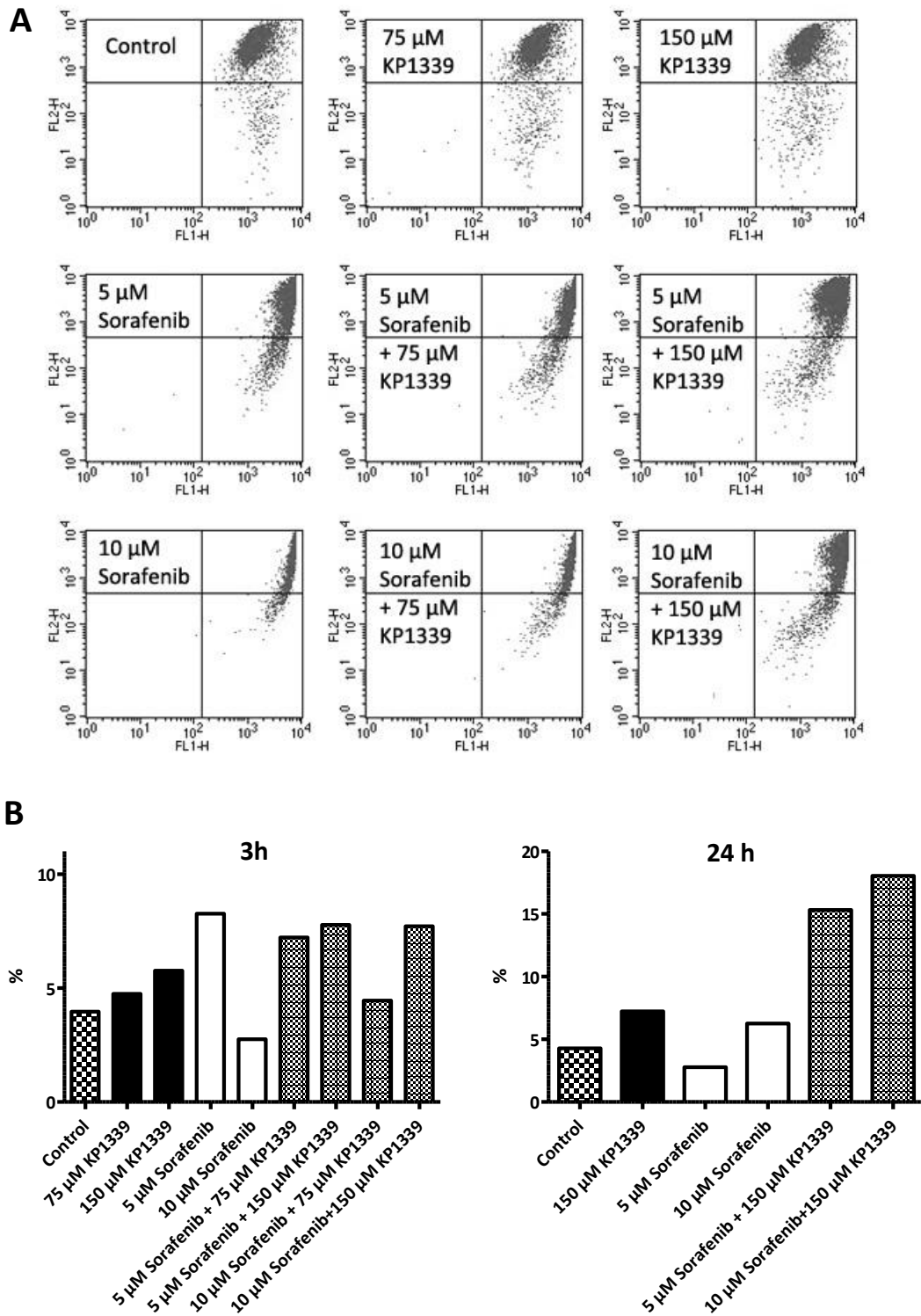


Figure 45: JC-1 stainings of Hep3B cells shown as histogram after 3 hours drug exposure (A) and as % cells with depolarized mitochondria after 3 hours and 24 hours drug exposure (B) at several sorafenib and KP1339 concentrations.

5.3.4. Effects of KP1339 and sorafenib co-treatment on DNA synthesis

To analyze the activity of KP1339 and sorafenib on DNA, Hep3B cells were treated for 6 hours, and the DNA synthesis levels in these samples were investigated using ^3H thymidine incorporation assay (Figure 46). This experiment showed that both drugs inhibited DNA synthesis. Cells exposed with sorafenib alone showed lower levels of DNA synthesis compared to cells after KP1339 treatment. Interestingly, the co-treatment did not induce any enhanced inhibition of DNA synthesis, although both drugs alone demonstrated decreasing levels of DNA synthesis. Unexpectedly, the combination with 10 μM sorafenib and 25 μM KP1339 caused lower activity in altering of DNA synthesis.

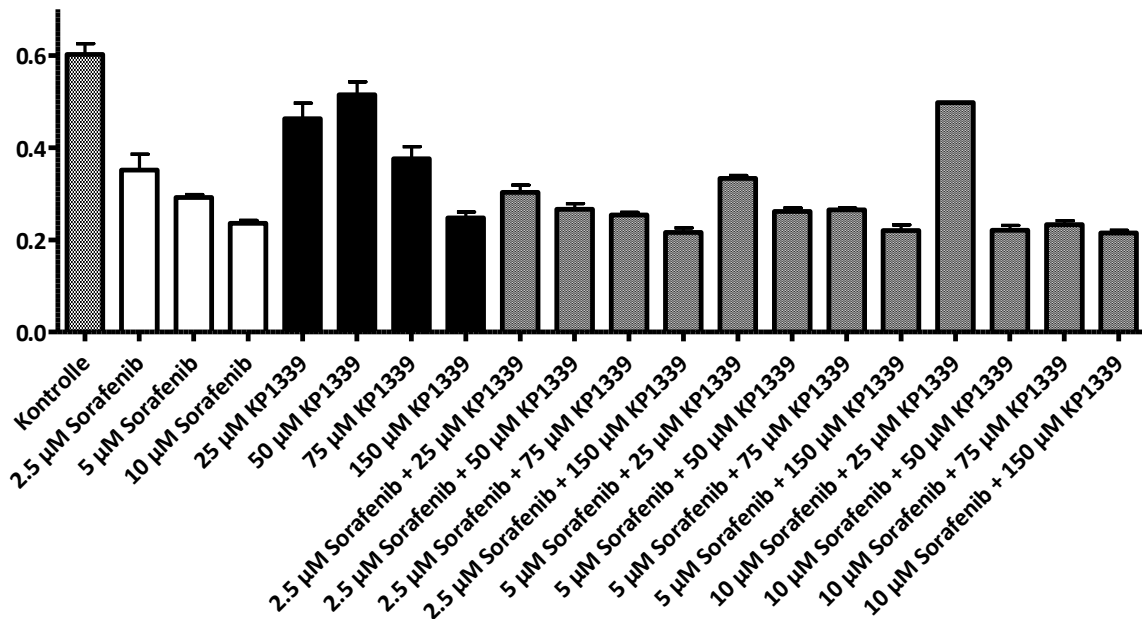


Figure 46: ^3H -thymidine incorporation in Hep3B cells after drug exposure for 6 hours. Sorafenib alone induced stronger inhibition of DNA synthesis in comparison to KP1339 alone. In the combination of these drugs, the levels of DNA synthesis did not differ from the samples treated with sorafenib alone.

5.3.5. Cell cycle alterations induced by KP1339 and sorafenib exposure

To identify the alterations in cell cycle induced by the combination of KP1339 with sorafenib, the cell cycle distribution after 24 hours treatment was evaluated using PI staining and flow cytometry (Figure 47). In all cell lines tested, KP1339 exposure alone resulted in increased G₂/M phase levels. Especially HCT116 and SPC111 cells were most responsive in this respect (from 14.57% to 55.29% and 19.9% to 51.95%, respectively), while in Hep3B only a small increase of cells in G₂/M phase (von 7.1% auf 16.63%) were observed. In general the effects of sorafenib mono-treatment on cell cycle distribution were less pronounced. In accordance to the literature [202-204], sorafenib mono-treatment mainly induced dependent on the cell type and the used concentration either G₀/G₁- or S-phase arrest. Also with regard to the drug combination, the effects were found to strongly differ depending on cell type and drug concentrations.

In Hep3B cells 5 µM sorafenib increased the number of cells in the G₂/M phase (from 8% and 17% by treatment with 75 µM and 150 µM KP1339 to 20% and 21%, respectively). This was accompanied mainly by a decrease of G₀/G₁ phase cells while the number of cells in S-phase remained constant. In contrast, co-treatment with 10 µM sorafenib completely abolished the KP1339-induced G₂/M arrest, leading to an 34% increase in the number of S-phase cells.

Similar effects were observed in HCC1.1 cells. At low drug concentrations (5 µM sorafenib with 75 µM KP1339) sorafenib enhanced the KP1339-induced G₂/M arrest by 40%, all other combinations induced ~ 65% increase of cells in S-phase. Comparable to previous cell lines tested, KP1339 again induced G₂/M arrest with an 2-fold and 1.6-fold increase, respectively. In contrast, 10 µM sorafenib caused a G₀/G₁ cell cycle arrest (from 51.62% to 66.65%). Moreover, the co-treatment of KP1339 and sorafenib led to a decrease by 56% of cells in S phase while the cells mainly arrested in G₀/G₁ phase (from 45.56% after 75 µM KP1339 exposure to 61.51% in combination with 5

μM sorafenib and to 63.52% in combination with 10 μM sorafenib, respectively).

In cell lines, where KP1339 treatment induced very strong G₂/M arrest, namely SW480, HCT116 and SPC111, combination with sorafenib was not able to completely abolish the increase of cells in G₂/M phase after KP1339 treatment. Nevertheless, sorafenib co-treatment decreased the KP1339-induced G₂/M arrest. In addition to the increase of G₂/M induced by KP1339, the sorafenib increased the amount of S-phase cells in these cell models. This led to a drastic reduction of G₀/G₁-phase cells, in the samples treated with the KP1339/sorafenib combination setting, especially at high drug concentrations (Figure 47).

5.3.6. Alterations in p38 MAPK and ERK pathway induced by KP1339/sorafenib combination

Furthermore, in response to stress mammalian cells activate three well-characterized subfamilies of mitogen-activated protein kinases (MAPKs): ERK1/2, Jun N-terminal kinases (JNKs), and p38s [205-206]. It is known that deregulation of MAPK signaling is one of the most common alterations in human cancers. Consequently, sorafenib has been shown to inhibit the MAPK pathway [78, 194, 207]. Therefore, the effects of KP1339/sorafenib combination on this pathway were tested. In all cell lines investigated (Hep3B, HepG2, HCT116, and VM-1 cells), pp38 upregulation was observed after KP1339 mono-treatment. However, addition of sorafenib led to decrease of pp38 in Hep3B and HepG2 cells or total disappear in HCT116 and VM-1 cells (Figure 48). In contrast, ERK1/2 level was not changed in HepG2 cells, while enhanced phosphorylation of ERK was detected after KP1339 mono-treatment and in combination with 5 μM sorafenib. Interestingly, co-treatment with 10 μM sorafenib decreased the pERK signal.

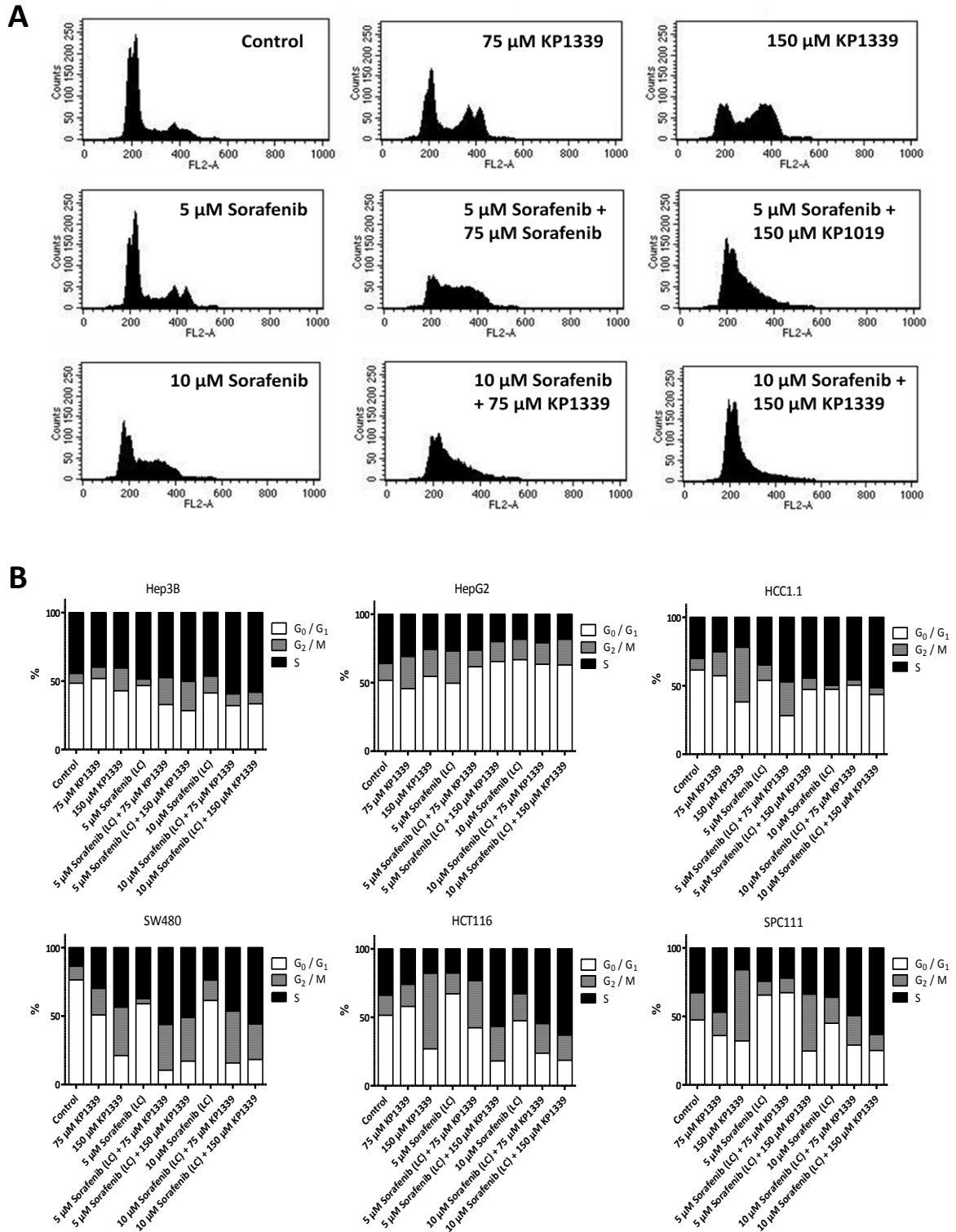


Figure 47: Impact of KP1339, sorafenib, and the combination on cell cycle detected via PI stainings of Hep3B as histogram (A) and several other cell lines as graphs (B. using GraphPad Prism 5.0.

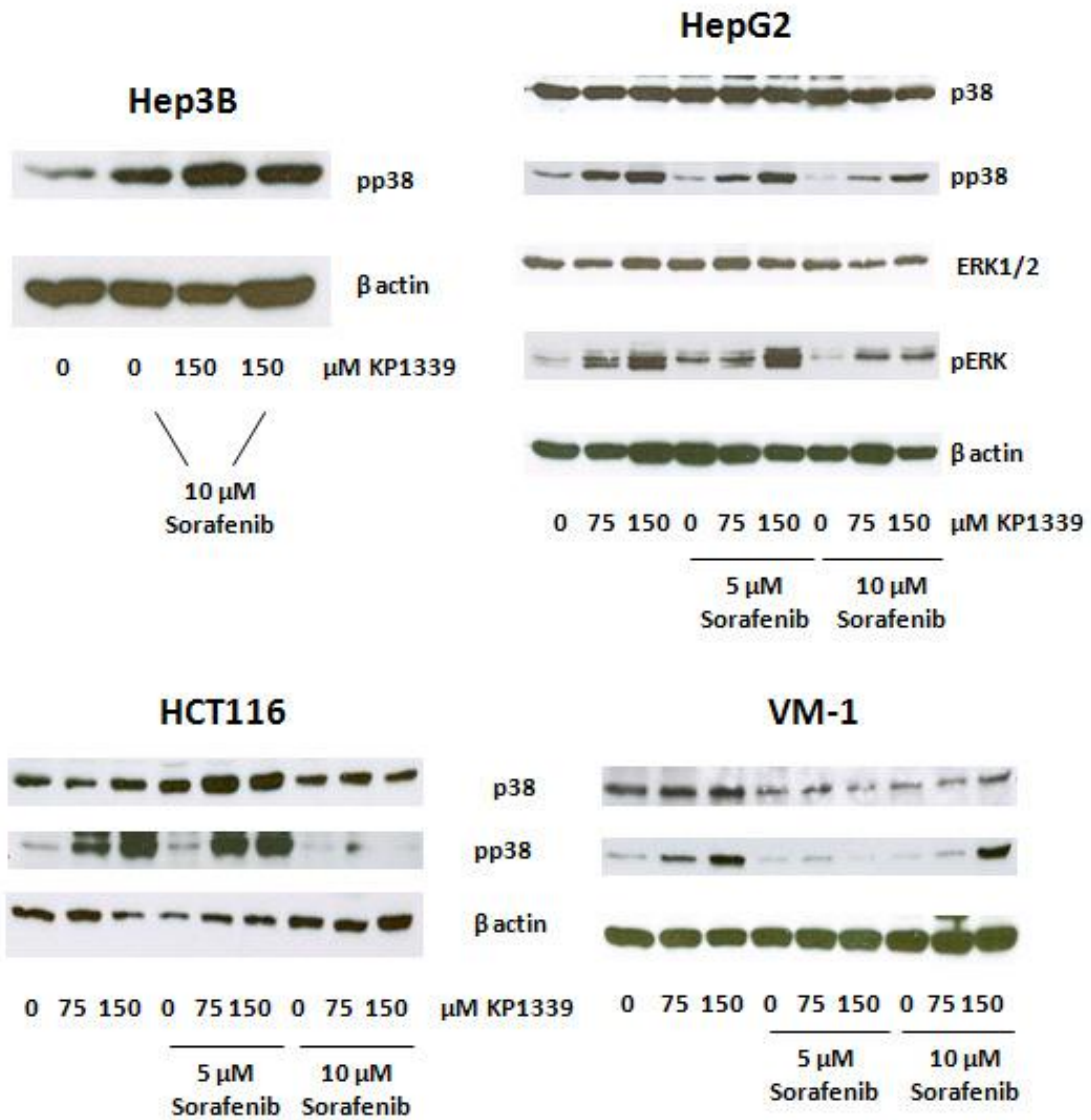


Figure 48: Western blot analyzes in Hep3B, HepG2, HCT116, and VM-1 cells after 24 hour KP1339 and sorafenib exposure. The protein extracts were tested against p38, pp38, ERK1/2 and pERK.

6. DISCUSSION

Cancer is a disease caused by genetic mutations as well as genome alterations in DNA. These alterations allow tumor tissues uncontrolled growth and spreading into diverse organs. When untreated, the development of such distant metastases leads inevitably to the patient's death [115]. The options to cure cancer patients especially surgery are mainly successful in the primary lesions at early-stage disease. At late stage, when the tumors are far progressed and distant metastases have developed, curative treatment by surgery or radiation therapy is often impossible. Therefore, systemic therapy with chemical drugs (or more recent antibodies) is often used to fight cancer at the metastatic stage. There is already a huge repertoire of clinical used chemotherapeutic drugs including several antibiotics (e.g. daunomycin, adriamycin), plant toxins (e.g. vincristine, paclitaxel), antimetabolites (e.g. 5-fluorouracil, cytarabine), as well as several metal compounds (e.g. cisplatin, oxaliplatin). However, especially the phenomena of drug resistance as well as unwanted side effects make the development of new anticancer drugs necessary. Thus, new drugs are frequently screened for their anticancer activity and there are currently several metal-based compounds with promising features [208].

Although the biological activities of ruthenium complexes were first recognized by Dwyer and co-workers in the 1950s [209-210], further researches were mainly performed after discovery and success of cisplatin in 1960s by Rosenberg *et al.* [106-107]. Ruthenium compounds have attracted much attention as promising alternatives to platinum complexes. They show several advantages like tumor-selective toxicity, lower side effects, ligand-exchange abilities analogous to platinum complexes and a well-understood chemistry. KP1019 and KP1339 belong to the group of ruthenium compounds currently developed for anti-cancer treatment. KP1339 is the sodium salt of KP1019 and differs from KP1019 in the indazolium counter ion. It was suggested that these agents might exhibit similar anticancer activities and modes of action

because of their almost identical chemistry [132]. Although KP1019 was tested in a phase I dose-escalation clinical trial, KP1339 was selected for further clinical development [136]. KP1339 showed better pharmaceutical properties, such as 30-fold more aqueous solubility in comparison to KP1019.

The aim of the study was to determine the anticancer activity of KP1339 and to clarify the mode of action of this ruthenium compound. Molecular mechanisms underlying this activity were investigated on gene expression and protein levels including additional experiments detecting inputs on cell cycle alterations, disruptions in DNA-synthesis or mitochondrial depolarization. Moreover, combinations with several other antitumor agents or tyrosine kinase inhibitors were performed in order to clarify their impact on the anticancer activity of KP1339 in the cell and to demonstrate possible synergistic molecular mechanisms induced by these co-treatments.

6.1. KP1019 vs. KP1339

Based on the close chemical relationship between KP1019 and KP1339, the evaluation of their effects on the tumor cells could help to get more information about the mode of action of ruthenium drugs as antitumor complexes. To this end, both drugs were analyzed using different approaches in hepatoma, cervix carcinoma, and colorectal carcinoma cell lines. Generally, it was observed that mechanistically both drugs act at least in most aspects very similar. The most obvious observation in all these experiments was the lower activity of KP1339 in comparison to KP1019.

KP1019 and KP1339 differ in their cytotoxicity in most cases. Almost all cell lines investigated (Hep3B, HepG2, HCC1.1, HCC1.2, KB-3-1 cells) displayed distinct higher sensitivity to KP1019. In contrast, HCT116 cells (a colon carcinoma cell line) were the most responsive cell line to both ruthenium compounds. This sensitivity is surprising as colon cancer cells are known to be highly chemo-resistant with characteristic

features such as p53 mutations [211], overexpression of pro-survival protein bcl₂ [212], and multidrug-resistance genes [213-214].

Furthermore, intracellular accumulation of both drugs was determined as a possible explanation for the different anticancer activity. Ruthenium complexes, such as KP1019 and KP1339, have chemical similarity to iron, and it has been suggested that they accumulate into the cell via transferrin [123, 215], which is able to transport iron and other species (for example gallium) into cells [216]. Transferrin receptors are upregulated in tumor cells because of the increased requirement for iron. Thus, ruthenium complexes can accumulate specifically in tumor cells by interaction with the iron binding sites of transferrin [215, 217]. Additionally, these drugs have also been shown to bind to albumin [218] and diverse intracellular molecules, such as nucleotides and glutathione [219-226]. These interactions and binding partners could act as natural drug carriers for ruthenium drugs like KP1019 and KP1339.

Interestingly, in all models investigated (Hep3B, HCC1.1, HCC1.2, KB-3-1, and HCT116 cells), KP1019 accumulated in higher amounts into the cell. However, the drug uptake could not fully clarify the mechanisms leading to differences in apoptosis induction between KP1019 and KP1339. The accumulation levels of KP1019 did not correlate with the anticancer activity determined by cytotoxicity assays. High KP1019 accumulation did not necessarily predict the cytotoxic activity, comparable to the study by Kapitza *et al.* [132]. Especially in Hep3B and HCC1.1 cells, highest KP1019 levels in the cell were detected, although they were comparable more resistant against KP1019 in cytotoxicity assays.

In further analyzes, the subcellular localization of KP1019 and KP1339 in the cell was analyzed as a possible mechanisms underlying the different activities of these ruthenium complexes. The accumulation of these ruthenium complexes was rapid as 1 hour drug exposure already induced significant anticancer activity, and ruthenium levels in the cell did not increase with longer drug incubation. Interestingly, KP1019

DISCUSSION

was mainly located in cytosol (~75%), although KP1339 was found in high levels in nuclei (~90%). As described previously, ruthenium drugs might target DNA [227] comparable to cisplatin [228] or doxorubicin [229]. KP1019 is able to bind strongly to serum proteins *in vitro* [1, 216], which interaction might be also found with proteins in the cytosol. These findings suggest that the higher cytotoxicity of KP1019 might be based on the anti-tumor activations in cytosol, while the nuclear localization of KP1339 seem to correspond to a lower cytotoxic activity. Consequently, DNA damages induced by ruthenium compounds cannot be major mechanism to trigger apoptosis in cancer cells. KP1019 and KP1339 lead to apoptosis via several mechanisms which might be initiated by targets residing in the cytosol.

In parallel to experiments regarding cytotoxicity and drug accumulation, DAPI stainings were performed to determine alterations in nuclear morphology after drug treatment. KP1019 induced more cells to undergo apoptosis in comparison to KP1339 which correlates with cytotoxicity tests. Moreover, KP1019 and KP1339 in highest concentrations demonstrated an inhibiting effect on cell proliferation as no mitotic cells could be detected in nuclear morphology analyzes. To determine the mechanisms for apoptosis induction, the integrity of the mitochondrial membrane potential was also measured. Mitochondrial membrane depolarization was observed in a drug-dependent manner. For similar level of mitochondrial depolarization induced by KP1019, ~2-fold higher concentrations of KP1339 were required. Comparable to other studies [131-132], KP1019 and KP1339 induced apoptosis by direct action on the mitochondrial membrane which is a characteristic of Ru(III) complexes.

Moreover, protein cleavages by caspases typical for apoptosis induction were detected in Hep3B, HepG2, and KB-3-1 cells. In all tested cell lines, PARP cleavage was observed after KP1019 as well as KP1339 exposure. Again, more potent cleavage was observed for KP1019. Moreover, it was also shown that caspase 3 and 8 levels remained unchanged in all cell lines tested, although Kapitza *et al.* [131] demonstrated a downregulation of procaspase 3 by KP1019 treatment of SW480 cells after 4 and 8

hours. Moreover, drug exposure triggered caspase 7 cleavage in all cell lines investigated and downregulation of caspase 9 only in HepG2 cells. These results indicate that the activation of intrinsic pathway of apoptosis by KP1019 or KP1339 is cell line-dependent at least with respect to caspase activation.

Following analyzes for apoptosis induction, impacts of ruthenium drugs on cell cycle distributions were analyzed using PI staining and FACS analyzes. The treatment with ruthenium complexes led KB-3-1 cells to arrest in G₂/M phase of the cell cycle in a drug- and dose-dependent manner. These alteration in cell cycle caused by KP1019 and KP1339 are observed in more or less all tested cell lines suggesting that both drugs act in a very similar manner to growth inhibition and to induce apoptosis. Together with the results obtained in DAPI stainings, it can be concluded that the tested ruthenium drugs target cell proliferation because of the disappearance of mitotic cells after drug treatment. Notably, many studies have shown that exposure to several ruthenium complexes, such as KP1019-analogue imidazolium salt NAMI-A, lead to the arrest of cells in G₂/M phase [230-231]. G₂ checkpoint prevents cells from initiating mitosis when they experience DNA damage during G₂, or they progress into G₂ with some unrepaired damage inflicted during S or G₁ phases [152, 232]. As described previously (compare to section 2.6.), the p53 tumor-suppressor protein, which controls genes involved in cell death and DNA repair, is a major transcription factor playing a key role in the regulation of G₂/M checkpoint activation after stress by suppressing or transactivating specific genes [233]. However, also tumor cells with mutant p53 tend to selectively accumulate in G₂ after treatment with KP1019/KP1339. This fact indicates that G₂ arrest is based on p53-independent mechanisms [147]. An alternative explanation for the observed G₂/M arrest might be the activation of p38. Phosphorylation of p38 leads to activation of other factors leading to cell cycle arrest or apoptosis [234-235]. To prove this hypothesis, p38-inhibitors can be used in combination with KP1339, and the changes in activity of this ruthenium compound can be investigated. Consequently, cell cycle arrest in G₂/M phase might be a typical

mechanism of heterocyclic ruthenium compounds with anti-tumor activity. Moreover, cell cycle arrest points towards DNA double strand breaks or genetic errors like the ones typical for platinum compounds like cisplatin [236].

Based on the chemical similarity of ruthenium to platinum, it is expected that ruthenium compounds show in some aspects similarities in anti-tumor activities with cisplatin. Treatment with cisplatin induced forming of DNA-adducts resulting in apoptosis [237]. Consequently, several studies have also shown that the ruthenium complex KP1019 might be able to interact with DNA and to form cross-links or induce strand breaks [131]. Although platinum compounds induce apoptosis mainly via monofunctional adducts, intrastrand and interstrand crosslinks [238-240], these ruthenium compounds trigger cell death via mitochondrial pathway additionally to induction of DNA damages [132]. Moreover, it was detected that endogenous bcl₂ down-modulation may explain lower sensitivity to ruthenium and platinum compounds in some cell lines [132, 241-242]. Activation of caspase 3, 8, and 9 is attenuated in cisplatin-resistant cells [1, 243-248], whereas downregulation of procaspase 3 [131] and caspase 9 beyond cleavage of caspase 7 were determined. Another similarity of these compounds is inducing G₂ cell cycle arrest typical for DNA damaging agents [236]. Nevertheless, the intracellular ruthenium-protein binding pattern of KP1019 and KP1339-treated cells distinctly differed from the platinum-protein-binding pattern observed after cisplatin treatment. Additionally, KP1019-induced cell death is independent of the p53 status in tumor cells [1], although p53 promotes increased sensitivity to cisplatin [249]. Interestingly, cisplatin is not a substrate for the P-glycoprotein which is overexpressed in multi-drug resistant cells and functions as a drug efflux pump [250-252]. In contrast, overexpression of P-glycoprotein reduced weakly but significantly KP1019 activity in cancer cells [134].

In summary, both ruthenium drugs are promising metallopharmaceuticals against several cancer types, especially against platinum-resistant cell lines. They have in most aspects similarities, although KP1019 showed generally higher anti-tumor activity.

They displayed correlating cytotoxicity, induction of mitochondrial depolarization, triggering of apoptosis through caspase 3 and 7, and cell cycle arrest in G₂/M phase. Based on the high activity of KP1019, it may be hypothesized that KP1019 might be able to accumulate at higher levels in the cell or might lead to inhibition of drug efflux pumps. Notably, several studies reported that KP1019 acts as a substrate and as an inhibitor of ATPase activity of P-glycoprotein, although the interaction between KP1019 and P-glycoprotein can be influenced by serum proteins [134]. This could suggest that KP1019 cannot be exported via this pump from the tumor cells. Nevertheless, higher accumulation levels of KP1019 cannot fully explain its higher cytotoxicity in all cell lines investigated. Another suggestion for different anti-tumor activities of KP1019 and KP1339 is their different localization in the cell. Apparently, KP1019 remains in cytosol, while KP1339 accumulates mainly in nuclei of tumor cells. Nevertheless, it was hypothesized that KP1019 induced DNA strand breaks characterized by ruthenium compounds although it localized mainly in cytosol. It is suggested that oxidative stress induced by KP1019 caused DNA damages [131]. KP1339 displayed lower activity although its localization in nuclei, and KP1339 higher cytotoxicity probably via protein interactions in cytosol. Consequently, the ability to damage DNA cannot be the only reason for anti-tumor activity of these ruthenium compounds, and major targets for this anticancer ruthenium compound seem to reside in the cytoplasm. Probably, the binding of KP1019 to cytosolic proteins corresponds its activity.

6.2. Combination tests with KP1339 and other chemical compounds

KP1339 is a ruthenium drug whose mode of action is not fully clarified yet. To gain more insights into the mechanism underlying the anti-tumor activity of KP1339, carcinoma cell lines were treated with this ruthenium drug in combination with several other chemical compounds. With regard to the theory that ruthenium complexes accumulate into the cell in a transferrin-dependent manner [253], cells were co-incubated with FeCl_3 and Gallium nitrate. These chemical complexes are known to utilize the transferrin-dependent pathway for accumulation into the cell [254-255].

Generally, FeCl_3 co-treatment enhanced activity of KP1339 in most hepatoma cell lines tested. In contrast, KB-3-1 cells did not display any enhanced anti-tumor activity of KP1339 in a FeCl_3 -dependent manner.

Iron is an essential element for virtually all living organisms. Iron is required for survival and proliferation, as a constituent of other hemoproteins, iron-sulfur (Fe-S) proteins, and proteins that use iron in other functional groups to carry out essential housekeeping functions for cellular metabolism. However, iron also is possible toxic agent because of the inter-conversion of Fe(II) and Fe(III) and side reactions between iron and oxygen [256]. To this end, cellular iron homeostasis necessitates tight control of iron uptake, storage, and export and management of intracellular iron distribution [257]. In mammals, iron is primarily absorbed from the diet by intestinal epithelial cells through the apical membrane protein divalent metal transporter 1 (DMT1). These cells export iron into the bloodstream through basolateral membrane protein ferroportin [257-259], and exported iron binds to the serum carrier transferrin for iron transport throughout the body. Body iron is sensed by the liver, and in response liver synthesizes and secretes hepcidin. Hepcidin negatively regulates iron export from intestinal cells via degradation of ferroportin, decrease of serum iron concentration, and increase of intracellular iron content [260]. Moreover, Tfr1 expression is

regulated by RNA binding-proteins IRP1 and IRP2. At low cellular iron concentrations, degradation of TfR1 mRNA is inhibited, and the expression is increased leading to transferrin-bound iron uptake [257, 261]. Intracellular iron levels are stringently regulated as a labile iron pool (LIP) which provides optimum iron levels for vital biochemical reactions and limits the availability of free iron for generation of ROS. Once iron enters the cell, the portion that is not needed for immediate use is stored by ferritin [262]. In accordance to this, treatment with FeCl₃ would lead to downregulation of TfR expression, upregulation of transferrin, and probably to oxidative stress because of presence of harmful “free” iron.

In humans, hepatic iron overload diseases may occur leading to the development of cirrhosis and hepatocellular carcinoma [263]. Furthermore, many studies have shown that transferrin receptor 2, which is responsible for iron internalization in addition to transferrin receptor 1 via binding to transferrin [264], is highly expressed in the liver [265]. The study by Heffeter *et al.* has shown that TfR-overexpressing cells were hypersensitive to KP1019 [134]. Thus, more transferrin-bound ruthenium compounds can be taken up into the cell via TfR. This might explain the higher sensitivity of hepatoma cell lines to KP1339 in combination with FeCl₃. However, it has been shown that Hep3B cells have no detectable TfR2 expression, while HepG2 cells express this receptor endogenously [266]. As the effect of FeCl₃ was not higher in HepG2 cells than in Hep3B cells, it cannot be explained by expression of TfR2 in hepatoma cell lines. Additionally, another study has shown that even in HepG2 cells TfR1 expression was much higher than TfR2 [267]. To this end, it can be suggested that KP1339 accumulation is TfR2-independent, and probably occurs mainly via TfR1.

Moreover, hepatocytes are the main storage site of iron in the body, and accordingly the liver is the organ most likely to be afflicted by iron overloading [268]. Iron overloading causes the generation of “free” iron (redox active) which catalyzes the formation of highly toxic reactive oxygen species (ROS) [269]. In accordance, ROS production leads to production of antioxidants to reduce any possible damages in the

cell. The major and most studied cofactors are ascorbic acid and glutathione (GSH), which are also linked to iron homeostasis [270-271]. Ascorbic acid, as a reducing agent, is able to release iron from ferritin and mobilize iron from the reticuloendothelial system to transferrin, which leads to increased iron availability and may prevent tissue iron overload [272-273]. Furthermore, GSH has been found to be elevated in a number of drug-resistant tumor cell lines [274-278]. Huang *et al.* have shown that GSH level is increased in human HCC [279]. Another feature of these reducing agents is that they lead to reduction of the ruthenium (III) complexes resulting in activation of these compounds such as KP1019 and KP1339 [225]. Moreover, it was shown that concentration-dependent accumulation of iron was accompanied by a biphasic change in the intracellular GSH level. Concentrations up to 80 μM iron, corresponding the concentrations tested in section 3.2, resulted in marked increase in GSH levels [280]. To this end, higher GSH levels dependent on iron overload and ROS production may explain the synergistic activity of KP1339 in combination therapy with FeCl_3 in hepatoma cell lines.

Additionally, combination therapy of KP1339 and Gallium nitrate was tested in Hep3B and KB-3-1 cells. Comparable to the results obtained with FeCl_3 , Hep3B cells displayed high synergism, while this effect was less pronounced in KB-3-1 cells. Gallium has been shown to share several properties with iron with respect to Tf binding [281], cellular uptake by TfRs [282-283], and incorporation into ferritin [283-284]. Both elements are present in intracellular “pools” in the cell and may compete for binding to macromolecules essential for cellular function [192]. Moreover, Chitambar *et al.* have demonstrated that exposure of HL60 cells (leukemia cell line) to Tf-Ga results in a decrease in iron uptake, an increase in cellular TfR number, and a subsequent growth arrest of these cells [285]. This increase of TfR expression might lead to higher accumulation and anti-cancer potential of KP1339. Furthermore, the inhibition of iron uptake after gallium treatment may render cells sensitive to the interference of iron/redox homeostasis by KP1339.

Also in case of doxorubicin (adriamycin), it was demonstrated that apoptosis is accompanied by a significant increase in TfR-mediated uptake of transferrin iron and that blockade of iron uptake by an anti-TfR antibody abolishes adriamycin-induced apoptosis [286]. Interestingly, combination of KP1339 with adriamycin showed additive to antagonistic activity, but no synergism. This observation can be explained by anti-cancer activity of adriamycin. Adriamycin belongs to the group of anthracyclines with ability to intercalate into DNA and induce DNA damages followed by growth arrest in G₁ and G₂ [287-289]. To this end, it suggests that adriamycin features additional mechanism resulting in apoptosis and may abolish the anti-tumor activity of KP1339.

Another drug, which has been shown to interfere with the cellular iron metabolism is triapine. Triapine is an iron chelator and known to inhibit the iron-dependent enzyme ribonucleotide reductase which catalyzes the reduction of ribonucleotides to deoxyribonucleotides and is essential for cell proliferation. After formation of an intracellular Fe-complex, triapine is also able to generate reactive oxygen species (ROS) [193], and the characteristic of this thiosemicarbazone makes it very interesting for co-treatment with KP1339. As mentioned previously, ruthenium drugs such as KP1019 are suggested to induce oxidative stress reactions resulting in DNA damages [131]. Based on these similarities in mode of action, the co-treatment of KP1339 with triapine was performed. Comparable to the results obtained with FeCl₃ and Gallium nitrate, combination of KP1339 and triapine showed strong synergistic effects in Hep3B cells, while KB-3-1 was very resistant against this co-treatment.

In general, all these complexes are known to play a role in iron metabolism based on their common uptake mechanism via transferrin and/or as an iron chelator. Especially hepatoma cell models showed enhanced sensitivity to KP1339 in combination with these compounds. Nevertheless, alterations in iron homeostasis and ROS production cannot fully explain the mode of action of KP1339 that probably features additionally mechanism to induce apoptosis.

6.3. Combination tests with KP1339 and tyrosine kinase inhibitor sorafenib

Previous analyzes have shown that KP1339 is able to trigger the intrinsic cell death pathway resulting in apoptosis, probably via ROS production and alterations in iron metabolism. In addition, this ruthenium drug showed high activity mainly in hepatoma cell models after mono-treatment as well as combination with several chemical compounds. As sorafenib (BAY 43-9006) is the currently approved first-line therapeutic against hepatocellular carcinoma (HCC), the effects of KP1339 on sorafenib efficacy were tested. Sorafenib is an oral, small-molecule tyrosine kinase inhibitor targeting vascular endothelial growth factor (VEGF) receptors 2 and 3, serine kinase B-Raf, Raf-1, and platelet-derived growth factor receptor (PDGFR) [78, 290]. Due to its impressive activity, sorafenib moved into phase II and III clinical trials [291], and FDA has approved sorafenib for treatment of renal cell carcinoma (RCC) and HCC.

In this study, combination of KP1339 and sorafenib was tested in several cell models with a focus on liver cancer. In all cell lines investigated, additive to synergistic activities were observed after co-treatment with KP1339 and sorafenib. Notably, this enhanced activity was detected especially in HCC cell lines. This observation might be explained by alterations of KP1339 accumulation levels induced by sorafenib. It was demonstrated that addition of sorafenib increased ruthenium levels up to ~10-fold higher in almost all cell lines tested (Hep3B, HepG2, HCC1.1, HCC1.2, VL-8, and HCT116 cells), except lung carcinoma model A549.

This might be explained by interactions of KP1339 and sorafenib with several drug transporters. It has been shown in some cell models that sorafenib is transported by the multidrug-resistance-conferring efflux transporters ABCB1 (P-gp) and ABCG2 (BCRP) and inhibits the function of these ABC transporters [195, 292]. As previously mentioned, KP1019 is a P-gp substrate and the overexpression of P-gp reduced KP1019 activity [134]. Consequently, sorafenib might inhibit the P-gp-dependent

KP1339 efflux resulting in higher ruthenium accumulation after co-treatment with sorafenib. This might be the reason why in HepG2 cells with higher P-gp levels a stronger enhancement of ruthenium accumulation in combination with sorafenib was observed as compared to Hep3B cells with lower P-gp levels (especially at higher sorafenib concentrations) [293]. In contrast, KB-C-1 cells with overexpressed P-gp and A549 cells with upregulated MRP1 did not demonstrate synergistic activity of KP1339 and sorafenib (data not shown).

Moreover, another study demonstrated that sorafenib is a substrate for efflux from cells by RLIP76. RLIP76 is a stress-responsive membrane protein and plays a key role in defending cancer cells from radiation, chemotherapeutic toxin-mediated apoptosis, and oxidant injury [291] via mediating efflux of GSH-conjugates and chemotherapeutic agents from cells [294]. Moreover, increased expression of RLIP76 was observed in several human tumors, such as kidney cancer [291, 295]. Sorafenib is a competitive inhibitor of RLIP76-mediated glutathione conjugate transport [291]. As mentioned previously, KP1019 can be reduced and get activated by glutathione. By Schluga *et al.* on interaction of GSH and KP1019 as well as with other ruthenium compounds was proven [225]. However, these investigations did not report any conjugates of GSH and KP1019 as well as KP1339 so far. Nevertheless, a possible conjugation to GSH might explain the higher accumulation and stronger cytotoxicity of KP1339 in combination with sorafenib.

Furthermore, additive to synergistic activity of the tested co-treatment might also be explained by enhanced cytotoxicity induction. Based on the assumption that the anti-tumor activity of KP1339 is mainly mediated by ROS production, any effect of sorafenib leading to imbalance of the intracellular redox homeostasis might serve as an explanation for the observed synergistic activity. Reactive oxygen species (ROS), including O^{2-} , OH and H_2O_2 , are important in signal transduction and regulation of several pathophysiological processes, such as cell cycle progression and apoptosis [296-297]. Cells produce ROS through multiple mechanisms. However, the major

source of ROS is mitochondria [298]. Electron leakage from the mitochondrial respiratory chain may react with molecular oxygen resulting in formation of superoxide, which can be converted to other ROS [299]. To prevent the cells from oxidative damage of lipids, proteins, and DNA, intracellular ROS levels must be strictly controlled [300]. For maintaining ROS homeostasis, cells balance ROS generation with their elimination by ROS-scavenging systems such as superoxide dismutases (SOD1, SOD2, and SOD3), glutathione peroxidase, peroxiredoxins, glutaredoxin, thioredoxin, and catalase. An increase in the level of ROS may result in transient cellular alteration and further in irreversible oxidative damage leading to cell death [299].

Moreover, several studies have shown that oxidative stress is involved in the process of carcinogenesis [301-304]. The regulation and recognition of ROS production occurs via Ras-Raf-MEK1/2-ERK1/2 signalling and the p38 mitogen activated protein kinases (MAPK) pathway. Notably, Ras-Raf-MEK1/2-ERK1/2 signalling is related to oncogenesis while p38 MAPK pathway participates in cancer suppression via inducing apoptosis or cellular senescence [234, 305-306]. Inhibition of Raf by sorafenib directly interferes with this pathway and inhibits the activation of ERK and p38.

Oxidative stress and Ras activation lead to the production of ROS [307]. In cells with activated Ras-Raf-MEK sorafenib, ROS cause non-apoptotic, oxidative cell death [308]. Furthermore, oncogenic Ras activates MEK, p38, and other downstream kinases and proteins which in turn suppress Ras-induced cell proliferation by blocking activation of JNK. In accordance to ROS production, p38 signalling cascade may be activated which is prerequisite for oxidative stress-mediated functions of ROS such as apoptosis in cancer cells [305, 309].

Through activation of Ras, several other components in the cell are upregulated or blocked. For example, oncogenic Ras induces upregulation of vascular endothelial growth factor (VEGF) [310] which has been reported as an additional target of

sorafenib. Notably, preliminary results obtained using the antibody array screen showed that KP1339 short term exposure enhanced phosphorylation of VEGFR in colon adenocarcinoma cell line SW480 cells (data not shown). Notably, the stimulation of VEGFR is an important antiapoptotic factor resulting in enhanced proliferation of tumor cells. Thus, KP1339 mono-treatment may result in escape of tumor cells from apoptosis by activation of several pathways strongly suppressed by addition of sorafenib. These observations suggest that enhanced anti-tumor efficacy of the KP1339/sorafenib combination might be based on inhibition of KP1339-induced activation of e.g. VEGFR by sorafenib.

Indeed, our data showed that KP1339 treatment stimulated phosphorylation of p38 and ERK. KP1339 mono-treatment led to strong increase of pERK phosphorylation which was downregulated after addition of sorafenib. Sorafenib has been shown to inhibit the MAPK signaling cascade in both melanomas and breast cancer preclinical models and ERK signaling in HCC models [78, 194, 207]. In case of the ERK1/2 pathway, phosphorylation activates ERK1/2, followed by translocation to the nucleus. Here, it phosphorylates several nuclear transcription factors such as Elk-1, Myc, CREB, and FOS, which subsequently bind promoters of many genes resulting in stimulation of cell proliferation, differentiation, and survival [311-313]. Similar to observations in VEGFR expression, KP1339 stimulated the phosphorylation of ERK1/2 probably based on its potential to produce ROS. The inhibition of KP1339-induced pERK by sorafenib suggests that tumor cells were not able to activate survival pathways and consequently underwent apoptosis triggered by KP1339 mono-treatment. Moreover, similar results were found for p38, where phosphorylation also increases after KP1339 treatment. Again, co-treatment with sorafenib blocked this survival pathway activation. With regard to these findings, ROS production by KP1339 may activate p38 MAPK while sorafenib inhibits the Ras-induced p38 phosphorylation. These alterations in phosphorylation of ERK and p38 correspond with other studies regarding activities of sorafenib [194, 207, 314]. Notably, in both cases the efficacy of 125sorafenib was

able to abolish partially or totally the upregulation of pERK and pp38 induced by KP1339.

Furthermore, cell cycle alterations dependent on 126orafenib/KP1339 co-treatment were investigated. In almost all cell lines investigated, KP1339 mono-treatment induced G₂/M cell cycle arrest (compare to section 5.3.5). Regarding to the suggestion that KP1339 causes ROS production, several studies have shown that ROS are able to trigger activation of cell cycle checkpoints [315]. Moreover, ROS production in cells has been reported to peak in the G₂/M phase of the cell cycle in some studies [316]. Additionally, other reports have indicated that phosphorylation of p38 MAPK is required for the induction of cell cycle arrest in the G₂ phase dependent on environmental stress [154, 317]. As p38 phosphorylation has been shown to increase in response to ROS [318], KP1339 might induce G₂/M phase arrest based on the activation of p38 through ROS generation. Moreover, an antibody array screen in SW480 cells indicated that other key regulators in G₂/M phase, such as CDK1 and Cdc25b, were downregulated by KP1339 mono-treatment (data not shown).

In contrast to KP1339, 126orafenib alone in our experiments caused G₀/G₁ or S cell cycle arrest. In accordance, other reports have also shown that sorafenib is able to cause G₁ [202-203] or S phase arrest [204]. Consequently, sorafenib decreased the expression of severe key regulators of the G₁/S transition such as cyclin D1, cyclin D3, CDK4, and CDK6 [202, 319]. Additionally, it was found that mouse embryonic fibroblasts were arrested in G₁ phase with a 70% decrease in cyclin D1 levels, when cells were treated with NAC resulting in reduction in intracellular redox state [320].

The combination of KP1339 and sorafenib showed mainly G₀/G₁ cell cycle arrest indicating that sorafenib abrogates or overrides the KP1339-induced G₂/M arrest. The enhanced G₀/G₁ cell cycle arrest in response to combination treatment is very similar to the study by Heim *et al.* who have worked with sorafenib in combination with oxaliplatin or cisplatin [321]. In this study, sorafenib abolished the G₂/M arrest

induced by cisplatin, which was suggested to be based on sorafenib-induced inhibition of CDC2 expression, a protein which is a regulator in G₂/M phase [321]. Similar interactions might be the underlying mechanisms explaining the reduction of KP1339-induced G₂/M arrest by sorafenib treatment.

Our data showed that the synergistic activity of KP1339/sorafenib combination may be based at least in part on uptake mechanisms, such as drug transporters, and/or intracellular processes caused by ROS production. Furthermore, another explanation for the synergistic activity of sorafenib and KP1339 might be the induction of ER stress via different but synergizing pathways. Rahmani *et al.* have suggested that sorafenib may induce apoptosis additionally to known mechanisms, such as targeting MAPK pathway and VEGFR, in a MEK1/2-ERK1/2-independent manner [322]. In this study, they have demonstrated that sorafenib induced cell death in human leukemia cells through generating of ER stress rather than inactivation of the MEK1/2-ERK1/2 pathway [322]. Sorafenib treatment led to rapid increase in phosphorylation of eIF2 α and PERK, which have been shown to protect cells against ER stress inducers [323-325]. They have reported that these events were accompanied by pronounced generation of ROS through a mechanism dependent on cytosolic-calcium mobilization and a significant decline in GRP78/Bip protein levels [322]. Interestingly, similar results were observed in our antibody array screen and Western blot analyzes (data not shown). After 1 hour KP1339 exposure of Hep3B and HCT116 cells, the level of phosphorylated eIF2 α was significantly decreased. Additionally, Rahmani *et al.* have found that sorafenib further induced IRE1 α upregulation [322]. Western blot analyzes of Hep3B extracts revealed that the protein level of IRE1 α increased after treatment with KP1339 and with sorafenib. Moreover, co-treatment of sorafenib and KP1339 caused a stronger increase of IRE1 α level (data not shown). These observations suggest that KP1339 and sorafenib induce via similar mechanisms and factors ER stress resulting in cell death. However, we suggest that ER stress induced by

DISCUSSION

KP1339/sorafenib combination cannot be the main mechanism to enhance anti-tumor activity and/or trigger apoptosis.

In summary, the observed synergism between sorafenib and KP1339 might be based on several mechanisms: 1) KP1339/sorafenib combination resulted in enhanced accumulation of KP1339. 2) Both sorafenib and KP1339 led to apoptosis via mitochondrial pathway, and they act additive to synergistic in depolarization of mitochondrial membrane potential. 3) Both compounds induce ER stress via different mechanisms in addition to inhibition of several tyrosine kinases and ROS production. 4) KP1339 induced several MAPK-pathways, which are believed to represent the major survival signaling upon stress situations. Sorafenib was shown to inhibit these survival pathways. Surprisingly, co-treatment was synergistic but did not cause higher levels of late stage apoptotic cells, indicating that the observed reduction of cell death is not based on reduced apoptosis induction but on hampered execution.

Overall, these data demonstrate that KP1339 and sorafenib act synergistically via multiple mechanisms, which makes this combination very promising against liver cancer. Especially, in the light of the tumor cell heterogeneity underlying frequent treatment failure, such multi-factorial treatment approaches are in the center of interest in experimental therapy research.

7. CONCLUSION

In this study, it was demonstrated that the ruthenium compound KP1339 represents a promising novel anticancer metal drug. Moreover, the synergistic activities of combinations with agents influencing intracellular iron homeostasis or ROS generation indicated that KP1339 interacts with the cellular iron and redox balance. Interestingly, co-treatment with tyrosine kinase inhibitor sorafenib (Nexavar®), currently representing the standard therapy in liver cancer, enhanced the cytotoxic and cytostatic effects of KP1339. Based on these findings, further in vivo analyses should be performed with this very promising ruthenium compound alone as well as in combination with other tyrosine kinase inhibitors to pave the way for clinical evaluations in cancer patients.

Diese Arbeit hat gezeigt, dass die Ruthenium-Verbindung KP1339 stellt ein neues vielversprechendes Anti-Krebs-Metall-Medikament. Weiters wurden synergistische Aktivitäten in KP1339-Kombinationen mit unterschiedlichen chemischen Verbindungen gezeigt, die intrazelluläre Eisenhomöostase oder ROS-Produktion beeinflussen. Dementsprechend wurde es festgestellt, dass KP1339 mit zellulärem Eisenspiegel und zellulärer Redox-Balance interagiert. Interessanterweise, die Kombination mit Tyrosin-Kinase-Inhibitor Sorafenib (Nexavar®), welcher zurzeit als Standardtherapie für Leberkarzinomen gilt, verstärkte die cytotoxischen und cyostatischen Wirkungen von KP1339. Anhand von diesen Ergebnissen sollen weitere in-vivo-Analysen durchgeführt werden, in denen dieser vielversprechende Ruthenium-Komplex sowohl alleine als auch in Kombinationen mit anderen Tyrosin-Kinase-Inhibitoren verwendet werden, um klinische Evaluationen in Krebspatienten zu ermöglichen.

8. ABBREVIATIONS

ABC	ATP-binding cassette
AFB1	Aflatoxin B1
ANT	Adenine nucleotide translocator
Apaf-1	Apoptosis protease-activating factor 1
ASC	Apoptosis-associated speck-like protein
ATP	Adenosine triphosphate
ATR	Ataxia telangiectasia- and Rad3-related
BSA	Bovin serum albumin
CDK	Cyclin-dependent kinase
CIN	Chromosome instability
Cisplatin	<i>cis</i> -diamminedichloroplatinum(II)
DAPI	4',6-diamidino-2-phenylindole
dATP	Deoxyadenosine triphosphate
DDR	DNA damage response
DLC1	Deleted in liver cancer 1
DMSO	Dimethyl sulfoxide
DMT1	Divalent metal transporter 1
DNA	Deoxyribonucleic acid
DSB	Double strand breaks
EGFR	Epidermal growth factor receptor
ER	Endoplasmic reticulum
FACS	Fluorescence-activated cell sortiment

ABBREVIATIONS

FCS	Fetal calf serum
FeCl ₃	Iron chloride
Fe-S	Iron-sulfur
FLT	FMS-like tyrosine kinase
GSH	Glutathione
HBV	Hepatitis B virus
HBX	Hepatitis B virus X protein
HCC	Hepatocellular carcinoma
HCV	Hepatitis C virus
HGF	Hepatocyte growth factor
HIF-1	Hypoxia inducible factor-1
ICP-MS	Inductively-coupled mass spectrometry
IGF	Insulin-like growth factor
IL-1 β	Interleukin-1 β
IL-6	Interleukin-6
JC-1	5,5',6,6'-tetrachloro-1,1',3,3'-tetraethyl-benzimidazolocarboyanine iodide
JNK	c-Jun N-terminal kinase
KP1019	trans-(tetrachlorobis(1H-indazole)ruthenate(III))
KP1339	Sodium trans-(tetrachlorobis(1H-indazole)ruthenate(III))
LIP	Labile iron pool
MAPK	Mitogen activated protein kinase
MDR	Multidrug resistance
MMP7	Matrix metalloproteinase 7
MRP	Multidrug resistance protein

MTT	Dimethyl thiazolyl diphenyl tetrazolium salt
NAC	N-acetyl-cysteine
NAMI-A	Imidazolium- <i>trans</i> -imidazoledimethyl-sulfoxide-tetrachlororuthenate
NEAA	Non-essential amino acids
NFκB	Nuclear factor κB
NSLC	Non-small lung carcinoma
PBS	Phosphate buffered saline
PCD	Programmed cell death
PDGF	Platelet-derived growth factor
P-gp	P-glycoprotein
PI	Propidium iodide
PI3K	Phosphatidylinositol-3-OH kinase
PIKK	Phosphatidylinositol-3-OH kinase-like kinase
PMSF	Phenylmethanesulfonylfluoride
PTP	Multiprotein pore
PVDF	Polyvinylidene fluoride
Rb	Retinoblastoma protein
RCC	Renal cell carcinoma
ROS	Reactive oxygen species
SCC	Squamous cervix carcinoma
SDS-PAGE	Sodium dodecyl sulfate polyacrylamide gel electrophoresis
SEC-ICP-MS	Size-exclusion chromatography-ICP-MS
SOD	Superoxide dismutase
TAM	Tumor-associated macrophage

ABBREVIATIONS

TBST	Tris-buffered saline with Tween
Tf	Transferrin
TfR	Transferrin receptor
TGF α	Tumor growth factor α
TF β	Tumor growth factor β
TMAH	Tetramethylammonium hydroxide
TNF α	Tumor necrosis factor α
VDAC	Voltage dependent anion channel
VEGF	Vascular endothelial growth factor

9. PUBLICATIONS

J Biol Inorg Chem
DOI 10.1007/s00775-010-0642-1

ORIGINAL PAPER

Intracellular protein binding patterns of the anticancer ruthenium drugs KP1019 and KP1339

Petra Heffeter · Katharina Böck · Bihter Atil · Mir Ali Reza Hoda · Wilfried Körner · Caroline Bartel · Ute Jungwirth · Bernhard K. Keppler · Michael Micksche · Walter Berger · Gunda Koellensperger

Received: 28 January 2010 / Accepted: 6 February 2010
© SBIC 2010

Abstract The ruthenium compound KP1019 has demonstrated promising anticancer activity in a pilot clinical trial. This study aims to evaluate the intracellular uptake/binding patterns of KP1019 and its sodium salt KP1339, which is currently in a phase I–IIa study. Although KP1339 tended to be moderately less cytotoxic than KP1019, IC_{50} values in several cancer cell models revealed significant correlation of the cytotoxicity profiles, suggesting similar targets for the two drugs. Accordingly, both drugs activated apoptosis, indicated by caspase activation via comparable pathways. Drug uptake determined by inductively coupled plasma mass spectrometry (ICP-MS) was completed after 1 h, corresponding to full cytotoxicity as early as after 3 h of drug exposure. Surprisingly, the total cellular drug uptake did not correlate with

cytotoxicity. However, distinct differences in intracellular distribution patterns suggested that the major targets for the two ruthenium drugs are cytosolic rather than nuclear. Consequently, drug–protein binding in cytosolic fractions of drug-treated cells was analyzed by native size-exclusion chromatography (SEC) coupled online with ICP-MS. Ruthenium–protein binding of KP1019- and KP1339-treated cells distinctly differed from the platinum binding pattern observed after cisplatin treatment. An adapted SEC-SEC-ICP-MS system identified large protein complexes/aggregates above 700 kDa as initial major binding partners in the cytosol, followed by ruthenium redistribution to the soluble protein weight fraction below 40 kDa. Taken together, our data indicate that KP1019 and KP1339 rapidly enter tumor cells, followed by binding to larger protein complexes/organelles. The different protein binding patterns as compared with those for cisplatin suggest specific protein targets and consequently a unique mode of action for the ruthenium drugs investigated.

P. Heffeter · B. Atil · M. A. Reza Hoda · U. Jungwirth · M. Micksche · W. Berger (✉)
Department of Medicine I,
Institute of Cancer Research,
Medical University Vienna,
Borschkegasse 8a,
1090 Vienna, Austria
e-mail: walter.berger@meduniwien.ac.at

K. Böck · G. Koellensperger
Division of Analytical Chemistry,
Department of Chemistry,
University of Natural Resources and Applied Life Sciences,
BOKU, Vienna, Austria

W. Körner
Institute for Geological Sciences,
University of Vienna,
Vienna, Austria

C. Bartel · B. K. Keppler
Institute of Inorganic Chemistry,
University of Vienna,
Vienna, Austria

Keywords Ruthenium · Size exclusion chromatography–inductively coupled plasma mass spectrometry · Drug uptake · Intracellular distribution · Anticancer

Abbreviations

GSH	Glutathione
HMW/LMW	Ruthenium-content ratio between the high molecular weight fraction and the low molecular weight fraction
ICP-MS	Inductively coupled plasma mass spectrometry
JC-1	5,5',6,6'-Tetrachloro-1,1',3,3'-tetraethylbenzimidazolylcarbocyanine iodide

KP1019	Indazolium <i>trans</i> -[tetrachlorobis(1 <i>H</i> -indazole)ruthenate(III)]
KP1339	Sodium <i>trans</i> -[tetrachlorobis(1 <i>H</i> -indazole)ruthenate(III)]
PARP	Poly(ADP-ribose)polymerase
PBS	Phosphate-buffered saline
SEC	Size-exclusion chromatography
Tris	Tris(hydroxymethyl)aminomethane

Introduction

Besides surgery and radiation therapy, chemotherapy is still one of the major therapy options for treatment of human malignancies. Platinum-containing drugs such as cisplatin and oxaliplatin are frequently used in diverse therapeutic regimens [1, 2]. However, owing to often observed complications, including severe side effects or ineffectiveness through drug resistance, the need for better chemotherapeutics still exists [3]. Ruthenium compounds belong to the most promising candidates of non-platinum-containing metal complexes for cancer therapy. Recently, indazolium *trans*-[tetrachlorobis(1*H*-indazole)ruthenate(III)] (KP1019) demonstrated exciting anticancer activity in a pilot clinical phase I study with disease stabilization for 8–10 weeks in five of six treated patients [2, 4]. Notably, only mild treatment-related toxicities were observed in this study, encouraging further clinical development of KP1019 [4]. On the basis of its higher water solubility, the sodium salt of KP1019, sodium *trans*-[tetrachlorobis(1*H*-indazole)ruthenate(III)] (KP1339), has been selected as a lead candidate for further clinical development. With regard to the mode of action, KP1019 has been suggested to induce oxidative stress and DNA damage comparable to that for other metal drugs such as cisplatin [5]. Moreover, treatment with KP1019 led to apoptosis via the mitochondrial pathway [6]. Profound depolarization of the mitochondrial membrane potential was observed after 24-h incubation with KP1019 in this study, indicating that there might be additional targets involved. KP1019 is known to strongly bind to serum proteins, including albumin and transferrin [4, 7, 8]. Consequently, it has been postulated that this serum protein binding is important for the drug accumulation into the tumor, probably involving the transferrin pathway [4, 7]. As cancer cells generally express elevated levels of transferrin receptor to serve their higher need for iron [9], KP1019 was expected to accumulate preferentially in tumor tissues to exert its anticancer activity. This hypothesis of “transferrin-mediated tumor targeting” is supported by the low toxicity of KP1019 observed in the clinical

phase I trial [4]. Moreover, the binding of KP1019 to serum proteins hampered P-glycoprotein-mediated KP1019 efflux, making this ruthenium drug interesting for treatment of multidrug-resistant tumor types [10].

Numerous studies have focused on the interaction of KP1019 with serum proteins, and the intracellular fate of KP1019 and KP1339 after uptake into tumor cells is widely unknown. Thus, the aim of this study was to gain more insight into the pharmacokinetics and intracellular distributions of KP1019 and KP1339, which should help to identify additional targets of these promising ruthenium compounds.

Materials and methods

Drugs

KP1019 and KP1339 were synthesized at the Institute of Inorganic Chemistry, University of Vienna, Austria, and by ChemCon (Freiburg, Germany), respectively, as previously reported [11, 12]. For *in vitro* studies, the compounds were dissolved in dimethyl sulfoxide and diluted into culture media at the concentrations indicated (dimethyl sulfoxide concentrations were always below 1%). Eluents were prepared from sodium hydroxide (pure pellets, Acros Organics, Geel, Belgium), hydrochloric acid (p.a. Merck, Darmstadt, Germany), tris(hydroxymethyl)aminomethane (Tris; p.a. Merck), and water purified in a water purification system (more than 18 M Ω cm resistance; HQ, USF, Vienna, Austria). HNO₃ was prepared by double subboiling distillation (Milestone-MLS, Leutkirch, Germany) of analytical reagent grade acid (Merck). H₂O₂ (ultrapure grade) was purchased from Merck. All other substances were from Sigma-Aldrich (St. Louis, MO, USA).

Cell culture

The cervical carcinoma-derived human cell line KB-3-1 was generously donated by D.W. Shen (Bethesda, MD, USA) [13]. The primary hepatocellular carcinoma cell lines HCC1.1 and HCC1.2 had been previously established at the Institute of Cancer Research, Vienna [14]. The mesothelioma cell model P31 and its respective cisplatin-resistant subline P31/cis were generously donated by K. Grankvist (Umeå University, Sweden) [15]. The colon carcinoma cell line HCT116 was generously donated by B. Vogelstein (Johns Hopkins University, Baltimore, MD, USA) [16]. The primary mesothelioma cell line VMC was established from patient material at the Institute of Cancer Research, Vienna. Additionally, the hepatocellular carcinoma cell line Hep3B and the colon carcinoma cell line SW480 (both from American Type Culture Collection,

Manassas, VA, USA) were used. SW480 cells were grown in minimal essential medium, HCT116 cells in McCoy's culture medium, and P31 cells in Eagle's minimal essential medium. All other cell lines were grown in RPMI 1640 supplemented with 10% fetal bovine serum. Cultures were regularly checked for *Mycoplasma* contamination.

Cytotoxicity assays

Cells were plated (2×10^3 cells in 100 μ l per well) in 96-well plates and allowed to recover for 24 h. Drugs were added in another 100 μ l of growth medium and cells were exposed for the time periods indicated. For pulsing experiments, test medium was replaced with fresh (drug-free) culture medium after the exposure times indicated. After 72-h drug treatment, the proportion of viable cells was determined by 3-(4,5-dimethylthiazol-2-yl)-2,5-diphenyltetrazolium bromide assay following the manufacturer's recommendations (EZ4U kit, Biomedica, Vienna, Austria).

Total ruthenium uptake levels

Cell lines derived from diverse cell models (1×10^5 per well) were exposed to 50 μ M KP1019 or KP1339 for 60 min at 37 °C. After three washes with ice-cold phosphate-buffered saline (PBS), cells were lysed by incubation at room temperature in 400 μ l tetramethylammonium hydroxide. Lysates were diluted in 0.6 N HNO₃ and ruthenium concentrations were determined by inductively coupled plasma mass spectrometry (ICP-MS) using an ELAN 6100 (PerkinElmer Sciex) at the Institute for Geological Sciences, University of Vienna. The values represent means of at least three independent experiments. As unspecific binding to cell culture plastic has been shown for KP1019 [17], the results were corrected for ruthenium levels of a blank well containing no cells.

Preparation of cytosolic versus nucleic fractions

KB-3-1 cells (2×10^6) were seeded in a T25 culture flask and allowed to attach for 24 h. Drugs were added in 5 ml of fresh growth medium. Cells were collected by trypsinization, washed twice with ice-cold PBS, and counted. For lysis, cell pellets were resuspended in lysis buffer containing 50 mM Tris-HCl, 300 mM NaCl, 0.5% Triton X-100. Additionally, 1 mM phenylmethylsulfonyl fluoride and 25 μ l/ml "complete" protease inhibitor mix (Roche, Mannheim, Germany) were added to the buffer immediately before use. Proper cell lysis was checked microscopically by trypan blue staining. After 5-min centrifugation (14,000 rpm) at 4 °C, supernatant (cytosolic fraction) was separated from the pellet (nucleic fraction)

and fractions were stored at -80 °C. Protein concentrations of the cytosolic fractions were determined using a micro bicinchoninic acid protein assay reagent kit (Pierce Biotechnology, Rockford, IL, USA).

Ruthenium levels in cytosolic and nucleic fractions

A 100- μ l volume of cytosolic fraction and the full nucleic fraction of each experiment were digested with 2 ml 20% HNO₃, 1 ml H₂O, and 200 μ l H₂O₂ in a high-performance microwave (MLS 1200 microwave, MLS, Leutkirch, Germany). Ruthenium levels were determined by ICP-MS. The quadrupole-based system used for these measurements was equipped with a dynamic reaction cell (ELAN DRC-II, PerkinElmer Sciex, Woodbridge, ON, Canada). Oxygen (purity 4.5, Linde Gas, Vienna, Austria) was used as the reaction gas. The values represent means of at least two independent experiments and were adjusted to the previously determined cell numbers. The values (arbitrary units) were expressed relative to the total ruthenium levels (cytosolic + nucleic) at 1-h exposure (50 μ M) set arbitrarily as 1.

Size-exclusion chromatography-inductively coupled plasma mass spectrometry

Size-exclusion chromatography (SEC) was combined with ICP-MS detection using the ELAN DRC-II (PerkinElmer Sciex, Woodbridge, ON, Canada). The metal-free chromatographic system consisted of an AS 50 autosampler (including a custom-made temperature-control device), a GP 40 gradient pump, and the Chromeleon Chromatography Management System (version 6.40), all from Dionex (Sunnyvale, CA, USA). The injection volume was 25 μ l. Injected samples were filtered in-line using a 0.45- μ m PEEK filter located in front of the column. A BioSuiteTM 125 column (300 mm \times 4.6 mm UHR SEC, 4- μ m particle diameter) from Waters (Milford, MA, USA) was used as the stationary phase for SEC. The eluent containing 150 mM NaCl and 20 mM Tris-HCl, pH 7.4 was delivered at a flow rate of 350 μ l/min. The SEC eluent was transferred directly to the ICP-MS introduction system consisting of a perfluoroalkoxy nebulizer and a cyclonic spray chamber. The values were assessed from four independently prepared samples.

The SEC column utilized for these experiments provided a size-exclusion limit of 150 kDa; hence, proteins larger than 150 kDa could not be separated and eluted in the void volume of the column at 6 min. A retention time of 8 min corresponded to the size range 80–60 kDa. Low molecular weight compounds as, e.g., peptides or metallothioneins, had a retention time of more than 10 min. A retention time of 13–14 min corresponded to small molecules (e.g. inorganic salts) [18]. The low molecular weight

fraction was defined as the integral of the ruthenium response from 11 to 14 min in the SEC chromatogram.

Tandem size-exclusion chromatography–inductively coupled plasma mass spectrometry

SEC-SEC-ICP-MS was performed by coupling two separation columns in-line in combination with ICP-MS detection using the ELAN DRC-II (PerkinElmer Sciex, Woodbridge, ON, Canada). The first column (BioSep-SEC-S 4000, 300 mm × 7.8 mm, 5 μm particle diameter) had an exclusion limit of 2,000 kDa and the second had a separation range from 66 to 670 kDa (BioSep-SEC-S 3000, 300 mm × 7.8 mm, 5-μm particle diameter), both from Phenomenex (Phenomenex, Ashaffenburg, Germany). The flow rate applied was 1 ml/min (injection volume 25 μl).

Cell fractionation

KB-3-1 cells (10^7) were seeded in a T150 culture flask and allowed to attach for 24 h. KP1019 or KP1339 was added in 20 ml of fresh growth medium. After 3-h drug incubation, cells were collected by trypsinization, washed twice with ice-cold PBS, and counted. After another centrifugation step, cell pellets were resuspended in Douce buffer containing 10 mM Tris–HCl pH 7.6 and 0.5 mM MgCl₂. Additionally, 1 mM phenylmethylsulfonyl fluoride and 25 μl/ml “complete” protease inhibitor mix (Roche, Mannheim, Germany) were added to the buffer immediately before use. After 15-min incubation on ice, cells were lysed by Douce homogenization. Total cell lysis was checked microscopically by trypan blue staining. After addition of NaCl (final concentration 150 mM), homogenates were centrifuged for 5 min at 3,500g. Pellets were separated from supernatants, washed once, and stored at –80 °C (fraction I). The supernatants were supplemented with EDTA (final concentration 5 mM) and centrifuged at 100,000g for 1 h at 4 °C. The resulting supernatant was stored at –80 °C (fraction II). The pellets (fraction III) were resuspended in lysis buffer containing 50 mM Tris–HCl, 300 mM NaCl, 0.5% Triton X-100, 1 mM phenylmethylsulfonyl fluoride, and 25 μl/ml “complete” protease inhibitor mix (Roche, Mannheim, Germany). Also this fraction was stored at –80 °C. Protein concentrations of the cytosolic fractions were determined using a micro bicinchoninic acid protein assay reagent kit (Pierce Biotechnology, Rockford, IL, USA).

4',6-Diamidino-2-phenylindole staining

KB-3-1 cells (1×10^5 per well) were plated in six well plates and after 24 h of recovery were treated with various concentrations of KP1019 and KP1339. After 24 h, cells were harvested, cytopspins were prepared, and apoptosis

was evaluated by staining with 4',6-diamidino-2-phenylindole (DAPI) containing antifade solution (Vector Laboratories, Burlingame, CA, USA). The nuclear morphology of cells was examined with a Leica DMRXA fluorescence microscope (Leica Mikroskopie and System, Wetzlar, Germany) equipped with appropriate epifluorescence filters and a Cohu charge-coupled-device camera. For each concentration at least two slides were evaluated, whereby at least 250 nuclei per experimental group were analyzed.

Western blot analyses

After 24 h of drug exposure, proteins were isolated, resolved by sodium dodecyl sulfate polyacrylamide gel electrophoresis, and transferred onto a poly(vinylidene difluoride) membrane for western blotting as described in [19, 20]. The anti-poly(ADP-ribose)polymerase (PARP), cleaved PARP, caspase 3, caspase 9, caspase 7, and cleaved caspase 7 antibodies (all polyclonal rabbit) from an apoptosis sampler kit (Cell Signalling Technology, Beverly, MA, USA) and the anti-β-actin monoclonal mouse AC-15 (Sigma) were used in a 1:1,000 dilution. Additionally, horseradish peroxidase labeled antibodies from Santa Cruz Biotechnology were used at working dilutions of 1:10,000.

Mitochondrial membrane potential detection

KB-3-1 cells (1×10^6 per well) were seeded in T25 flasks. After 24-h recovery, cells were treated with various concentrations of KP1019 and KP1339 for another 24 h. Cell staining was performed as published [21]. Cell suspensions were incubated with 10 μl/ml of the fluorescent dye 5,5',6,6'-tetrachloro-1,1',3,3'-tetraethylbenzimidazolylcarbocyanine iodide (JC-1; mitochondrial membrane potential detection kit; Stratagene, La Jolla, CA, USA) in full culture medium for 10 min at 37 °C. At the end of the incubation period, cells were washed twice with cold PBS, resuspended in PBS, and analyzed by flow cytometry using a Calibur fluorescence-activated cell sorting instrument (Becton-Dickinson, Palo Alto, CA, USA).

Statistical analysis

Linear regression analyses were performed using GraphPad Prism 4.0 (GraphPad Software, La Jolla, CA, USA).

Results

Exposure-time dependency of cytotoxicity

The anticancer activity of KP1339 was compared with that of KP1019 after 72 h in several cancer cell lines (Table 1).

Table 1 IC₅₀ values after 72 h

	KP1019 (μM)		KP1339 (μM)	
	IC ₅₀	SD	IC ₅₀	SD
KB-3-1	99.3	29.3	135.3	25.8
HCC1.1	108.1	56.0	148.9	42.1
HCC1.2	82.9	0.2	88.3	26.4
Hep3B	98.4	25.3	143.1	15.3
SW480	58.2	21.4	110.2	31.7
HCT116	36.6	17.0	34.7	3.6
P31	151.2	12.9	148.0	9.2
P31/cis	147.0	8.0	150.0	0.8
VMC	56.4	9.6	77.5	6.3

SD standard deviation

For both drugs, the colon cancer cell line HCT116 was found to be most responsive, whereas the mesothelioma cell model P31 and P31/cis displayed the highest resistance. In general, KP1339 tended to be less cytotoxic than KP1019, with a mean IC₅₀ values of 93.1 μM for KP1019 and 115.1 μM for KP1339 over all cell lines tested. However, linear regression analysis of the respective IC₅₀ values revealed significant correlation of the anticancer activity of KP1019 and KP1339 ($p = 0.0035$). With regard to exposure time dependency, the ruthenium drugs were tested by pulsing experiments using KB-3-1 cells. To this end, KP1019- and KP1339-containing test mediums were replaced with fresh culture medium after 1-, 2-, and 3-h exposure for a total experimental time of 72 h (Fig. 1). Again KP1019 displayed moderately enhanced cytotoxicity at all time points tested. With regard to the exposure-time dependency, as little as 1 h of drug contact induced significant anticancer activity, with IC₅₀ values of 136 μM for KP1019 and 182 μM for KP1339. Moreover, 3 h of drug contact was found to be sufficient for about 95% anticancer activity (3-h IC₅₀ values of KP1019 and KP1339 were 85.0 and 117.6 μM, respectively, versus 82.6 and 108.9 μM after 72 h).

Comparison of KP1019 and KP1339 drug uptake

To evaluate whether the higher cytotoxicity of KP1019 (compared with KP1339) might be based on enhanced drug uptake, total intracellular ruthenium levels were determined by ICP-MS after 1-h incubation. In general, drug uptake was detectable at levels of nanograms of ruthenium per 10⁵ cells for both drugs. In most cell lines tested, KP1019 accumulation was up to twofold higher than KP1339 uptake (mean of all cell lines, 4.4 ng ruthenium per 10⁵ cells for KP1019 vs. 2.3 ng ruthenium per 10⁵ cells for KP1339; Table 2). Comparable to the vitality assays, linear regression analysis revealed significant correlation of

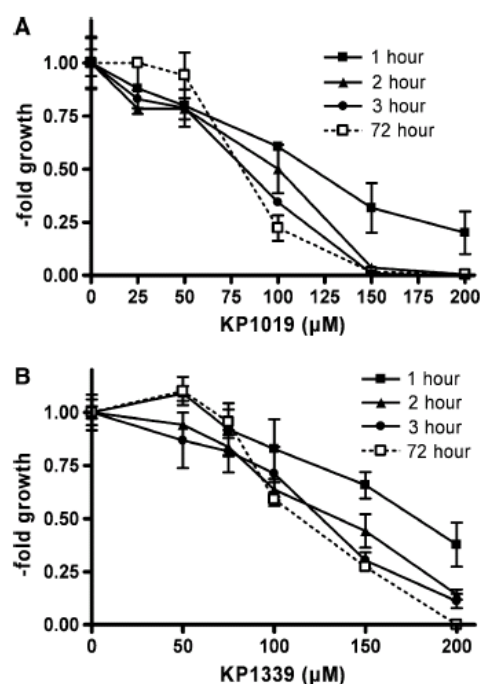


Fig. 1 Exposure-time dependency of KP1019 and KP1339 cytotoxicity. Pulsing experiments were performed in KB-3-1 cells by replacing a KP1019- and b KP1339-containing test mediums after 1, 2, and 3 h with fresh culture medium. Following a total experimental time of 72 h, cell vitality was determined by 3-(4,5-dimethylthiazol-2-yl)-2,5-diphenyltetrazolium bromide assays. The values given are means and standard deviations (SD) of three independent experiments in triplicate

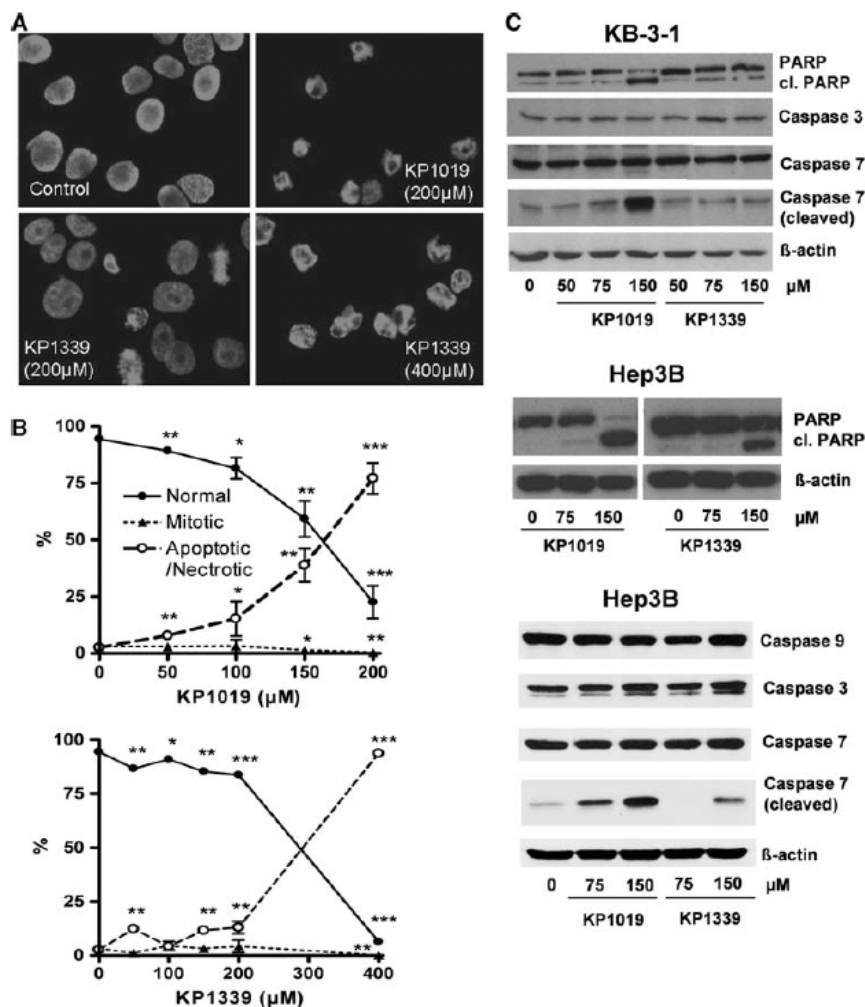
Table 2 Total uptake after 1-h exposure using 50 μM of the respective drug

	KP1019		KP1339	
	Ru/10 ⁵ cells (ng)	±SD	Ru/10 ⁵ cells (ng)	±SD
KB-3-1	5.3	0.56	3.0	0.06
HCC1.1	7.7	2.55	5.1	0.96
HCC1.2	4.4	0.35	3.1	0.46
Hep3B	7.5	0.43	3.2	0.14
SW480	2.6	0.15	2.4	0.40
HCT116	3.0	0.3	1.4	1.5
P31	2.4	0.66	0.24	0.36
P31/cis	1.9	0.35	ND	–
VMC	5.59	0.51	1.97	0.15

ND below detection limit

KP1019 and KP1339 uptake ($p = 0.049$). However, no correlation between total cellular drug uptake and cytotoxicity was found in the case of both drugs (KP1019 $p = 0.76$ and KP1339 $p = 0.81$), indicating that mere drug

Fig. 2 Comparison of the apoptosis-inducing potential of KP1019 with KP1339. **a** Induction of apoptosis in KB-3-1 cells was determined after treatment for 24 h. 4',6-Diamidino-2-phenylindole (DAPI) staining of nuclei is shown in untreated controls and cells treated with the drug concentrations indicated. **b** Morphological features of 300–500 nuclei of at least two slides for each concentration were analyzed by DAPI staining. The percentages of normal, mitotic, and apoptotic/necrotic nuclei at the concentrations indicated are shown. **c** Apoptosis-induced cleavage of poly(ADP-ribose)polymerase (PARP), caspase 7, and caspase 3 in KB-3-1 and Hep3B cells after 24-h treatment was determined via western blot. The antibodies used are described in “Materials and methods”



accumulation is not decisive for the exerted level of cytotoxicity.

Comparison of KP1019- and KP1339-induced apoptosis

Next, it was tested whether the difference in activity of KP1019 and KP1339 is accompanied by differences in the induction of apoptosis. To this end KB-3-1 cells were treated with increasing concentrations of KP1019 and KP1339 for 24 h (Fig. 2a, b). Pronounced apoptosis induction was observed after treatment with 150 μM (38.9%) and 200 μM (77.1%) KP1019. In accordance with the cytotoxicity and uptake data, apoptosis levels induced by KP1339 were distinctly lower at these concentrations (11.5 and 12.9%, respectively). Treatment with 400 μM

KP1339 strongly increased the proportion of apoptotic cells to 93.7%. Additionally, apoptotic body formation after KP1019 and KP1339 treatment was accompanied with an increase in cleavage of caspase 7 as well as of the caspase substrate PARP, another indicator for apoptotic cell death (Fig. 2c). In contrast to reports on SW480 cells [6], no caspase 3 cleavage was observed.

As a next step, the mitochondrial integrity was determined by JC-1 staining after 24-h treatment with KP1019 and KP1339 (Fig. 3a). A detectable increase (from 4.57 to 8.33%) of cells with depolarized mitochondria was observed using only 100 μM KP1019. Treatment with 200 μM KP1019 resulted in profound mitochondrial depolarization (78.72%). KP1339 was about half as active as KP1019, with 7.03% of cells with depolarized mitochondria at 200 μM and 65.67% of cells at 400 μM.

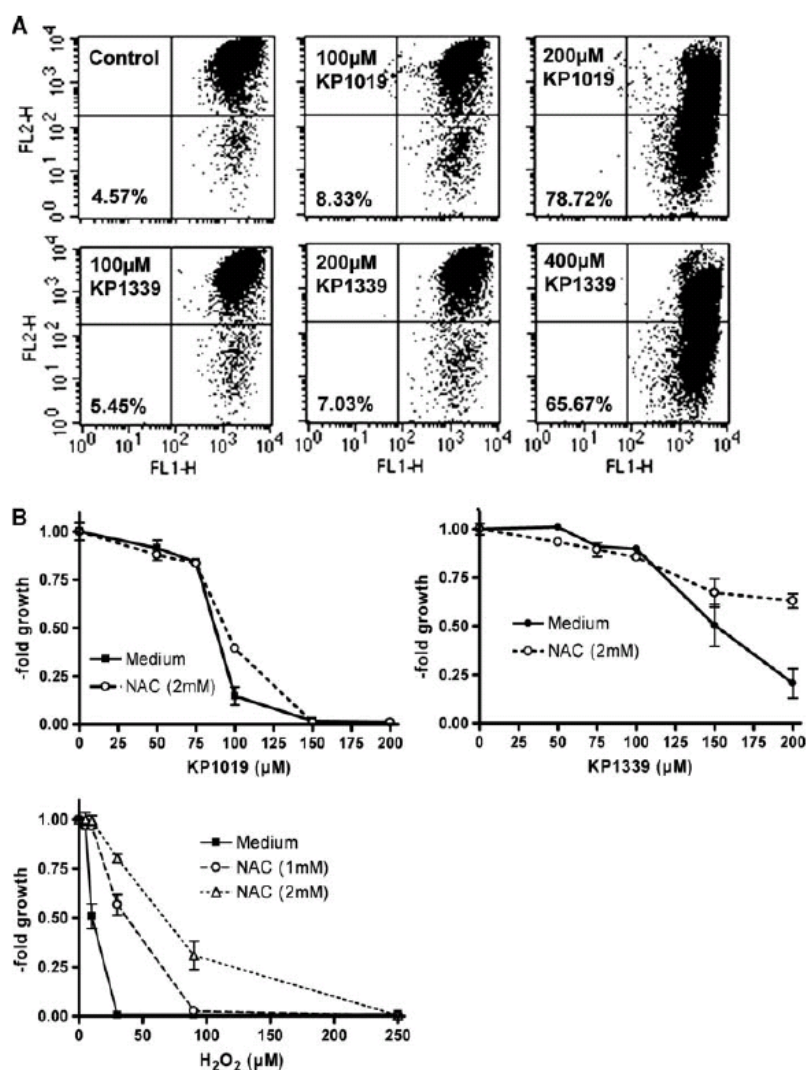


Fig. 3 Characterization of KP1019 and KP1339 apoptosis. **a** Loss of mitochondrial membrane potential after 24-h treatment was determined by 5,5',6,6'-tetrachloro-1,1',3,3'-tetraethylbenzimidazolylcarbocyanine iodide (JC-1) staining. Increase of the green fluorescent apoptotic populations of KB-3-1 cells at the drug concentrations

indicated (cells in the lower right field) are indicated (30,000 events were analyzed in total per group). **b** Effects of 30-min pretreatment with the radical scavenger *N*-acetylcysteine (NAC) on the anticancer activity of KP1019, KP1339, and H₂O₂ (positive control) were analyzed after 72-h drug exposure by an EZ4U kit

Earlier studies indicated that oxidative stress might be involved in apoptosis induction by KP1019 [5, 6]. Thus, the impact of the radical scavenger *N*-acetylcysteine (NAC) on the cytotoxic activity of KP1019 and KP1339 was compared. Protective NAC effects were observed for both drugs at concentrations in their IC₅₀ range (Fig. 3b). However, this effect was significantly less pronounced as compared with that for H₂O₂, the positive control for oxidative stress production.

Intracellular distribution of KP1019 and KP1339

The intracellular fate of the ruthenium compounds tested is still widely unknown. Figure 4 shows the ruthenium distribution between cytoplasm and nucleic cell fractions after 1-, 3-, and 6-h treatment with 50, 75, and 150 μM KP1019 and KP1339, respectively. In accordance with already published observations [10], KP1019 and KP1339 were significantly and completely accumulated in tumor cells

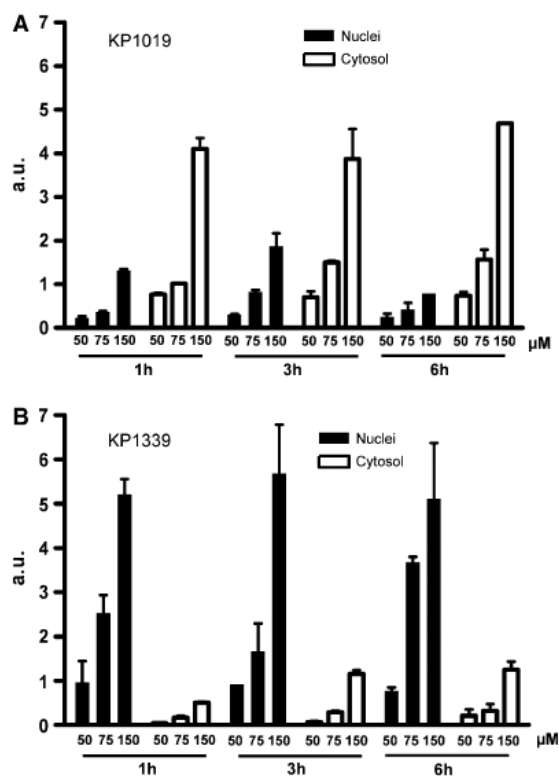


Fig. 4 Drug accumulation and intracellular drug distribution. Cytosolic and nucleic ruthenium levels of **a** KP1019- and **b** KP1339-treated KB-3-1 cells were determined after 1-, 3-, and 6-h drug exposure by inductively coupled plasma mass spectrometry (ICP-MS). The values given are relative means and the SD from at least two independent experiments

within the first hour of drug incubation. Further increase of the incubation time up to 6 h did not result in a change of total drug uptake or the patterns of distribution between the nucleus and the cytoplasm. This was also in good agreement with the findings of the pulsing experiment data (see Fig. 1), which had already indicated that only short drug contact is sufficient for full KP1019 and KP1339 anticancer activity. Drug uptake of KP1019 as well as KP1339 followed a linear and dose-dependent pattern. With regard to intracellular distribution at all concentrations and time points tested, about 75% of KP1019 was detected in the cytosolic fraction. In contrast, KP1339 accumulated preferentially in the nuclei (approximately 90%).

Protein binding patterns of KP1019 and KP1339

As a next step, the protein binding of the drugs tested was investigated in culture medium as well as in cytoplasm samples from drug-exposed cells. For this purpose SEC

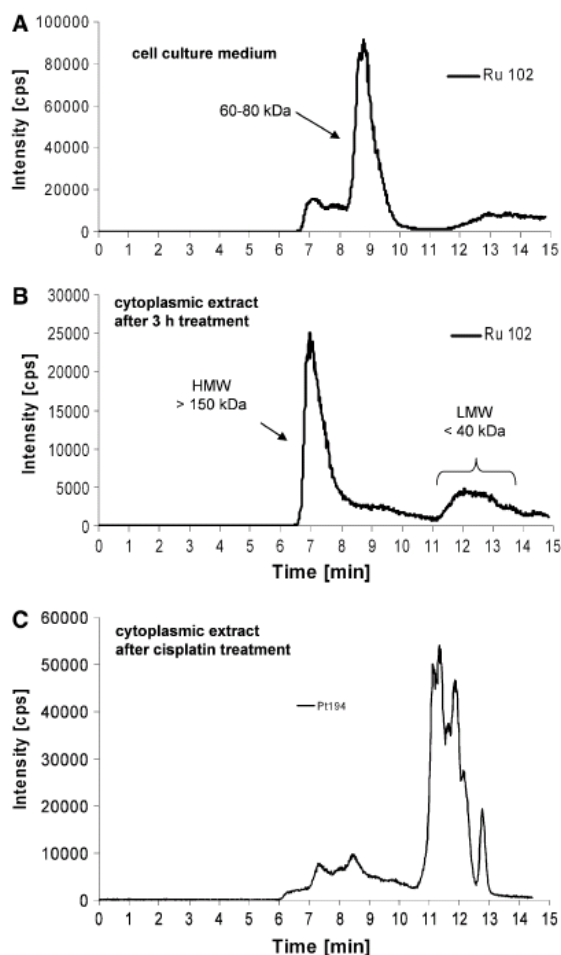


Fig. 5 Drug-protein binding patterns of KP1019. **a** Size-exclusion chromatography (SEC)-ICP-MS determination of cell culture medium supplemented with fetal calf serum after 3 h of incubation with KP1019. **b** Cytosolic fractions of KP1019-treated KB-3-1 cells were isolated after 3-h treatment and protein-bound ruthenium was determined by SEC-ICP-MS. **c** Cytosolic fractions of cisplatin-treated KB-3-1 cells were isolated after 3-h treatment with 50 μ M cisplatin and protein-bound platinum was determined by SEC-ICP-MS. One representative experiment out of three is shown

was combined with element-selective detection by ICP-MS [22, 23]. Figure 5a shows the protein binding pattern of the cell culture medium of cells after 3-h incubation with 50 μ M KP1019. The major fraction of ruthenium was detected on proteins in the size range 60–80 kDa, i.e., the fraction of albumin and transferrin, present in the medium owing to fetal calf serum supplementation. Only small amounts of KP1019 (including free KP1019) could be detected in the low molecular weight fraction. The column recovery was 70% in these experiments. This is in

accordance with findings of earlier studies on drug–protein binding in human serum of patients [8].

In the cytoplasmic fraction isolated from drug-treated cells (Fig. 5b), KP1019 delivered basically two ruthenium-containing peaks: a prominent high molecular weight peak close to the exclusion limit of the column and a broad peak after 11–14 min corresponding to the low molecular weight fraction. The ruthenium-content ratio between the high molecular weight fraction and the low molecular weight fraction (HMW/LMW) was 3.5 ± 0.8 ($n = 5$ independently prepared samples) upon 3 h of drug exposure. Comparable intracellular protein binding patterns were also observed in Hep3B, HCC1.2, and HL60 cells (data not shown). Comparative experiments with KP1339 revealed concordant protein binding in the culture medium and in the cytoplasm (data not shown). KP1339 exposure for 3 h resulted in an HMW/LMW of 4 ± 0.8 ($n = 2$ independently prepared samples). Although KP1339 exhibits less accumulation in the cytoplasm, the cytoplasmic protein binding pattern was comparable to that of KP1019. Thus, for further analysis only KP1019-treated cells were used. Notably, the ruthenium binding patterns of KP1019 and KP1339 were in contrast to the platinum binding pattern of cisplatin-treated cells (Fig. 5c), which were characterized by distinct protein binding in the low molecular weight fraction.

As a next step, KP1019 incubation was extended from 3 to 24 h (Fig. 6a). A significantly changed HMW/LMW of 1.0 ± 0.4 ($n = 2$ independently performed experiments) was observed in the cytoplasmic samples; hence, the drug binding shifted toward low molecular weight proteins. To test the hypothesis that these observations resulted from changes in the distribution of the early accumulated

KP1019, pulsing experiments were performed. To this end, KP1019-containing medium was replaced after 3 h with drug-free cell culture medium. SEC-ICP-MS was performed 24 h after the beginning of the experiment. In analogy to the 24-h continuous incubation experiments, the low molecular weight fraction increased, giving an HMW/LMW of 0.5 in this experiment (Fig. 6b).

Characterization of the high molecular weight fraction

The column utilized for the SEC-ICP-MS measurements provided a size-exclusion limit of 150 kDa; hence proteins larger than 150 kDa could not be separated and eluted in the void volume of the column at 6 min. To further characterize the high molecular weight fraction, which was observed in all cytoplasmic samples, an alternative size-exclusion system was implemented. This new high-end technology allowed the separation of large proteins by increasing the protein size-exclusion limit from 150 to 2,000 kDa. The separation efficiency for the low molecular weight fraction was retained by setting up a novel SEC-SEC-ICP-MS method with two size-exclusion columns online. The first column was designed for separation of large proteins (exclusion limit 2,000 kDa, separation range 66–670 kDa), and the second column provided separation for mid-to-large proteins (exclusion limit 700 kDa, 5–700 kDa separation range). Notably, the SEC-SEC-ICP-MS investigation of KB-3-1 cells incubated with 50 μ M KP1019 for 3 h (Fig. 7a) again revealed only two peaks: one at high molecular weight (again at the exclusion limit of the column, corresponding to proteins larger than 2,000 kDa), and the other at low molecular weight. Similar to our previous experiments, an HMW/LMW of 3.6 was observed. Hence, it could be concluded that monomeric proteins in the size range 60–700 kDa were not major targets of the ruthenium compounds in the cytoplasm. Since the native fractionation protocol applied did not separate cytoplasm from membrane-bound proteins and cell organelles, the metaldrug adducts detected in the void volume of the SEC-SEC-ICP-MS system can be explained by drug bound to membrane protein agglomerates, large protein complexes (e.g., ribosomes, vaults), and/or other cell organelles. This hypothesis was further confirmed by applying a different cell lysis protocol ($n = 2$). This allowed the separation of different cell compartments: the nucleic fraction (fraction I), a fraction containing all soluble (cytoplasmic) proteins (fraction II), as well as a particular fraction containing all membrane proteins and organelles (fraction III). The overall ruthenium levels in fractions I, II, and III were 2.9 ± 0.6 , 1.8 ± 0.1 , and 2.8 ± 1.8 fg per cell, respectively. Figure 7b shows the intracellular/cytoplasmic distribution obtained of 50 μ M KP1019 in the soluble

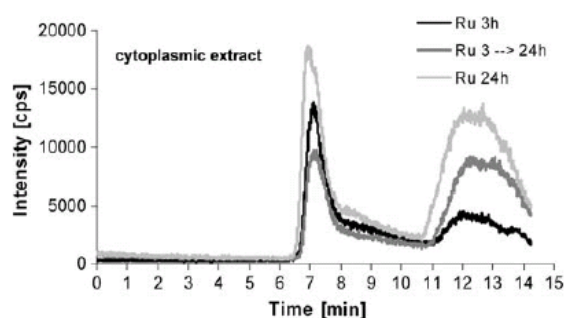


Fig. 6 Drug–protein binding patterns of KP1019 in pulsing experiments. KB-3-1 cells were treated with 50 μ M KP1019, and after 3-h drug exposure drug-containing medium was replaced with fresh, drug-free cell culture medium. SEC-ICP-MS of cytosolic fractions was performed 24 h after the beginning of the experiment. Cytosolic fractions of cells treated for 3 and 24 h were prepared and analyzed in parallel. The respective cell numbers for the experiment were 1.58×10^7 , 3.2×10^7 , and 2.95×10^7 for the 3-, 3–24-, and 24-h samples

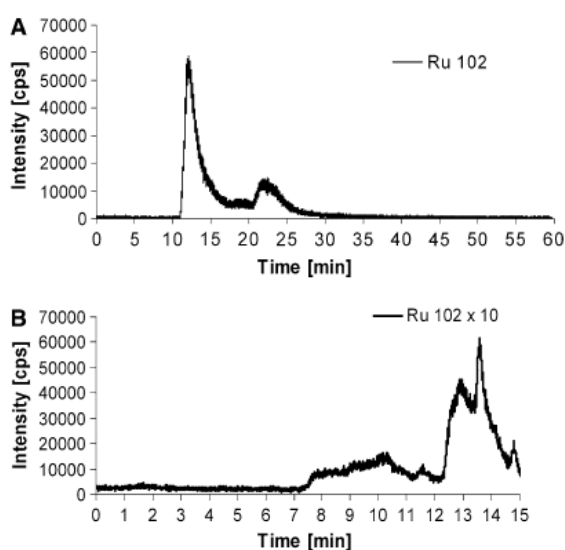


Fig. 7 a Drug-protein binding pattern of KP1019 determined by SEC-SEC-ICP-MS (designed for the separation of large proteins). Cytosolic fractions of KP1019-treated KB-3-1 cells were prepared after 3-h drug treatment. b Drug-protein binding pattern of KP1019 determined by SEC-ICP-MS after implementation of an alternative cell compartment fractionation protocol. Cytosolic 100,000g supernatant fractions not containing organelles, particular protein complexes, as well as membrane-bound proteins (fraction III) of KP1019-treated KB-3-1 cells were prepared after 3-h drug treatment

fraction (fraction II) of KB-3-1 cells after 3 h of incubation. In accordance with the above-mentioned hypothesis, only the low molecular weight fraction was detectable, and the prominent high molecular weight peak was missing from the SEC-ICP-MS spectrum. This indicates that KP1019 does not bind to soluble, monomeric proteins larger than 100 kDa. The low molecular weight ruthenium peaks correspond to small protein- and/or peptide-bound drug. Detection of free drug is unlikely as comparable amounts of KP1019 from protein-free solutions could not be recovered from the column (data not shown).

Discussion

Metal compounds belong to the most important chemotherapeutics for the treatment of human malignancies at the disseminated stage. In addition to platinum-containing drugs, ruthenium compounds such as KP1019 and KP1339 are also promising candidates in the development of new cancer therapeutics [4]. Recently, KP1019—containing an indazolium counterion—demonstrated considerable anti-cancer activity in a pilot clinical phase I study with low

side effects [2, 4]. However, KP1019's poor pharmaceutical properties, especially its poor aqueous solubility, did not allow the dose escalation in the trial to be done beyond a certain point. The maximum tolerated dose and optimal dose could not be reached. Hence, the sodium salt (KP1339) was selected for further clinical development. KP1339 has superior pharmaceutical properties, including more than 30 times better aqueous solubility. In this study, we compared the modes of action and activity patterns of these two ruthenium compounds *in vitro*. KP1019 was generally more active than KP1339. Nevertheless, linear regression analyses showed that both cytotoxic activity and the drug accumulation profile correlated between both drugs, indicating that they share similar modes of action. Moreover, both drugs were found to induce caspase-mediated apoptosis via the mitochondrial pathway, which is in agreement with previous data showing mitochondrial membrane depolarization and apoptosis induction by KP1019 in SW480 cells [5, 6]. Experiments using the glutathione (GSH) precursor and radical scavenger NAC indicated that the mechanisms underlying the anticancer activity of KP1019 and KP1339 share common effectors and/or metabolic pathways.

The present study reveals that KP1019 and KP1339 distinctly differ in their intracellular distribution: KP1339 preferentially accumulated into the nucleus (approximately 90%), whereas KP1019 was mainly localized in the cytoplasm (approximately 75%). This is of special interest as it challenges the widespread view that DNA is the major target of ruthenium drugs [24]. Pronounced nucleic localization has been reported for several DNA-damaging agents such as cisplatin [25] and doxorubicin [26]. Unlike the cytotoxicity of cisplatin or other DNA-damaging agents, our studies show that the KP1019 and KP1339 cytotoxicity is independent of p53 status ([10], data not shown). Similarly, the caspase activation and cytosolic drug-protein binding profiles indicate that both ruthenium drugs exert apoptosis via similar pathways, despite their different intracellular distribution pattern. Therefore, it seems unlikely that nucleic localization and DNA targeting is the primary mechanism underlying the anticancer activity of KP1019 and KP1339. In support of this, ruthenium compounds have been shown to involve targets other than DNA [27]. For example, the designed ruthenium-containing glycogen synthase kinase-3 β inhibitor DW1/2 was recently reported to reduce the intracellular levels of MDM2 and MDM4. Consequently, p53 is stabilized, leading to apoptosis via the mitochondrial pathway in melanoma cells [28]. Moreover, DW1/2 was found to potently inhibit phosphatidylinositol 3-kinase [29] as well as the serine/threonine kinase PIM1 [30]. Also, for NAMI-A, a specific antimetastatic activity was described independent from DNA targeting [31, 32]. Altogether, these

reports and our data suggest that cytosolic protein targets are involved in the anticancer activity of some ruthenium compounds including KP1019 and KP1339.

KP1019 has been repeatedly shown to bind to serum proteins *in vitro* as well as in patient blood samples [4, 7, 8]. However, the intracellular protein binding patterns of anticancer drugs, in general, and of ruthenium compounds such as KP1019 and KP1339, in particular, are widely unexplored. This is the first study to elucidate the intracellular distribution and protein binding patterns of KP1019 and KP1339. A highly advanced SEC-ICP-MS analytical method has been adapted to address ruthenium contents of native (cytosolic) protein preparations from drug-exposed human cancer cells [22, 23]. This method is an ideal tool for studying interactions between metallo-drugs and proteins in live cells on a quantitative basis. It combines native protein separation with ICP-MS detection, allowing the determination of covalent as well as noncovalent drug–protein binding. Such noncovalent interactions (e.g., with serum proteins) are believed to play a crucial role in the anticancer activity of KP1019 and KP1339 [4]. Our time-course activity and cellular accumulation experiments show that uptake and damage leading to cytotoxicity of KP1019 and KP1339 is rapid and completed within the first hours of drug incubation. Moreover, the cytosol to nucleus distribution remained unchanged for more than 6 h, arguing for rapid drug compartmentalization. With regard to the binding of KP1019 or KP1339 to cytosolic proteins, ruthenium binding was predominantly found in the high molecular weight fraction (more than 700 kDa). This fraction probably contains mainly polymeric proteins (e.g., cytoskeleton components) or large protein complexes (e.g., ribosomes, proteins from the respiratory chain, multimeric channels). Accordingly, preliminary proteome profiling using shotgun analyses identified multiple ribosomal and cytoskeletal proteins in this fraction (data not shown). To further dissect the observed ruthenium–protein binding patterns, a second cell fractionation approach using detergent-free buffer for separation of nuclei and large (protein) particles from smaller, soluble proteins was employed. Corroborating the data above, the larger ruthenium binding fraction was completely lost following 100,000*g* centrifugation in these settings. Only ruthenium bound to cytosolic proteins smaller than 100 kDa was still detectable, with distinct separation into several subpeaks. The characterization of these KP1019 and KP1339 targets is currently being addressed by developing immunoaffinity-assisted SEC-ICP-MS methods with higher selectivity for potential protein targets. Notably, the intracellular drug binding patterns of KP1019- and KP1339-treated cells strongly differed from those exposed to cisplatin, where cytosolic platinum

binding was mainly detected in the low molecular weight protein fraction. This again illustrates that KP1019 and KP1339 have a mechanism of action different from that of cisplatin.

To further investigate the intracellular processing of ruthenium binding, protein extracts of KP1019-treated cells were prepared after a longer drug-free recovery period (21 h). Notably, the initiative ruthenium–protein binding pattern shifted to the low molecular weight fraction (below 40 kDa) in these experiments. Again the underlying mechanisms are widely speculative and need further evaluation. However, one explanation for the increase in small ruthenium-bound proteins could be the appearance of KP1019 and KP1339 detoxification products. In SEC-ICP-MS measurements, peptides or metallothioneins have a retention time of more than 10 min [18]. Thus, GSH conjugation or metallothionein binding would explain the increased ruthenium content in this fraction. This is supported by the interaction and coordination of KP1019 to GSH [33] and metallothioneins (unpublished results) in cell-free systems. Also, the protective activity of NAC against KP1339- and KP1019-mediated cytotoxicity would support this hypothesis (see Fig. 3b and [5]). However, our previous studies revealed that KP1019 is not a substrate for the GSH conjugate efflux pump MRP1 and long-term KP1019 treatment did not induce expression of any GSH-dependent ABC transporters [2, 10]. This suggests that GSH conjugation is not a major factor protecting cells from KP1019. Another explanation for the increased low molecular weight ruthenium-containing protein peaks might be the proteosomal degradation of damaged proteins due to ruthenium-adduct formation [34, 35]. KP1019 has previously been shown to induce the formation of reactive (oxygen) species [5]. Moreover, preliminary results revealed induction of several chaperons including heat shock proteins after KP1339 treatment (unpublished results), which also points toward induction of protein stress. Accordingly, in a recent study activation of endoplasmic reticulum stress was described as a major contributor to the cytotoxic activity of the poorly DNA interacting ruthenium compound RDC11 [36].

Taken together, the findings of our study revealed that KP1019 and KP1339 rapidly enter tumor cells, where they bind to multiple small soluble proteins as well as large (multimeric) complexes/organelles. The higher cytosolic retention of the more cytotoxic compound KP1019 suggests that protein targets in the cytoplasm are key components of the cytotoxicity exerted. Moreover, the cytosolic protein binding pattern strongly differs from that observed for cisplatin, supporting the hypothesis that KP1019 and KP1339 exert a specific mode of action different from that of platinum drugs.

Acknowledgments We are indebted to Vera Bachinger and Maria Eisenbauer for the skilful handling of cell cultures, Elisabeth Rabensteiner, Rosa-Maria Weiss, as well as Christian Balcarek for competent technical assistance, and Irene Herbacek for fluorescence-activated cell sorting analysis. Many thanks go to Rita Dornetshuber, Christian Hartinger, Leonilla Elbling, and Michael Jakupec for inspiring discussions. This work was performed within the Research Platform Translational Cancer Therapy Research Vienna and supported by the Austrian Science Fond grants L212 and L473, by Bürgermeister Fond der Stadt Wien grant 2460, as well as by FFG grant 811591.

References

1. Bruijninx PC, Sadler PJ (2008) *Curr Opin Chem Biol* 12:197–206
2. Heffeter P, Jungwirth U, Jakupec M, Hartinger C, Galanski M, Elbling L, Micksche M, Keppler B, Berger W (2008) *Drug Resist Updat* 11:1–16
3. Cossa G, Gatti L, Zunino F, Perego P (2009) *Curr Med Chem* 16:2355–2365
4. Hartinger CG, Zorbas-Seifried S, Jakupec MA, Kynast B, Zorbas H, Keppler BK (2006) *J Inorg Biochem* 100:891–904
5. Kapitzka S, Jakupec MA, Uhl M, Keppler BK, Marian B (2005) *Cancer Lett* 226:115–121
6. Kapitzka S, Pongratz M, Jakupec MA, Heffeter P, Berger W, Lackinger L, Keppler BK, Marian B (2004) *J Cancer Res Clin Oncol* 226:115–121
7. Cetinbas N, Webb MI, Dubland JA, Walsby CJ (2010) *J Biol Inorg Chem* 15:131–145
8. Sulyok M, Hann S, Hartinger CG, Keppler BK, Stingeder G, Koellensperger G (2005) *J Anal At Spectrom* 20:856–863
9. MacKenzie EL, Iwasaki K, Tsuji Y (2008) *Antioxid Redox Signal* 10:997–1030
10. Heffeter P, Pongratz M, Steiner E, Chiba P, Jakupec MA, Elbling L, Marian B, Korner W, Sevelde F, Micksche M, Keppler BK, Berger W (2005) *J Pharmacol Exp Ther* 312:281–289
11. Lipponer KG, Vogel E, Keppler BK (1996) *Met Based Drugs* 3:243–260
12. Peti W, Pieper T, Sommer, Keppler BK, Giester G (1999) *Eur J Inorg Chem* 1551–1555
13. Heffeter P, Jakupec MA, Korner W, Wild S, von Keyserlingk NG, Elbling L, Zorbas H, Korynevska A, Knasmuller S, Sutterluty H, Micksche M, Keppler BK, Berger W (2006) *Biochem Pharmacol* 71:426–440
14. Sagmeister S, Eisenbauer M, Pirker C, Mohr T, Holzmann K, Zwickl H, Bichler C, Kandioler D, Wrba F, Mikulits W, Gerner C, Shehata M, Majdic O, Streubel B, Berger W, Micksche M, Zatloukal K, Schulte-Hermann R, Grasl-Kraupp B (2008) *Br J Cancer* 99:151–159
15. Janson V, Andersson B, Behnam-Motlagh P, Engstrom KG, Henriksson R, Grankvist K (2008) *Cell Physiol Biochem* 22:45–56
16. Bunz F, Fauth C, Speicher MR, Dutriaux A, Sedivy JM, Kinzler KW, Vogelstein B, Lengauer C (2002) *Cancer Res* 62:1129–1133
17. Egger A, Rappel C, Jakupec MA, Hartinger CG, Heffeter P, Keppler BK (2009) *J Anal At Spectrom* 24:51–61
18. Koellensperger G, Daubert S, Erdmann R, Hann S, Rottensteiner HP (2007) *Chem Biol* 388:1209–1214
19. Heffeter P, Jakupec MA, Korner W, Chiba P, Pirker C, Dornetshuber R, Elbling L, Sutterluty H, Micksche M, Keppler BK, Berger W (2007) *Biochem Pharmacol* 73:1873–1886
20. Berger W, Elbling L, Micksche M (2000) *Int J Cancer* 88:293–300
21. Korynevska A, Heffeter P, Matselyukh B, Elbling L, Micksche M, Stoika R, Berger W (2007) *Biochem Pharmacol* 74:1713–1726
22. Hall AG (1999) *Adv Exp Med Biol* 457:199–203
23. Hann S, Obinger C, Stingeder G, Paumann M, Furtmüller PG, Koellensperger G (2006) *J Anal At Spectrom* 21:1224–1231
24. Pizarro AM, Sadler PJ (2009) *Biochimie* 91:1198–1211
25. Sakurai H, Okamoto M, Hasegawa M, Satoh T, Oikawa M, Kammiya T, Arakawa K, Nakano T (2008) *Cancer Sci* 99:901–904
26. Pawarode A, Shukla S, Minderman H, Fricke SM, Pinder EM, O’Loughlin KL, Ambudkar SV, Baer MR (2007) *Cancer Chemother Pharmacol* 60:179–188
27. Brabec V, Novakova O (2006) *Drug Resist Updat* 9:111–122
28. Smalley KS, Contractor R, Haass NK, Kulp AN, Atilla-Gokcumen GE, Williams DS, Bregman H, Flaherty KT, Soengas MS, Meggers E, Herlyn M (2007) *Cancer Res* 67:209–217
29. Xie P, Williams DS, Atilla-Gokcumen GE, Milk L, Xiao M, Smalley KS, Herlyn M, Meggers E, Marmorstein R (2008) *ACS Chem Biol* 3:305–316
30. Bullock AN, Russo S, Amos A, Pagano N, Bregman H, Debreczeni JE, Lee WH, von Delft F, Meggers E, Knapp S (2009) *PLoS One* 4:e7112
31. Bergamo A, Sava G (2007) *Dalton Trans* 1267–1272
32. Alessio E, Mestroni G, Bergamo A, Sava G (2004) *Curr Top Med Chem* 4:1525–1535
33. Schluga P, Hartinger CG, Egger A, Reisner E, Galanski M, Jakupec MA, Keppler BK (2006) *Dalton Trans* 1796–1802
34. Bursch W, Karwan A, Mayer M, Dornetshuber J, Frohwein U, Schulte-Hermann R, Fazi B, Di Sano F, Piredda L, Piacentini M, Petrovski G, Fesus L, Gerner C (2008) *Toxicology* 254:147–157
35. Jung T, Grune T (2008) *IUBMB Life* 60:743–752
36. Meng X, Leyva ML, Jenny M, Gross I, Benosman S, Fricker B, Harlepp S, Hebraud P, Boos A, Wlosik P, Bischoff P, Sirlin C, Pfeiffer M, Loeffler JP, Gaidon C (2009) *Cancer Res* 69:5458–5466

10. REFERENCES

1. Hartinger, C.G., et al., *From bench to bedside--preclinical and early clinical development of the anticancer agent indazolium trans-[tetrachlorobis(1H-indazole)ruthenate(III)] (KP1019 or FFC14A)*. J Inorg Biochem, 2006. **100**(5-6): p. 891-904.
2. Berger, M.R., et al., *Efficacy of new ruthenium complexes against chemically induced autochthonous colorectal carcinoma in rats*. Anticancer Res, 1989. **9**(3): p. 761-5.
3. Knowles, M.A. and P.J. Selby, *Introduction to the Cellular and Molecular Biology of Cancer*. 2005: p. 552.
4. Weinberg, R.A., *The Biology of Cancer*. 2007, Massachusetts, USA: Garland Science.
5. Smith, C., A.D. Marks, and M. Lieberman, *Marks' Basic Medical Biochemistry*. 3 ed. 2009: Lippincott Williams & Wilkins. 1024.
6. Franks, L.M. and N.M. Teich, *Introduction to the Cellular and Molecular Biology of Cancer*. Third Edition ed. 2003: Oxford University Press.
7. Hanahan, D. and R.A. Weinberg, *The hallmarks of cancer*. Cell, 2000. **100**(1): p. 57-70.
8. Grander, D., *How do mutated oncogenes and tumor suppressor genes cause cancer?* Med Oncol, 1998. **15**(1): p. 20-6.
9. Heppner, G.H. and F.R. Miller, *The cellular basis of tumor progression*. Int Rev Cytol, 1998. **177**: p. 1-56.
10. Cairns, J., *The cancer problem*. Sci Am, 1975. **233**(5): p. 64-72, 77-8.
11. Reya, T., et al., *Stem cells, cancer, and cancer stem cells*. Nature, 2001. **414**(6859): p. 105-11.
12. Luo, J., N.L. Solimini, and S.J. Elledge, *Principles of cancer therapy: oncogene and non-oncogene addiction*. Cell, 2009. **136**(5): p. 823-37.
13. Fedi, P., S.R. Tronick, and S.A. Aaronson, *Growth factors*. Cancer Medicine, 1997: p. 41-46.
14. Slamon, D.J., et al., *Human breast cancer: correlation of relapse and survival with amplification of the HER-2/neu oncogene*. Science, 1987. **235**(4785): p. 177-82.
15. Yarden, Y. and A. Ullrich, *EGF and erbB2 receptor overexpression in human tumors*. Annu Rev Biochem, 1988. **57**: p. 443-478.
16. Giancotti, F.G. and E. Ruoslahti, *Integrin signaling*. Science, 1999. **285**(5430): p. 1028-32.
17. Weinberg, R.A., *The retinoblastoma protein and cell cycle control*. Cell, 1995. **81**(3): p. 323-30.
18. Datto, M.B., et al., *The viral oncoprotein E1A blocks transforming growth factor beta-mediated induction of p21/WAF1/Cip1 and p15/INK4B*. Mol Cell Biol, 1997. **17**(4): p. 2030-7.
19. Hannon, G.J. and D. Beach, *p15INK4B is a potential effector of TGF-beta-induced cell cycle arrest*. Nature, 1994. **371**(6494): p. 257-61.
20. Kerr, J.F., A.H. Wyllie, and A.R. Currie, *Apoptosis: a basic biological phenomenon with wide-ranging implications in tissue kinetics*. Br J Cancer, 1972. **26**(4): p. 239-57.
21. Korsmeyer, S.J., *Chromosomal translocations in lymphoid malignancies reveal novel proto-oncogenes*. Annu Rev Immunol, 1992. **10**: p. 785-807.

REFERENCES

22. Vaux, D.L., S. Cory, and J.M. Adams, *Bcl-2 gene promotes haemopoietic cell survival and cooperates with c-myc to immortalize pre-B cells*. *Nature*, 1988. **335**(6189): p. 440-2.
23. McDonnell, T.J. and S.J. Korsmeyer, *Progression from lymphoid hyperplasia to high-grade malignant lymphoma in mice transgenic for the t(14; 18)*. *Nature*, 1991. **349**(6306): p. 254-6.
24. Levine, A.J., *p53, the cellular gatekeeper for growth and division*. *Cell*, 1997. **88**(3): p. 323-31.
25. Evan, G. and T. Littlewood, *A matter of life and cell death*. *Science*, 1998. **281**(5381): p. 1317-22.
26. Bodnar, A.G., et al., *Extension of life-span by introduction of telomerase into normal human cells*. *Science*, 1998. **279**(5349): p. 349-52.
27. Vaziri, H. and S. Benchimol, *Reconstitution of telomerase activity in normal human cells leads to elongation of telomeres and extended replicative life span*. *Curr Biol*, 1998. **8**(5): p. 279-82.
28. Kimura, T., et al., *Interactions of ginsenosides with ligand-bindings of GABA(A) and GABA(B) receptors*. *Gen Pharmacol*, 1994. **25**(1): p. 193-9.
29. Cao, Y., T.M. Bryan, and R.R. Reddel, *Increased copy number of the TERT and TERC telomerase subunit genes in cancer cells*. *Cancer Sci*, 2008. **99**(6): p. 1092-9.
30. Lansdorp, P.M., *Telomeres and disease*. *Embo J*, 2009. **28**(17): p. 2532-40.
31. Hartwell, L.H. and M.B. Kastan, *Cell cycle control and cancer*. *Science*, 1994. **266**(5192): p. 1821-8.
32. Maser, R.S. and R.A. DePinho, *Connecting chromosomes, crisis, and cancer*. *Science*, 2002. **297**(5581): p. 565-9.
33. Rak, J., et al., *Oncogenes as inducers of tumor angiogenesis*. *Cancer Metastasis Rev*, 1995. **14**(4): p. 263-77.
34. Maxwell, P.H., et al., *The tumour suppressor protein VHL targets hypoxia-inducible factors for oxygen-dependent proteolysis*. *Nature*, 1999. **399**(6733): p. 271-5.
35. Sporn, M.B., *The war on cancer*. *Lancet*, 1996. **347**(9012): p. 1377-81.
36. Christofori, G. and H. Semb, *The role of the cell-adhesion molecule E-cadherin as a tumour-suppressor gene*. *Trends Biochem Sci*, 1999. **24**(2): p. 73-6.
37. Coussens, L.M. and Z. Werb, *Matrix metalloproteinases and the development of cancer*. *Chem Biol*, 1996. **3**(11): p. 895-904.
38. Chambers, A.F. and L.M. Matrisian, *Changing views of the role of matrix metalloproteinases in metastasis*. *J Natl Cancer Inst*, 1997. **89**(17): p. 1260-70.
39. Kroemer, G. and J. Pouyssegur, *Tumor cell metabolism: cancer's Achilles' heel*. *Cancer Cell*, 2008. **13**(6): p. 472-82.
40. Condeelis, J. and J.W. Pollard, *Macrophages: obligate partners for tumor cell migration, invasion, and metastasis*. *Cell*, 2006. **124**(2): p. 263-6.
41. Cramer, T., et al., *HIF-1alpha is essential for myeloid cell-mediated inflammation*. *Cell*, 2003. **112**(5): p. 645-57.
42. Bartkova, J., et al., *Oncogene-induced senescence is part of the tumorigenesis barrier imposed by DNA damage checkpoints*. *Nature*, 2006. **444**(7119): p. 633-7.
43. Di Micco, R., et al., *Oncogene-induced senescence is a DNA damage response triggered by DNA hyper-replication*. *Nature*, 2006. **444**(7119): p. 638-42.
44. Halazonetis, T.D., V.G. Gorgoulis, and J. Bartek, *An oncogene-induced DNA damage model for cancer development*. *Science*, 2008. **319**(5868): p. 1352-5.

45. Harper, J.W. and S.J. Elledge, *The DNA damage response: ten years after*. Mol Cell, 2007. **28**(5): p. 739-45.
46. Komarova, N.L., et al., *Dynamics of genetic instability in sporadic and familial colorectal cancer*. Cancer Biol Ther, 2002. **1**(6): p. 685-92.
47. Cahill, D.P., et al., *Mutations of mitotic checkpoint genes in human cancers*. Nature, 1998. **392**(6673): p. 300-3.
48. Denko, N.C., et al., *The human Ha-ras oncogene induces genomic instability in murine fibroblasts within one cell cycle*. Proc Natl Acad Sci U S A, 1994. **91**(11): p. 5124-8.
49. Pollack, J.R., et al., *Microarray analysis reveals a major direct role of DNA copy number alteration in the transcriptional program of human breast tumors*. Proc Natl Acad Sci U S A, 2002. **99**(20): p. 12963-8.
50. Torres, E.M., et al., *Effects of aneuploidy on cellular physiology and cell division in haploid yeast*. Science, 2007. **317**(5840): p. 916-24.
51. Tsafirir, D., et al., *Relationship of gene expression and chromosomal abnormalities in colorectal cancer*. Cancer Res, 2006. **66**(4): p. 2129-37.
52. Denoyelle, C., et al., *Anti-oncogenic role of the endoplasmic reticulum differentially activated by mutations in the MAPK pathway*. Nat Cell Biol, 2006. **8**(10): p. 1053-63.
53. Ganem, N.J., Z. Storchova, and D. Pellman, *Tetraploidy, aneuploidy and cancer*. Curr Opin Genet Dev, 2007. **17**(2): p. 157-62.
54. Torres, E.M., B.R. Williams, and A. Amon, *Aneuploidy: cells losing their balance*. Genetics, 2008. **179**(2): p. 737-46.
55. DeBerardinis, R.J., et al., *Beyond aerobic glycolysis: transformed cells can engage in glutamine metabolism that exceeds the requirement for protein and nucleotide synthesis*. Proc Natl Acad Sci U S A, 2007. **104**(49): p. 19345-50.
56. Warburg, O., *On the origin of cancer cells*. Science, 1956. **123**(3191): p. 309-14.
57. Sztatowski, T.P. and C.F. Nathan, *Production of large amounts of hydrogen peroxide by human tumor cells*. Cancer Res, 1991. **51**(3): p. 794-8.
58. Lee, A.C., et al., *Ras proteins induce senescence by altering the intracellular levels of reactive oxygen species*. J Biol Chem, 1999. **274**(12): p. 7936-40.
59. Gogvadze, V., S. Orrenius, and B. Zhivotovsky, *Mitochondria in cancer cells: what is so special about them?* Trends Cell Biol, 2008. **18**(4): p. 165-73.
60. Dewhirst, M.W., Y. Cao, and B. Moeller, *Cycling hypoxia and free radicals regulate angiogenesis and radiotherapy response*. Nat Rev Cancer, 2008. **8**(6): p. 425-37.
61. Hogge, D.E., *Cytogenetics and oncogenes in leukemia*. Curr Opin Oncol, 1994. **6**(1): p. 3-13.
62. Campana, D. and C.H. Pui, *Detection of minimal residual disease in acute leukemia: methodologic advances and clinical significance*. Blood, 1995. **85**(6): p. 1416-34.
63. Cotter, F.E., *Molecular pathology of lymphomas*. Cancer Surv, 1993. **16**: p. 157-74.
64. Thomas, M.B. and A.X. Zhu, *Hepatocellular carcinoma: the need for progress*. J Clin Oncol, 2005. **23**(13): p. 2892-9.
65. Kensler, T.W., et al., *Translational strategies for cancer prevention in liver*. Nat Rev Cancer, 2003. **3**(5): p. 321-9.
66. Voiculescu, M., et al., *Chemotherapies and targeted therapies in advanced hepatocellular carcinoma: from laboratory to clinic*. J Gastrointestin Liver Dis, 2008. **17**(3): p. 315-22.
67. Cozza, P., A. Giancotti, and A. Petrosino, *Butterfly expander for use in the mixed dentition*. J Clin Orthod, 1999. **33**(10): p. 583-7 contd.

REFERENCES

68. Kim, N.W., et al., *Specific association of human telomerase activity with immortal cells and cancer*. Science, 1994. **266**(5193): p. 2011-5.
69. Chan, K.T. and M.L. Lung, *Mutant p53 expression enhances drug resistance in a hepatocellular carcinoma cell line*. Cancer Chemother Pharmacol, 2004. **53**(6): p. 519-26.
70. Bush, J.A. and G. Li, *Cancer chemoresistance: the relationship between p53 and multidrug transporters*. Int J Cancer, 2002. **98**(3): p. 323-30.
71. Nguyen, K.T., et al., *Transactivation of the human multidrug resistance (MDR1) gene promoter by p53 mutants*. Oncol Res, 1994. **6**(2): p. 71-7.
72. Sampath, J., et al., *Mutant p53 cooperates with ETS and selectively up-regulates human MDR1 not MRP1*. J Biol Chem, 2001. **276**(42): p. 39359-67.
73. Chin, K.V., et al., *Modulation of activity of the promoter of the human MDR1 gene by Ras and p53*. Science, 1992. **255**(5043): p. 459-62.
74. Strauss, B.E., et al., *The MDR1 downstream promoter contains sequence-specific binding sites for wild-type p53*. Biochem Biophys Res Commun, 1995. **217**(3): p. 825-31.
75. Strunin, L., *Metabolism of drugs by the liver*. Ann R Coll Surg Engl, 1971. **48**(2): p. 76-7.
76. Keating, G.M. and A. Santoro, *Sorafenib: a review of its use in advanced hepatocellular carcinoma*. Drugs, 2009. **69**(2): p. 223-40.
77. Adnane, L., et al., *Sorafenib (BAY 43-9006, Nexavar), a dual-action inhibitor that targets RAF/MEK/ERK pathway in tumor cells and tyrosine kinases VEGFR/PDGFR in tumor vasculature*. Methods Enzymol, 2006. **407**: p. 597-612.
78. Wilhelm, S.M., et al., *BAY 43-9006 exhibits broad spectrum oral antitumor activity and targets the RAF/MEK/ERK pathway and receptor tyrosine kinases involved in tumor progression and angiogenesis*. Cancer Res, 2004. **64**(19): p. 7099-109.
79. Farazi, P.A. and R.A. DePinho, *Hepatocellular carcinoma pathogenesis: from genes to environment*. Nat Rev Cancer, 2006. **6**(9): p. 674-87.
80. Bartosch, B., et al., *Hepatitis C virus-induced hepatocarcinogenesis*. J Hepatol, 2009. **51**(4): p. 810-20.
81. Matsuda, Y. and T. Ichida, *Impact of hepatitis B virus X protein on the DNA damage response during hepatocarcinogenesis*. Med Mol Morphol, 2009. **42**(3): p. 138-42.
82. Hollinger, F.B., *Hepatitis B virus*. 3 ed. Fields virology. 1996, Philadelphia: Lippincott.Raven.
83. Paterlini, P., et al., *Selective accumulation of the X transcript of hepatitis B virus in patients negative for hepatitis B surface antigen with hepatocellular carcinoma*. Hepatology, 1995. **21**(2): p. 313-21.
84. Unsal, H., et al., *Genetic heterogeneity of hepatocellular carcinoma*. Proc Natl Acad Sci U S A, 1994. **91**(2): p. 822-6.
85. Feitelson, M.A., *Hepatitis B virus in hepatocarcinogenesis*. J Cell Physiol, 1999. **181**(2): p. 188-202.
86. Twu, J.S. and W.S. Robinson, *Hepatitis B virus X gene can transactivate heterologous viral sequences*. Proc Natl Acad Sci U S A, 1989. **86**(6): p. 2046-50.
87. Moradpour, D., F. Penin, and C.M. Rice, *Replication of hepatitis C virus*. Nat Rev Microbiol, 2007. **5**(6): p. 453-63.
88. McClain, C.J., et al., *Monocyte activation in alcoholic liver disease*. Alcohol, 2002. **27**(1): p. 53-61.

89. McClain, C.J., et al., *S-Adenosylmethionine, cytokines, and alcoholic liver disease*. Alcohol, 2002. **27**(3): p. 185-92.
90. Hoek, J.B. and J.G. Pastorino, *Ethanol, oxidative stress, and cytokine-induced liver cell injury*. Alcohol, 2002. **27**(1): p. 63-8.
91. Coussens, L.M. and Z. Werb, *Inflammation and cancer*. Nature, 2002. **420**(6917): p. 860-7.
92. Wild, C.P. and P.C. Turner, *The toxicology of aflatoxins as a basis for public health decisions*. Mutagenesis, 2002. **17**(6): p. 471-81.
93. Liang, T.J., *p53 proteins and aflatoxin b1: the good, the bad, and the ugly*. Hepatology, 1995. **22**(4 Pt 1): p. 1330-2.
94. Riley, J., et al., *In vitro activation of the human Harvey-ras proto-oncogene by aflatoxin B1*. Carcinogenesis, 1997. **18**(5): p. 905-10.
95. Kew, M.C., *Synergistic interaction between aflatoxin B1 and hepatitis B virus in hepatocarcinogenesis*. Liver Int, 2003. **23**(6): p. 405-9.
96. Gregorieff, A. and H. Clevers, *Wnt signaling in the intestinal epithelium: from endoderm to cancer*. Genes Dev, 2005. **19**(8): p. 877-90.
97. Feitelson, M.A., et al., *Genetic mechanisms of hepatocarcinogenesis*. Oncogene, 2002. **21**(16): p. 2593-604.
98. Daveau, M., et al., *Hepatocyte growth factor, transforming growth factor alpha, and their receptors as combined markers of prognosis in hepatocellular carcinoma*. Mol Carcinog, 2003. **36**(3): p. 130-41.
99. Matsuda, Y., et al., *p16(INK4) is inactivated by extensive CpG methylation in human hepatocellular carcinoma*. Gastroenterology, 1999. **116**(2): p. 394-400.
100. Murata, H., et al., *Promoter hypermethylation silences cyclooxygenase-2 (Cox-2) and regulates growth of human hepatocellular carcinoma cells*. Lab Invest, 2004. **84**(8): p. 1050-9.
101. Schmoll, H.J., K. Höffken, and K. Possinger, *Kompendium Internistische Onkologie*. 1999. **1**.
102. Hardman, J.G. and L.E. Limbird, *The Pharmacological Basis of Therapeutics*. 10 ed, ed. G. Gilman.
103. Chu, G., *Cellular responses to cisplatin. The roles of DNA-binding proteins and DNA repair*. J Biol Chem, 1994. **269**(2): p. 787-90.
104. Twentyman, P.R., *Bleomycin--mode of action with particular reference to the cell cycle*. Pharmacol Ther, 1983. **23**(3): p. 417-41.
105. Smets, L.A., *Programmed cell death (apoptosis) and response to anti-cancer drugs*. Anticancer Drugs, 1994. **5**(1): p. 3-9.
106. Rosenberg, B., L. Vancamp, and T. Krigas, *Inhibition of Cell Division in Escherichia Coli by Electrolysis Products from a Platinum Electrode*. Nature, 1965. **205**: p. 698-9.
107. Rosenberg, B., et al., *Platinum compounds: a new class of potent antitumour agents*. Nature, 1969. **222**(5191): p. 385-6.
108. Rebillard, A., D. Lagadic-Gossmann, and M.T. Dimanche-Boitrel, *Cisplatin cytotoxicity: DNA and plasma membrane targets*. Curr Med Chem, 2008. **15**(26): p. 2656-63.
109. Sheikh-Hamad, D., *Cisplatin-induced cytotoxicity: is the nucleus relevant?* Am J Physiol Renal Physiol, 2008. **295**(1): p. F42-3.
110. Johnson, E.R., et al., *Metal Antitumor Compounds: The Mechanism of Action of Platinum Complexes*. Prog. Clin. Biochem. Med., 1989. **10**: p. 1-24.

REFERENCES

111. Reedijk, J., *Medicinal Applications of Metal Complexes Binding to Biological Macromolecules*. Macromolecular Symposium, 2008. **270**: p. 193-201.
112. Weiss, R.B. and M.C. Christian, *New cisplatin analogues in development. A review*. Drugs, 1993. **46**(3): p. 360-77.
113. Wong, E. and C.M. Giandomenico, *Current status of platinum-based antitumor drugs*. Chem Rev, 1999. **99**(9): p. 2451-66.
114. Giaccone, G., *Clinical perspectives on platinum resistance*. Drugs, 2000. **59 Suppl 4**: p. 9-17; discussion 37-8.
115. Kostova, I., *Ruthenium complexes as anticancer agents*. Curr Med Chem, 2006. **13**(9): p. 1085-107.
116. Barabas, K., et al., *Cisplatin: a review of toxicities and therapeutic applications*. Vet Comp Oncol, 2008. **6**(1): p. 1-18.
117. Wernyj, R.P. and P.J. Morin, *Molecular mechanisms of platinum resistance: still searching for the Achilles' heel*. Drug Resist Updat, 2004. **7**(4-5): p. 227-32.
118. Sava, G. and A. Bergamo, *Ruthenium-based compounds and tumour growth control (review)*. Int J Oncol, 2000. **17**(2): p. 353-65.
119. Fruhauf, S. and W.J. Zeller, *New platinum, titanium, and ruthenium complexes with different patterns of DNA damage in rat ovarian tumor cells*. Cancer Res, 1991. **51**(11): p. 2943-8.
120. Coluccia, M., et al., *Anti-leukaemic action of RuCl₂ (DMSO)₄ isomers and prevention of brain involvement on P388 leukaemia and on P388/DDP subline*. Eur J Cancer, 1993. **29A**(13): p. 1873-9.
121. Clarke, M.J., *Ruthenium metallopharmaceuticals*. Coordination Chemistry Reviews, 2002. **236**(1-2): p. 209-233.
122. Alessio, E., et al., *Ruthenium anticancer drugs*. Met Ions Biol Syst, 2004. **42**: p. 323-51.
123. Kratz, F., et al., *The binding properties of two antitumor ruthenium(III) complexes to apotransferrin*. J Biol Chem, 1994. **269**(4): p. 2581-8.
124. Frasca, D., et al., *Effects of hypoxia and transferrin on toxicity and DNA binding of ruthenium antitumor agents in hela cells*. Met Based Drugs, 1996. **3**(4): p. 197-209.
125. Wike-Hooley, J.L.H., J; Reinhold, H. S., *Radiotherapeutical Oncology*, 1984. **2**: p. 343.
126. Anghileri, L.J., *The in vivo inhibition of tumor growth by ruthenium red: its relationship with the metabolism of calcium in the tumor*. Z Krebsforsch Klin Onkol Cancer Res Clin Oncol, 1975. **83**(3): p. 213-7.
127. Seelig, M.H., M.R. Berger, and B.K. Keppler, *Antineoplastic activity of three ruthenium derivatives against chemically induced colorectal carcinoma in rats*. J Cancer Res Clin Oncol, 1992. **118**(3): p. 195-200.
128. Galeano, A., M.R. Berger, and B.K. Keppler, *Antitumor activity of some ruthenium derivatives in human colon cancer cell lines in vitro*. Arzneimittelforschung, 1992. **42**(6): p. 821-4.
129. Frasca, D.R., L.E. Gehrig, and M.J. Clarke, *Cellular effects of transferrin coordinated to*. J Inorg Biochem, 2001. **83**(2-3): p. 139-49.
130. Jakupec, M.A., et al., *Redox-active antineoplastic ruthenium complexes with indazole: correlation of in vitro potency and reduction potential*. J Med Chem, 2005. **48**(8): p. 2831-7.
131. Kapitza, S., et al., *The heterocyclic ruthenium(III) complex KP1019 (FFC14A) causes DNA damage and oxidative stress in colorectal tumor cells*. Cancer Lett, 2005. **226**(2): p. 115-21.

132. Kapitzka, S., et al., *Heterocyclic complexes of ruthenium(III) induce apoptosis in colorectal carcinoma cells*. J Cancer Res Clin Oncol, 2005. **131**(2): p. 101-10.
133. Messori, L., et al., *Binding of Antitumor Ruthenium(III) Complexes to Plasma Proteins*. Met Based Drugs, 2000. **7**(6): p. 335-42.
134. Heffeter, P., et al., *Intrinsic and acquired forms of resistance against the anticancer ruthenium compound KP1019 [indazolium trans-[tetrachlorobis(1H-indazole)ruthenate (III)] (FFC14A)]*. J Pharmacol Exp Ther, 2005. **312**(1): p. 281-9.
135. Goda, K., Z. Bacso, and G. Szabo, *Multidrug resistance through the spectacle of P-glycoprotein*. Curr Cancer Drug Targets, 2009. **9**(3): p. 281-97.
136. Hartinger, C.G., et al., *KP1019, a new redox-active anticancer agent--preclinical development and results of a clinical phase I study in tumor patients*. Chem Biodivers, 2008. **5**(10): p. 2140-55.
137. Alberts, B., et al., *Molecular Biology of the Cell*. 2001: WILEY-VCH.
138. Lundberg, A.S. and R.A. Weinberg, *Control of the cell cycle and apoptosis*. Eur J Cancer, 1999. **35**(14): p. 1886-94.
139. Pardee, A.B., *A restriction point for control of normal animal cell proliferation*. Proc Natl Acad Sci U S A, 1974. **71**(4): p. 1286-90.
140. Evan, G.I. and K.H. Vousden, *Proliferation, cell cycle and apoptosis in cancer*. Nature, 2001. **411**(6835): p. 342-8.
141. Roovers, K. and R.K. Assoian, *Integrating the MAP kinase signal into the G1 phase cell cycle machinery*. Bioessays, 2000. **22**(9): p. 818-26.
142. Blume-Jensen, P. and T. Hunter, *Oncogenic kinase signalling*. Nature, 2001. **411**(6835): p. 355-65.
143. Harbour, J.W. and D.C. Dean, *The Rb/E2F pathway: expanding roles and emerging paradigms*. Genes Dev, 2000. **14**(19): p. 2393-409.
144. Janicke, R.U., et al., *Specific cleavage of the retinoblastoma protein by an ICE-like protease in apoptosis*. EMBO J, 1996. **15**(24): p. 6969-78.
145. Baudino, T.A. and J.L. Cleveland, *The Max network gone mad*. Mol Cell Biol, 2001. **21**(3): p. 691-702.
146. Hartwell, L.H. and T.A. Weinert, *Checkpoints: controls that ensure the order of cell cycle events*. Science, 1989. **246**(4930): p. 629-34.
147. Kastan, M.B. and J. Bartek, *Cell-cycle checkpoints and cancer*. Nature, 2004. **432**(7015): p. 316-23.
148. Dynlacht, B.D., *Regulation of transcription by proteins that control the cell cycle*. Nature, 1997. **389**(6647): p. 149-52.
149. Bartek, J., C. Lukas, and J. Lukas, *Checking on DNA damage in S phase*. Nat Rev Mol Cell Biol, 2004. **5**(10): p. 792-804.
150. Bartek, J. and J. Lukas, *Chk1 and Chk2 kinases in checkpoint control and cancer*. Cancer Cell, 2003. **3**(5): p. 421-9.
151. Donzelli, M. and G.F. Draetta, *Regulating mammalian checkpoints through Cdc25 inactivation*. EMBO Rep, 2003. **4**(7): p. 671-7.
152. Nyberg, K.A., et al., *Toward maintaining the genome: DNA damage and replication checkpoints*. Annu Rev Genet, 2002. **36**: p. 617-56.
153. Mailand, N., et al., *Regulation of G(2)/M events by Cdc25A through phosphorylation-dependent modulation of its stability*. EMBO J, 2002. **21**(21): p. 5911-20.
154. Bulavin, D.V., et al., *Initiation of a G2/M checkpoint after ultraviolet radiation requires p38 kinase*. Nature, 2001. **411**(6833): p. 102-7.

REFERENCES

155. Newbold, R.F. and R.W. Overell, *Fibroblast immortality is a prerequisite for transformation by EJ c-Ha-ras oncogene*. *Nature*, 1983. **304**(5927): p. 648-51.
156. Serrano, M., et al., *Oncogenic ras provokes premature cell senescence associated with accumulation of p53 and p16INK4a*. *Cell*, 1997. **88**(5): p. 593-602.
157. Askew, D.S., et al., *Constitutive c-myc expression in an IL-3-dependent myeloid cell line suppresses cell cycle arrest and accelerates apoptosis*. *Oncogene*, 1991. **6**(10): p. 1915-22.
158. Evan, G.I., et al., *Induction of apoptosis in fibroblasts by c-myc protein*. *Cell*, 1992. **69**(1): p. 119-28.
159. Lane, D.P., *Cancer. p53, guardian of the genome*. *Nature*, 1992. **358**(6381): p. 15-6.
160. Johnstone, R.W., A.A. Ruefli, and S.W. Lowe, *Apoptosis: a link between cancer genetics and chemotherapy*. *Cell*, 2002. **108**(2): p. 153-64.
161. Allan, L.A. and P.R. Clarke, *Apoptosis and autophagy: Regulation of caspase-9 by phosphorylation*. *FEBS J*, 2009. **276**(21): p. 6063-73.
162. Bras, M., B. Queenan, and S.A. Susin, *Programmed cell death via mitochondria: different modes of dying*. *Biochemistry (Mosc)*, 2005. **70**(2): p. 231-9.
163. Virchow, R., *Die Cellularpathologie in ihrer Begründung auf physiologische Gewebelehre*. 4 ed. 1871.
164. Clarke, P.G., *Developmental cell death: morphological diversity and multiple mechanisms*. *Anat Embryol (Berl)*, 1990. **181**(3): p. 195-213.
165. Schweichel, J.U. and H.J. Merker, *The morphology of various types of cell death in prenatal tissues*. *Teratology*, 1973. **7**(3): p. 253-66.
166. Henze, K. and W. Martin, *Evolutionary biology: essence of mitochondria*. *Nature*, 2003. **426**(6963): p. 127-8.
167. McBride, H.M., M. Neuspiel, and S. Wasiak, *Mitochondria: more than just a powerhouse*. *Curr Biol*, 2006. **16**(14): p. R551-60.
168. Green, D.R., *Apoptotic pathways: paper wraps stone blunts scissors*. *Cell*, 2000. **102**(1): p. 1-4.
169. Wang, X., *The expanding role of mitochondria in apoptosis*. *Genes Dev*, 2001. **15**(22): p. 2922-33.
170. Chipuk, J.E. and D.R. Green, *How do BCL-2 proteins induce mitochondrial outer membrane permeabilization?* *Trends Cell Biol*, 2008. **18**(4): p. 157-64.
171. Zou, H., et al., *Apaf-1, a human protein homologous to C. elegans CED-4, participates in cytochrome c-dependent activation of caspase-3*. *Cell*, 1997. **90**(3): p. 405-13.
172. Li, P., et al., *Cytochrome c and dATP-dependent formation of Apaf-1/caspase-9 complex initiates an apoptotic protease cascade*. *Cell*, 1997. **91**(4): p. 479-89.
173. Liu, X., et al., *Induction of apoptotic program in cell-free extracts: requirement for dATP and cytochrome c*. *Cell*, 1996. **86**(1): p. 147-57.
174. Cain, K., et al., *Apaf-1 oligomerizes into biologically active approximately 700-kDa and inactive approximately 1.4-MDa apoptosome complexes*. *J Biol Chem*, 2000. **275**(9): p. 6067-70.
175. Kurokawa, M. and S. Kornbluth, *Caspases and kinases in a death grip*. *Cell*, 2009. **138**(5): p. 838-54.
176. Slee, E.A., et al., *Ordering the cytochrome c-initiated caspase cascade: hierarchical activation of caspases-2, -3, -6, -7, -8, and -10 in a caspase-9-dependent manner*. *J Cell Biol*, 1999. **144**(2): p. 281-92.

177. Van de Craen, M., et al., *The proteolytic procaspase activation network: an in vitro analysis*. Cell Death Differ, 1999. **6**(11): p. 1117-24.
178. Galluzzi, L. and G. Kroemer, *Mitochondrial apoptosis without VDAC*. Nat Cell Biol, 2007. **9**(5): p. 487-9.
179. Kim, J.S., L. He, and J.J. Lemasters, *Mitochondrial permeability transition: a common pathway to necrosis and apoptosis*. Biochem Biophys Res Commun, 2003. **304**(3): p. 463-70.
180. Belzacq, A.S., et al., *The adenine nucleotide translocator in apoptosis*. Biochimie, 2002. **84**(2-3): p. 167-76.
181. Marzo, I., et al., *Bax and adenine nucleotide translocator cooperate in the mitochondrial control of apoptosis*. Science, 1998. **281**(5385): p. 2027-31.
182. Shimizu, S., M. Narita, and Y. Tsujimoto, *Bcl-2 family proteins regulate the release of apoptogenic cytochrome c by the mitochondrial channel VDAC*. Nature, 1999. **399**(6735): p. 483-7.
183. Bergamini, C.M., et al., *Oxygen, reactive oxygen species and tissue damage*. Curr Pharm Des, 2004. **10**(14): p. 1611-26.
184. Huang, P., et al., *Superoxide dismutase as a target for the selective killing of cancer cells*. Nature, 2000. **407**(6802): p. 390-5.
185. Pelicano, H., et al., *Inhibition of mitochondrial respiration: a novel strategy to enhance drug-induced apoptosis in human leukemia cells by a reactive oxygen species-mediated mechanism*. J Biol Chem, 2003. **278**(39): p. 37832-9.
186. Waterhouse, N.J., et al., *Cytochrome c maintains mitochondrial transmembrane potential and ATP generation after outer mitochondrial membrane permeabilization during the apoptotic process*. J Cell Biol, 2001. **153**(2): p. 319-28.
187. Volm, M., *Multidrug resistance and its reversal*. Anticancer Res, 1998. **18**(4C): p. 2905-17.
188. Dang, C.V. and G.L. Semenza, *Oncogenic alterations of metabolism*. Trends Biochem Sci, 1999. **24**(2): p. 68-72.
189. Lipponer, K.G., E. Vogel, and B.K. Keppler, *Synthesis, Characterization and Solution Chemistry of trans-Indazoliumtetrachlorobis(Indazole)Ruthenate(III), a New Anticancer Ruthenium Complex. IR, UV, NMR, HPLC Investigations and Antitumor Activity. Crystal Structures of trans-1-Methyl-Indazoliumtetrachlorobis-(1-Methylindazole)Ruthenate(III) and its Hydrolysis Product trans-Monoaquatrchlorobis-(1-Methylindazole)-Ruthenate(III)*. Met Based Drugs, 1996. **3**(5): p. 243-60.
190. Elion, G.B., S. Singer, and G.H. Hitchings, *Antagonists of nucleic acid derivatives. VIII. Synergism in combinations of biochemically related antimetabolites*. J Biol Chem, 1954. **208**(2): p. 477-88.
191. Eliopoulos, G.M., P. Lorian, and R.C. Moellering, *Antibiotics in Laboratorz Medicine*. 4 ed. 1991: Lippincott, Williams & Wilkins.
192. Chitambar, C.R., et al., *Development of drug resistance to gallium nitrate through modulation of cellular iron uptake*. Cancer Res, 1990. **50**(15): p. 4468-72.
193. Shao, J., et al., *A Ferrous-Triapine complex mediates formation of reactive oxygen species that inactivate human ribonucleotide reductase*. Mol Cancer Ther, 2006. **5**(3): p. 586-92.
194. Wilhelm, S., et al., *Discovery and development of sorafenib: a multikinase inhibitor for treating cancer*. Nat Rev Drug Discov, 2006. **5**(10): p. 835-44.

REFERENCES

195. Hu, S., et al., *Interaction of the multikinase inhibitors sorafenib and sunitinib with solute carriers and ATP-binding cassette transporters*. Clin Cancer Res, 2009. **15**(19): p. 6062-9.
196. Chen, Y.N., et al., *Characterization of adriamycin-resistant human breast cancer cells which display overexpression of a novel resistance-related membrane protein*. J Biol Chem, 1990. **265**(17): p. 10073-80.
197. Nakagawa, M., et al., *Reduced intracellular drug accumulation in the absence of P-glycoprotein (mdr1) overexpression in mitoxantrone-resistant human MCF-7 breast cancer cells*. Cancer Res, 1992. **52**(22): p. 6175-81.
198. Yang, C.J., et al., *Cross-resistance to camptothecin analogues in a mitoxantrone-resistant human breast carcinoma cell line is not due to DNA topoisomerase I alterations*. Cancer Res, 1995. **55**(18): p. 4004-9.
199. Burger, H., et al., *Imatinib mesylate (STI571) is a substrate for the breast cancer resistance protein (BCRP)/ABCG2 drug pump*. Blood, 2004. **104**(9): p. 2940-2.
200. Elkind, N.B., et al., *Multidrug transporter ABCG2 prevents tumor cell death induced by the epidermal growth factor receptor inhibitor Iressa (ZD1839, Gefitinib)*. Cancer Res, 2005. **65**(5): p. 1770-7.
201. Shen, D.W., et al., *Multiple drug-resistant human KB carcinoma cells independently selected for high-level resistance to colchicine, adriamycin, or vinblastine show changes in expression of specific proteins*. J Biol Chem, 1986. **261**(17): p. 7762-70.
202. Jane, E.P., D.R. Premkumar, and I.F. Pollack, *Coadministration of sorafenib with rottlerin potently inhibits cell proliferation and migration in human malignant glioma cells*. J Pharmacol Exp Ther, 2006. **319**(3): p. 1070-80.
203. Peng, C.L., et al., *Sorafenib induces growth inhibition and apoptosis in human synovial sarcoma cells via inhibiting the RAF/MEK/ERK signaling pathway*. Cancer Biol Ther, 2009. **8**(18): p. 1729-36.
204. Li, N., et al., *[Schedule-dependent effects of sorafenib in combination with paclitaxel on human hepatocellular carcinoma cell line BEL-7402.]*. Chin J Cancer, 2009. **28**(8): p. 838-43.
205. Davis, R.J., *Signal transduction by the JNK group of MAP kinases*. Cell, 2000. **103**(2): p. 239-52.
206. Johnson, G.L. and R. Lapadat, *Mitogen-activated protein kinase pathways mediated by ERK, JNK, and p38 protein kinases*. Science, 2002. **298**(5600): p. 1911-2.
207. Liu, L., et al., *Sorafenib blocks the RAF/MEK/ERK pathway, inhibits tumor angiogenesis, and induces tumor cell apoptosis in hepatocellular carcinoma model PLC/PRF/5*. Cancer Res, 2006. **66**(24): p. 11851-8.
208. Brabec, V. and O. Novakova, *DNA binding mode of ruthenium complexes and relationship to tumor cell toxicity*. Drug Resist Updat, 2006. **9**(3): p. 111-22.
209. Dwyer, F.P., et al., *Biological activity of complex ions*. Nature, 1952. **170**(4318): p. 190-1.
210. Dwyer, F.P., et al., *Inhibition of Landschuetz Ascites Tumour Growth by Metal Chelates Derived from 3,4,7,8-Tetramethyl-1,10-Phenanthroline*. Br J Cancer, 1965. **19**: p. 195-9.
211. Fearon, E.R. and B. Vogelstein, *A genetic model for colorectal tumorigenesis*. Cell, 1990. **61**(5): p. 759-67.
212. Krajewska, M., et al., *Elevated expression of Bcl-X and reduced Bak in primary colorectal adenocarcinomas*. Cancer Res, 1996. **56**(10): p. 2422-7.

213. Hinoshita, E., et al., *Increased expression of an ATP-binding cassette superfamily transporter, multidrug resistance protein 2, in human colorectal carcinomas*. Clin Cancer Res, 2000. **6**(6): p. 2401-7.
214. Peng, K.C., et al., *Tissue and cell distribution of the multidrug resistance-associated protein (MRP) in mouse intestine and kidney*. J Histochem Cytochem, 1999. **47**(6): p. 757-68.
215. Kratz, F., et al., *Protein-binding Properties of two Antitumour Ru(III) Complexes to Human Apotransferrin and Apolactoferrin*. Met Based Drugs, 1994. **1**(2-3): p. 169-73.
216. Cetinbas, N., et al., *Serum-protein interactions with anticancer Ru(III) complexes KP1019 and KP418 characterized by EPR*. J Biol Inorg Chem, 2010. **15**(2): p. 131-45.
217. Messori, L., F. Kratz, and E. Alessio, *The Interaction of the Antitumor Complexes Na[trans-RuCl(4)(DMSO)(Im)] and Na[trans-RuCl(4)(DMSO)(Ind)] With Apotransferrin: a Spectroscopic Study*. Met Based Drugs, 1996. **3**(1): p. 1-9.
218. Messori, L., et al., *A spectroscopic study of the reaction of NAMI, a novel ruthenium(III)anti-neoplastic complex, with bovine serum albumin*. Eur J Biochem, 2000. **267**(4): p. 1206-13.
219. Malina, J., et al., *Biophysical analysis of natural, double-helical DNA modified by anticancer heterocyclic complexes of ruthenium(III) in cell-free media*. J Biol Inorg Chem, 2001. **6**(4): p. 435-45.
220. Bacac, M., et al., *The hydrolysis of the anti-cancer ruthenium complex NAMI-A affects its DNA binding and antimetastatic activity: an NMR evaluation*. J Inorg Biochem, 2004. **98**(2): p. 402-12.
221. Egger, A., et al., *Reactions of potent antitumor complex trans-[Ru(III)Cl4(indazole)2]- with a DNA-relevant nucleobase and thioethers: insight into biological action*. Inorg Chem, 2005. **44**(1): p. 122-32.
222. Groessl, M., et al., *CZE-ICP-MS as a tool for studying the hydrolysis of ruthenium anticancer drug candidates and their reactivity towards the DNA model compound dGMP*. J Inorg Biochem, 2008. **102**(5-6): p. 1060-5.
223. Kung, A., T. Pieper, and B.K. Keppler, *Investigations into the interaction between tumor-inhibiting ruthenium(III) complexes and nucleotides by capillary electrophoresis*. J Chromatogr B Biomed Sci Appl, 2001. **759**(1): p. 81-9.
224. Pluim, D., et al., *Cytotoxicity of the orgallium nitratec ruthenium anticancer drug Nami-A is correlated with DNA binding in four different human tumor cell lines*. Cancer Chemother Pharmacol, 2004. **54**(1): p. 71-8.
225. Schluga, P., et al., *Redox behavior of tumor-inhibiting ruthenium(III) complexes and effects of physiological reductants on their binding to GMP*. Dalton Trans, 2006(14): p. 1796-802.
226. Tan, C., et al., *Differences in structure, physiological stability, electrochemistry, cytotoxicity, DNA and protein binding properties between two Ru(III) complexes*. J Inorg Biochem, 2008. **102**(2): p. 347-58.
227. Pizarro, A.M. and P.J. Sadler, *Unusual DNA binding modes for metal anticancer complexes*. Biochimie, 2009. **91**(10): p. 1198-211.
228. Sakurai, H., et al., *Direct visualization and quantification of the anticancer agent, cis-diamminedichloro-platinum(II), in human lung cancer cells using in-air microparticle-induced X-ray emission analysis*. Cancer Sci, 2008. **99**(5): p. 901-4.

REFERENCES

229. Pawarode, A., et al., *Differential effects of the immunosuppressive agents cyclosporin A, tacrolimus and sirolimus on drug transport by multidrug resistance proteins*. *Cancer Chemother Pharmacol*, 2007. **60**(2): p. 179-88.
230. Bergamo, A., et al., *In vitro cell cycle arrest, in vivo action on solid metastasizing tumors, and host toxicity of the antimetastatic drug NAMI-A and cisplatin*. *J Pharmacol Exp Ther*, 1999. **289**(1): p. 559-64.
231. Zorzet, S., et al., *Lack of In vitro cytotoxicity, associated to increased G(2)-M cell fraction and inhibition of matrigel invasion, may predict In vivo-selective antimetastasis activity of ruthenium complexes*. *J Pharmacol Exp Ther*, 2000. **295**(3): p. 927-33.
232. Xu, B., et al., *Two molecularly distinct G(2)/M checkpoints are induced by ionizing irradiation*. *Mol Cell Biol*, 2002. **22**(4): p. 1049-59.
233. Taylor, W.R. and G.R. Stark, *Regulation of the G2/M transition by p53*. *Oncogene*, 2001. **20**(15): p. 1803-15.
234. Han, J. and P. Sun, *The pathways to tumor suppression via route p38*. *Trends Biochem Sci*, 2007. **32**(8): p. 364-71.
235. Hui, L., et al., *p38alpha: a suppressor of cell proliferation and tumorigenesis*. *Cell Cycle*, 2007. **6**(20): p. 2429-33.
236. Sorenson, C.M. and A. Eastman, *Influence of cis-diamminedichloroplatinum(II) on DNA synthesis and cell cycle progression in excision repair proficient and deficient Chinese hamster ovary cells*. *Cancer Res*, 1988. **48**(23): p. 6703-7.
237. Jamieson, E.R. and S.J. Lippard, *Structure, Recognition, and Processing of Cisplatin-DNA Adducts*. *Chem Rev*, 1999. **99**(9): p. 2467-98.
238. Reed, E., et al., *Platinum-DNA adducts in leukocyte DNA correlate with disease response in ovarian cancer patients receiving platinum-based chemotherapy*. *Proc Natl Acad Sci U S A*, 1987. **84**(14): p. 5024-8.
239. Reed, E., et al., *The measurement of cisplatin-DNA adduct levels in testicular cancer patients*. *Carcinogenesis*, 1988. **9**(10): p. 1909-11.
240. Reed, E., et al., *Platinum-DNA adduct in leukocyte DNA of a cohort of 49 patients with 24 different types of malignancies*. *Cancer Res*, 1993. **53**(16): p. 3694-9.
241. Chresta, C.M., J.R. Masters, and J.A. Hickman, *Hypersensitivity of human testicular tumors to etoposide-induced apoptosis is associated with functional p53 and a high Bax:Bcl-2 ratio*. *Cancer Res*, 1996. **56**(8): p. 1834-41.
242. Lutzker, S.G. and A.J. Levine, *A functionally inactive p53 protein in teratocarcinoma cells is activated by either DNA damage or cellular differentiation*. *Nat Med*, 1996. **2**(7): p. 804-10.
243. Blanc, C., et al., *Caspase-3 is essential for procaspase-9 processing and cisplatin-induced apoptosis of MCF-7 breast cancer cells*. *Cancer Res*, 2000. **60**(16): p. 4386-90.
244. Micheau, O., et al., *Sensitization of cancer cells treated with cytotoxic drugs to fas-mediated cytotoxicity*. *J Natl Cancer Inst*, 1997. **89**(11): p. 783-9.
245. Muller, M., et al., *p53 activates the CD95 (APO-1/Fas) gene in response to DNA damage by anticancer drugs*. *J Exp Med*, 1998. **188**(11): p. 2033-45.
246. Henkels, K.M. and J.J. Turchi, *Cisplatin-induced apoptosis proceeds by caspase-3-dependent and -independent pathways in cisplatin-resistant and -sensitive human ovarian cancer cell lines*. *Cancer Res*, 1999. **59**(13): p. 3077-83.

247. Asselin, E., G.B. Mills, and B.K. Tsang, *XIAP regulates Akt activity and caspase-3-dependent cleavage during cisplatin-induced apoptosis in human ovarian epithelial cancer cells*. *Cancer Res*, 2001. **61**(5): p. 1862-8.
248. Ono, Y., et al., *Loss of p73 induction in a cisplatin-resistant bladder cancer cell line*. *Mol Urol*, 2001. **5**(1): p. 25-30.
249. Pestell, K.E., et al., *Effect of p53 status on sensitivity to platinum complexes in a human ovarian cancer cell line*. *Mol Pharmacol*, 2000. **57**(3): p. 503-11.
250. Toffoli, G., et al., *Pleiotropic-resistant phenotype is a multifactorial phenomenon in human colon carcinoma cell lines*. *Br J Cancer*, 1991. **63**(1): p. 51-6.
251. Kuppen, P.J., et al., *cis-diamminedichloroplatinum(II)-resistant sublines derived from two human ovarian tumor cell lines*. *Cancer Res*, 1988. **48**(12): p. 3355-9.
252. Gottesman, M.M. and I. Pastan, *The multidrug transporter, a double-edged sword*. *J Biol Chem*, 1988. **263**(25): p. 12163-6.
253. Som, P., et al., *⁹⁷Ru-transferrin uptake in tumor and abscess*. *Eur J Nucl Med*, 1983. **8**(11): p. 491-4.
254. Chua, A.C., et al., *The regulation of cellular iron metabolism*. *Crit Rev Clin Lab Sci*, 2007. **44**(5-6): p. 413-59.
255. Larson, S.M., Z. Grunbaum, and J.S. Rasey, *The role of transferrins in gallium uptake*. *Int J Nucl Med Biol*, 1981. **8**(4): p. 257-66.
256. Kuhn, L.C., *How iron controls iron*. *Cell Metab*, 2009. **10**(6): p. 439-41.
257. Hentze, M.W., M.U. Muckenthaler, and N.C. Andrews, *Balancing acts: molecular control of mammalian iron metabolism*. *Cell*, 2004. **117**(3): p. 285-97.
258. Pantopoulos, K., *Iron metabolism and the IRE/IRP regulatory system: an update*. *Ann N Y Acad Sci*, 2004. **1012**: p. 1-13.
259. Muckenthaler, M.U., B. Galy, and M.W. Hentze, *Systemic iron homeostasis and the iron-responsive element/iron-regulatory protein (IRE/IRP) regulatory network*. *Annu Rev Nutr*, 2008. **28**: p. 197-213.
260. Pietrangelo, A. and C. Trautwein, *Mechanisms of disease: The role of hepcidin in iron homeostasis--implications for hemochromatosis and other disorders*. *Nat Clin Pract Gastroenterol Hepatol*, 2004. **1**(1): p. 39-45.
261. Rouault, T.A., *The role of iron regulatory proteins in mammalian iron homeostasis and disease*. *Nat Chem Biol*, 2006. **2**(8): p. 406-14.
262. Torti, F.M. and S.V. Torti, *Regulation of ferritin genes and protein*. *Blood*, 2002. **99**(10): p. 3505-16.
263. Niederau, C., et al., *Survival and causes of death in cirrhotic and in noncirrhotic patients with primary hemochromatosis*. *N Engl J Med*, 1985. **313**(20): p. 1256-62.
264. Kawabata, H., et al., *Transferrin receptor 2-alpha supports cell growth both in iron-chelated cultured cells and in vivo*. *J Biol Chem*, 2000. **275**(22): p. 16618-25.
265. Kawabata, H., et al., *Molecular cloning of transferrin receptor 2. A new member of the transferrin receptor-like family*. *J Biol Chem*, 1999. **274**(30): p. 20826-32.
266. Johnson, M.B., et al., *Transferrin receptor 2: evidence for ligand-induced stabilization and redirection to a recycling pathway*. *Mol Biol Cell*, 2007. **18**(3): p. 743-54.
267. Chloupkova, M., A.S. Zhang, and C.A. Enns, *Stoichiometries of transferrin receptors 1 and 2 in human liver*. *Blood Cells Mol Dis*, 2010. **44**(1): p. 28-33.
268. Kew, M.C., *Hepatic iron overload and hepatocellular carcinoma*. *Cancer Lett*, 2009. **286**(1): p. 38-43.

REFERENCES

269. Graf, E., et al., *Iron-catalyzed hydroxyl radical formation. Stringent requirement for free iron coordination site.* J Biol Chem, 1984. **259**(6): p. 3620-4.
270. Toth, I. and K.R. Bridges, *Ascorbic acid enhances ferritin mRNA translation by an IRP/aconitase switch.* J Biol Chem, 1995. **270**(33): p. 19540-4.
271. Sturm, B., et al., *Intravenous iron preparations and ascorbic acid: effects on chelatable and bioavailable iron.* Kidney Int, 2005. **67**(3): p. 1161-70.
272. Bienfait, H.F. and M.L. van den Briel, *Rapid mobilization of ferritin iron by ascorbate in the presence of oxygen.* Biochim Biophys Acta, 1980. **631**(3): p. 507-10.
273. Tarng, D.C. and T.P. Huang, *A parallel, comparative study of intravenous iron versus intravenous ascorbic acid for erythropoietin-hyporesponsive anaemia in haemodialysis patients with iron overload.* Nephrol Dial Transplant, 1998. **13**(11): p. 2867-72.
274. Lu, S.C., *Regulation of hepatic glutathione synthesis: current concepts and controversies.* FASEB J, 1999. **13**(10): p. 1169-83.
275. Mulcahy, R.T., H.H. Bailey, and J.J. Gipp, *Up-regulation of gamma-glutamylcysteine synthetase activity in melphalan-resistant human multiple myeloma cells expressing increased glutathione levels.* Cancer Chemother Pharmacol, 1994. **34**(1): p. 67-71.
276. Mulcahy, R.T., S. Untawale, and J.J. Gipp, *Transcriptional up-regulation of gamma-glutamylcysteine synthetase gene expression in melphalan-resistant human prostate carcinoma cells.* Mol Pharmacol, 1994. **46**(5): p. 909-14.
277. Godwin, A.K., et al., *High resistance to cisplatin in human ovarian cancer cell lines is associated with marked increase of glutathione synthesis.* Proc Natl Acad Sci U S A, 1992. **89**(7): p. 3070-4.
278. Oguri, T., et al., *Expression of gamma-glutamylcysteine synthetase (gamma-GCS) and multidrug resistance-associated protein (MRP), but not human canalicular multispecific orgallium nitratec anion transporter (cMOAT), genes correlates with exposure of human lung cancers to platinum drugs.* Br J Cancer, 1998. **77**(7): p. 1089-96.
279. Huang, Z.Z., et al., *Mechanism and significance of increased glutathione level in human hepatocellular carcinoma and liver regeneration.* FASEB J, 2001. **15**(1): p. 19-21.
280. Nunez, M.T., et al., *Progressive iron accumulation induces a biphasic change in the glutathione content of neuroblastoma cells.* Free Radic Biol Med, 2004. **37**(7): p. 953-60.
281. Harris, W.R. and V.L. Pecoraro, *Thermodynamic binding constants for gallium transferrin.* Biochemistry, 1983. **22**(2): p. 292-9.
282. Larson, S.M., et al., *Common pathway for tumor cell uptake of gallium-67 and iron-59 via a transferrin receptor.* J Natl Cancer Inst, 1980. **64**(1): p. 41-53.
283. Chitambar, C.R. and Z. Zivkovic, *Uptake of gallium-67 by human leukemic cells: demonstration of transferrin receptor-dependent and transferrin-independent mechanisms.* Cancer Res, 1987. **47**(15): p. 3929-34.
284. Hegge, F.N., D.J. Mahler, and S.M. Larson, *The incorporation of Ga-67 into the ferritin fraction of rabbit hepatocytes in vivo.* J Nucl Med, 1977. **18**(9): p. 937-9.
285. Chitambar, C.R. and P.A. Seligman, *Effects of different transferrin forms on transferrin receptor expression, iron uptake, and cellular proliferation of human leukemic HL60 cells. Mechanisms responsible for the specific cytotoxicity of transferrin-gallium.* J Clin Invest, 1986. **78**(6): p. 1538-46.

286. Kotamraju, S., et al., *Transferrin receptor-dependent iron uptake is responsible for doxorubicin-mediated apoptosis in endothelial cells: role of oxidant-induced iron signaling in apoptosis*. J Biol Chem, 2002. **277**(19): p. 17179-87.
287. Minotti, G., et al., *Anthracyclines: molecular advances and pharmacologic developments in antitumor activity and cardiotoxicity*. Pharmacol Rev, 2004. **56**(2): p. 185-229.
288. Perego, P., et al., *Role of apoptosis and apoptosis-related genes in cellular response and antitumor efficacy of anthracyclines*. Curr Med Chem, 2001. **8**(1): p. 31-7.
289. Zunino, F., G. Pratesi, and P. Perego, *Role of the sugar moiety in the pharmacological activity of anthracyclines: development of a novel series of disaccharide analogs*. Biochem Pharmacol, 2001. **61**(8): p. 933-8.
290. Ma, W.W. and A.A. Adjei, *Novel agents on the horizon for cancer therapy*. CA Cancer J Clin, 2009. **59**(2): p. 111-37.
291. Singhal, S.S., et al., *Relip76 transports sunitinib and sorafenib and mediates drug resistance in kidney cancer*. Int J Cancer, 2010. **126**(6): p. 1327-38.
292. Lagas, J.S., et al., *Breast cancer resistance protein and P-glycoprotein limit sorafenib brain accumulation*. Mol Cancer Ther, 2010. **9**(2): p. 319-26.
293. Kim, J.H., et al., *Combined use of tamoxifen, cyclosporin A, and verapamil for modulating multidrug resistance in human hepatocellular carcinoma cell lines*. Yonsei Med J, 1993. **34**(1): p. 35-44.
294. Vatsyayan, R., et al., *RLIP76: A versatile transporter and an emerging target for cancer therapy*. Biochem Pharmacol, 2010.
295. Awasthi, S., et al., *RLIP76 and Cancer*. Clin Cancer Res, 2008. **14**(14): p. 4372-7.
296. Boonstra, J. and J.A. Post, *Molecular events associated with reactive oxygen species and cell cycle progression in mammalian cells*. Gene, 2004. **337**: p. 1-13.
297. Gourlay, C.W. and K.R. Ayscough, *The actin cytoskeleton: a key regulator of apoptosis and ageing?* Nat Rev Mol Cell Biol, 2005. **6**(7): p. 583-9.
298. Gruber, J., S. Schaffer, and B. Halliwell, *The mitochondrial free radical theory of ageing--where do we stand?* Front Biosci, 2008. **13**: p. 6554-79.
299. Trachootham, D., J. Alexandre, and P. Huang, *Targeting cancer cells by ROS-mediated mechanisms: a radical therapeutic approach?* Nat Rev Drug Discov, 2009. **8**(7): p. 579-91.
300. Perry, G., et al., *How important is oxidative damage? Lessons from Alzheimer's disease*. Free Radic Biol Med, 2000. **28**(5): p. 831-4.
301. Klaunig, J.E. and L.M. Kamendulis, *The role of oxidative stress in carcinogenesis*. Annu Rev Pharmacol Toxicol, 2004. **44**: p. 239-67.
302. Halliwell, B., *Oxidative stress and cancer: have we moved forward?* Biochem J, 2007. **401**(1): p. 1-11.
303. Toyokuni, S., *Novel aspects of oxidative stress-associated carcinogenesis*. Antioxid Redox Signal, 2006. **8**(7-8): p. 1373-7.
304. Gius, D. and D.R. Spitz, *Redox signaling in cancer biology*. Antioxid Redox Signal, 2006. **8**(7-8): p. 1249-52.
305. Pan, J.S., M.Z. Hong, and J.L. Ren, *Reactive oxygen species: a double-edged sword in oncogenesis*. World J Gastroenterol, 2009. **15**(14): p. 1702-7.
306. Sun, P., et al., *PRAK is essential for ras-induced senescence and tumor suppression*. Cell, 2007. **128**(2): p. 295-308.

REFERENCES

307. Heyworth, P.G., et al., *Regulation of NADPH oxidase activity by Rac GTPase activating protein(s)*. Mol Biol Cell, 1993. **4**(11): p. 1217-23.
308. Yagoda, N., et al., *RAS-RAF-MEK-dependent oxidative cell death involving voltage-dependent anion channels*. Nature, 2007. **447**(7146): p. 864-8.
309. Kang, Y.H. and S.J. Lee, *The role of p38 MAPK and JNK in Arsenic trioxide-induced mitochondrial cell death in human cervical cancer cells*. J Cell Physiol, 2008. **217**(1): p. 23-33.
310. Komatsu, D., et al., *NADPH oxidase 1 plays a critical mediating role in oncogenic Ras-induced vascular endothelial growth factor expression*. Oncogene, 2008. **27**(34): p. 4724-32.
311. Aplin, A.E., et al., *Integrin-mediated adhesion regulates ERK nuclear translocation and phosphorylation of Elk-1*. J Cell Biol, 2001. **153**(2): p. 273-82.
312. Deng, T. and M. Karin, *c-Fos transcriptional activity stimulated by H-Ras-activated protein kinase distinct from JNK and ERK*. Nature, 1994. **371**(6493): p. 171-5.
313. Davis, R.J., *Transcriptional regulation by MAP kinases*. Mol Reprod Dev, 1995. **42**(4): p. 459-67.
314. Ahmad, T. and T. Eisen, *Kinase inhibition with BAY 43-9006 in renal cell carcinoma*. Clin Cancer Res, 2004. **10**(18 Pt 2): p. 6388S-92S.
315. Burhans, W.C. and N.H. Heintz, *The cell cycle is a redox cycle: linking phase-specific targets to cell fate*. Free Radic Biol Med, 2009. **47**(9): p. 1282-93.
316. Havens, C.G., et al., *Regulation of late G1/S phase transition and APC Cdh1 by reactive oxygen species*. Mol Cell Biol, 2006. **26**(12): p. 4701-11.
317. Wang, X., et al., *Involvement of the MKK6-p38gamma cascade in gamma-radiation-induced cell cycle arrest*. Mol Cell Biol, 2000. **20**(13): p. 4543-52.
318. Dolado, I., et al., *p38alpha MAP kinase as a sensor of reactive oxygen species in tumorigenesis*. Cancer Cell, 2007. **11**(2): p. 191-205.
319. Sherr, C.J. and J.M. Roberts, *Living with or without cyclins and cyclin-dependent kinases*. Genes Dev, 2004. **18**(22): p. 2699-711.
320. Menon, S.G., et al., *Redox regulation of the G1 to S phase transition in the mouse embryo fibroblast cell cycle*. Cancer Res, 2003. **63**(9): p. 2109-17.
321. Heim, M., et al., *The Raf kinase inhibitor BAY 43-9006 reduces cellular uptake of platinum compounds and cytotoxicity in human colorectal carcinoma cell lines*. Anticancer Drugs, 2005. **16**(2): p. 129-36.
322. Rahmani, M., et al., *The kinase inhibitor sorafenib induces cell death through a process involving induction of endoplasmic reticulum stress*. Mol Cell Biol, 2007. **27**(15): p. 5499-513.
323. Harding, H.P., Y. Zhang, and D. Ron, *Protein translation and folding are coupled by an endoplasmic-reticulum-resident kinase*. Nature, 1999. **397**(6716): p. 271-4.
324. Lu, P.D., et al., *Cytoprotection by pre-emptive conditional phosphorylation of translation initiation factor 2*. EMBO J, 2004. **23**(1): p. 169-79.
325. Scheuner, D., et al., *Translational control is required for the unfolded protein response and in vivo glucose homeostasis*. Mol Cell, 2001. **7**(6): p. 1165-76.

Bihter Atil

+43 – 06769557249

bihteratil@hotmail.com, a0409144@unet.univie.ac.at

Address:

Wurlitzergasse 41 Top:11, 1160 Vienna – Austria

Date of Birth

31.08.1985

Place of Birth

Istanbul, Turkey

Citizenship

Turkey

Education

- 01/2009 – 04/2010 Diploma thesis (Molecular Determinants of the Anti-cancer Activity of Ruthenium Compound KP1339) at the Institute of Cancer Research (ICR), Department of Medicine I, Medical University of Vienna. Supervision by Univ.-Prof. Mag. Dr. Renée Schroeder (University of Vienna, Department of Biochemistry and Cell Biology) and a. o. Univ.-Prof. Dr. Walter Berger (ICR)
- 10/2004 – 04/2010 Diploma study in Microbiology/Genetics at the University of Vienna, Austria
- 06/2004 School leaving examination (Matura) at secondary school St. Georg College
- 09/1996 – 06/2004 Secondary school St. Georg College (Bundesrealgymnasium), Istanbul – Turkey
- 09/1991 – 06/1996 Primary school Özel Efdal Ana ve İlkokulu, Istanbul – Turkey

Publications

Heffeter P., Boeck K., **Atil B.**, Reza Hoda M.A., Körner W., Bartel C., Jungwirth U., Keppler B.K., Micksche M., Berger W., Koellensperger G.. Intracellular protein binding patterns of the anticancer ruthenium drugs KP1019 and KP1339. J Biol Inorg Chem 2010. Supplied by publisher

Posters

Heffeter P., **Atil B.**, Jungwirth U., Koerner W., Micksche M., Keppler B.K., Berger W. In vitro and in vivo anticancer activity of the new ruthenium compounds KP1339 against human liver cancer models. Molecular Cancer Therapeutics 8:C103-103C; doi: 10.1158/1535-7163.TARG-09-C103, 15 – 19 November 2009, Boston, MA.